

# **Evaluation of Cardiac Mitochondrial Function in the Fructose-Fed Rat**

by

Katrina Yvonne Scott

A thesis submitted in partial fulfillment of the requirements for the degree of

Master of Science

Department of Pharmacology

University of Alberta

© Katrina Yvonne Scott, 2016

# Abstract

Multiple sources suggest that insulin resistance and derangements of cardiac metabolism are among the earliest signs of type-2 diabetes detected in the heart. Unfortunately, limited evidence reflects early changes in cardiac mitochondrial metabolism linked to the development of this disease. Thus, pinpointing the location of early alterations was the objective of this study. The fructose-fed insulin resistant rat at six weeks of fructose feeding was selected as an appropriate model for the characterization of early type-2 diabetes.

The respiration of mitochondria isolated from the left ventricular wall of healthy and fructose-fed rats was measured in response to different substrate and/or inhibitor combinations using the Oroboros Oxygraph-2K high-resolution respirometry system. These measurements were supplemented with assessments of key metabolic protein levels by immunoblotting and enzymatic activities by biochemical assays.

Respiratory state differences in the fructose-fed group consisted of the increased oxidative phosphorylation of certain fatty acids, i.e. palmitoyl-CoA and octanoylcarnitine, with malate. Increases in the uptake and the oxidation of fatty acids were suggested by: (i) the elevated sarcolemmal expression of cluster of differentiation 36 (CD36), (ii) the augmented expression of the primary cardiac isoform of carnitine palmitoyltransferase-I (CPT1), (iii) the increased mitochondrial expression of CD36, (iv) the reduced presence of CPT1's inhibitor malonyl-CoA, (v) the reduced sensitivity of CPT1 to malonyl-CoA, and (vi) the enhanced activity of the fatty acid  $\beta$ -oxidation (FAO) enzyme  $\beta$ -hydroxyacyl-CoA dehydrogenase. Furthermore, the upregulated expressions of peroxisome proliferator-activated receptor- $\alpha$  (PPAR $\alpha$ ) and peroxisome

proliferator-activated receptor- $\gamma$  coactivator-1 $\alpha$  (PGC-1 $\alpha$ ) indicate the heightened potential for PPAR $\alpha$ /PGC-1 $\alpha$  signaling, which is intimately involved in FAO. The decreased activity of the pyruvate dehydrogenase complex and the increased expression of pyruvate dehydrogenase kinase 4 revealed a less prominent glucose oxidation. Sirtuin 1 and sirtuin 3 were more abundantly expressed in hearts of fructose-fed rats. However, the extent of their activity is unclear. These changes were accompanied by indications of oxidative stress, i.e. increased hydroxynoneal Michael adducts and decreased aconitase activity, in the absence of major antioxidant responses. Diminished mitochondrial markers, i.e. citrate synthase activity and cytochrome *c* oxidase IV expression, were also observed. In conclusion, there are significant metabolic changes combined with signs of decompensation in the fructose-fed rat model of early type-2 diabetes.

# Preface

The research project on which this thesis is based received research ethics approval from the University of Alberta Research Ethics Board: Project Name “Cardioprotective Mechanisms in Rat Hearts”, No. AUP00000239, September 2015.

# Acknowledgements

This thesis was completed under the supervision of Dr. Michael Zaugg and Dr. H el ene Lemieux, in collaboration with supervisory committee member Dr. Alexander Clanachan. Teaching and additional support was also provided by Dr. Eliana Lucchinetti. Dr. John Seubert will act as the external examiner at the thesis defense. The following research included in this thesis was conducted by Dr. Phing-How Lou: hydroxynoneal Michael adducts immunoblots, electron transport system complex activities, pyruvate dehydrogenase complex activity, carnitine palmitoyltransferase activity, superoxide dismutase activity,  $\beta$ -hydroxyacyl-CoA dehydrogenase activity, NAD(P)<sup>+</sup>/NAD(P)H levels, and malonyl-CoA concentrations.

# Table of Contents

<b>Chapter 1 – Introduction</b>	1
<b>Chapter 2 – Methodology</b>	8
2.1 Animals	8
2.2 Integrated Mitochondrial Function Measurement	8
2.2.1 Mitochondrial Isolation	8
2.2.2 High-Resolution Respirometry	10
2.3 Protein Samples	14
2.3.1 Total Tissue Homogenate	14
2.3.2 Subcellular Fractions	15
2.4 Immunoblots	17
2.5 Enzyme Activity Assays	19
2.5.1 Electron Transport System Complexes	19
2.5.2 Citrate Synthase	24
2.5.3 Pyruvate Dehydrogenase Complex	25
2.5.4 Aconitase	25
2.5.5 Carnitine Palmitoyltransferase	27

2.5.6 Superoxide Dismutase _____	28
2.5.7 Aldehyde Dehydrogenase 2 _____	29
2.5.8 $\beta$ -Hydroxyacyl-CoA Dehydrogenase _____	30
2.6 Assays for NAD(P) <sup>+</sup> /NAD(P)H and Malonyl-CoA _____	31
2.6.1 NAD(P) <sup>+</sup> /NAD(P)H _____	31
2.6.2 Malonyl-CoA _____	32
2.7 Data Analysis _____	32
<b>Chapter 3 – Results</b> _____	<b>33</b>
3.1 Reduced Mitochondrial Glucose Oxidation _____	33
3.1.1 Pyruvate Dehydrogenase Complex Activity _____	33
3.1.2 Pyruvate Dehydrogenase Kinase 2 and 4 Expressions _____	33
3.2 Altered Mitochondrial Function _____	34
3.2.1 Integrated Mitochondrial Function _____	34
3.2.2 Electron Transport System Complex Activities _____	37
3.3 Increased Mitochondrial Fatty Acid Oxidation _____	39
3.3.1 Mitochondrial Fatty Acid Uptake _____	39
3.3.2 $\beta$ -Hydroxyacyl-CoA Dehydrogenase Activity _____	42
3.3.3 Regulation of Fatty Acid Oxidation _____	43

3.4 Elevated Oxidative Stress in Mitochondria _____	46
3.4.1 Markers of Oxidative Stress _____	46
3.4.2 Antioxidant Defenses _____	47
3.5 SIRT1 and SIRT3 Signaling _____	50
3.5.1 SIRT1 and SIRT3 Expressions _____	50
3.5.2 NAD <sup>+</sup> /NADH Levels _____	51
3.6 Evidence of Decreased Mitochondrial Content _____	51
<b>Chapter 4 – Discussion</b> _____	<b>54</b>
4.1 Impaired Glucose Oxidation and Insulin Resistance _____	54
4.2 Mitochondrial Electron Transport System Function _____	56
4.3 Mitochondrial Fatty Acid Oxidation _____	57
4.4 Oxidative Stress and Antioxidant Response _____	59
4.5 Sirtuin Signaling _____	63
4.6 Mitochondrial Content _____	65
4.7 Comparison of Cardiac and Skeletal Muscles _____	66
4.8 Overall Significance _____	69
4.9 Limitations _____	70
4.10 Future Directions _____	71

**References** \_\_\_\_\_ 73

**Appendices** \_\_\_\_\_ 95

# List of Tables

2.1 Assays for mitochondrial respiration in isolated rat heart mitochondria _____	10
3.1 OXPHOS (pmol O <sub>2</sub> /s/μg) _____	35
3.2 LEAK (pmol O <sub>2</sub> /s/μg) _____	35
4.1 Characteristics of muscle metabolism in early type-2 diabetes _____	69

# List of Figures

2.1 Presence of subcellular compartment markers in subcellular fractions _____	16
3.1 PDH complex activity (mOD/min/CS) and PDK2 and PDK4 expressions _____	34
3.2 UCP3 expression in mitochondria _____	37
3.3 ETS complex activities ( $\mu\text{mol}/\text{min}/\text{mg}$ ) _____	38
3.4 CPT1B and mitochondrial CD36 expressions _____	39
3.5 CPT activities ( $\mu\text{mol}/\text{min}/\text{mg}$ ) and malonyl-CoA tissue levels (ng/mg) _____	41
3.6 $\beta\text{HADH}$ activity ( $\mu\text{mol}/\text{min}/\text{mg}$ ) _____	42
3.7 Total tissue and nuclear PPAR $\alpha$ and PGC-1 $\alpha$ expressions _____	43
3.8 Cell membrane CD36 expression _____	44
3.9 Cytosolic pAMPK $\alpha$ expression _____	45
3.10 Aconitase activity (nmol/min/mg) and mitochondrial HNE expression _____	46
3.11 Nuclear NRF2 expression _____	47
3.12 Antioxidant protein activities ( $\mu\text{mol}/\text{min}/\text{mg}$ ; SOD units/mg) and expressions _____	48
3.13 Mitochondrial and cytosolic NADPH/NADP $^+$ _____	49
3.14 Nuclear SIRT1 and mitochondrial SIRT3 expressions _____	50
3.15 Mitochondrial, cytosolic, and nuclear NAD $^+$ /NADH _____	51

3.16 Citrate synthase activity ( $\mu\text{mol}/\text{min}/\text{mg}$ ) and total COXIV expression _____	52
3.17 Total and mitochondrial TFAM expressions _____	53

# Chapter 1

## Introduction

At a global scale, approximately 347 million people suffer from diabetes (World Health Organization 2014). According to the Canadian Diabetes Association (2005), only a small proportion of Canada's cases are attributed to type-1 diabetes, an autoimmune disease resulting in a disrupted production of insulin by the pancreas. On the other hand, an estimated ninety per cent of the diabetic patients in Canada are afflicted with type-2 of this disease (Canadian Diabetes Association 2005), which is characterized by increased insulin production and insulin resistance. Regardless of the disease type, the lack of insulin response to the presence of glucose is associated with severe medical complications, such as blindness, neuropathy, kidney disease, stroke, and heart disease (Canadian Diabetes Association 2005). Furthermore, the national prevalence of diabetes is projected to increase from approximately nine to twelve per cent by 2025 (Canadian Diabetes Association 2015). This presents catastrophic implications for the overall quality of life of Canadians and the future of our health care system. A detailed understanding of the development of diabetes is, therefore, necessary to uncover new targets for potential therapies.

Unfortunately, studies using human tissues are limited by the availability of viable samples and are complicated by the heterogeneity of different stages of diabetes. To overcome these restrictions, various animal models are employed to examine specific manifestations of diabetes. Obesity is often used to induce glucose intolerance and insulin resistance – features of type-2 diabetes – in animal models via (i) over-nutrition feeding regimens, such as high fat (Kraegen et

al. 1991; Winzell and Ahrén 2004), high sugar (Musselman et al. 2011), and high fat/high sugar (Zhuhua et al. 2015) diets and (ii) disrupted leptin signaling, as seen in the Lep<sup>ob/ob</sup> mouse (Zhang et al. 1994), the Lepr<sup>db/db</sup> mouse (Chen et al. 1996), and the Zucker fatty rat (Phillips et al. 1996). While pertinent studies of some of these models of late stages of diabetes will be referenced in the discussion of our results (Chapter 4), the current study was conducted using the fructose-fed rat at six weeks of fructose feeding, a model of early type-2 diabetes.

Fructose-rich foods and beverages from corn syrup play an important role in the acquisition of type-2 diabetes in industrialized countries (Canadian Diabetes Association 2005). The intake of dietary fructose differs from that of glucose at the level of metabolic and hormonal regulation. The hepatic metabolism of fructose produces C<sub>3</sub>-phosphate intermediates, which enter glycolysis after the rate-limiting step of glucose uptake. Therefore, the metabolism of fructose is not subject to the feedback inhibition that controls hepatic glucose uptake. This lack of regulation produces additional pyruvate, which favours the generation of acetyl-CoA and the subsequent formation of long-chain fatty acids and triglycerides. In this respect, fructose feeding resembles the nutritional overload of high fat feeding. Moreover, the release of hormones in response to glucose, i.e. insulin and leptin, is not triggered by fructose consumption (Teff et al. 2004). Ultimately, the consequence of homeostatic dysregulation by fructose feeding is manifested in a range of symptoms – hypertriglyceridemia, hyperinsulinemia, insulin resistance, and hypertension – known as the metabolic syndrome. These symptoms were initially reported in the fructose-fed rat by Hwang et al. (1987). Changes in this model also include a reduced  $\beta$ -cell mass (Maiztegui et al. 2009), mirroring the  $\beta$ -cell deficit observed in type-2 diabetic patients (reviewed by Klöppel et al. 1985). Although weight gain is not observed in the rat during four to eight weeks of fructose feeding (Iyer et al. 1994; Verma et al. 1994; Dai and McNeill 1995; Iyer et al. 1996; Galipeau et al. 2001), there

is significant deposition of fat in organs and the abdomen termed “abdominal obesity” (Allen and Leahy 1966; Crescenzo et al. 2014).

As the body’s most important glucose sink, skeletal muscle is a tissue of great interest in the investigation of type-2 diabetes. Skeletal muscle regulates glucose levels in conjunction with insulin action. Therefore, reduced insulin-stimulated glucose uptake into the muscle plays a role in the development of whole body insulin resistance and type 2 diabetes. Low mitochondrial capacity (Mogensen et al. 2007; Phielix et al. 2008), high levels of reactive oxygen species (Houstis et al. 2006; Anderson et al. 2009b), and small mitochondrial size (Kelley et al. 2002) have been previously reported in skeletal muscle of type-2 diabetic patients. To respond to the dynamic demands of the body’s musculoskeletal system, skeletal muscles with contrasting functions possess fibres that metabolize different substrates: (i) fast-twitch muscle fibres, e.g. the extensor digitorum longus (EDL), are glycolytic, and (ii) slow-twitch muscle fibres, e.g. the soleus, are oxidative. A study by our laboratory revealed that the mitochondrial content of the glycolytic EDL and oxidative soleus skeletal muscles was unaffected in the fructose-fed rat (Warren et al. 2014). However, the soleus was more resilient than the EDL in terms of coping with the energy supply, i.e. cellular fat overload, and the oxidative balance. Whereas the soleus only showed signs of an enhanced fatty acid  $\beta$ -oxidation (FAO), the EDL exhibited a reduced pyruvate dehydrogenase (PDH) complex activity, a dysfunctional FAO, and a decreased aconitase activity consistent with increased oxidative stress (Warren et al. 2014). This was largely attributed to a relatively lesser abundance of antioxidant enzymes in the EDL (Warren et al. 2014).

However, the heart is also particularly affected by diabetes. Even though cardiac muscle is striated like skeletal muscles, metabolic diversity does not exist between cardiac muscle fibres. Thus, metabolic flexibility is essential to sustain proper cardiac function during changes in the body’s

state of nutrition, i.e. fed or starved conditions. In the diabetic heart, neither cardiac function nor energetic efficiency are maintained, leading to a host of symptoms known as diabetic cardiomyopathy. Diabetic cardiomyopathy was originally identified by Rubler et al. (1972). It encompasses all modifications to the structure and function of the diabetic heart that are independent of confounding factors, such as obesity, hypertension, and coronary artery disease. Diabetic hearts are at risk of experiencing diastolic and systolic dysfunction (Redfield et al. 2003), which are thought to develop in this respective order (Liu et al. 2001; Schannwell et al. 2002). On the same note, diastolic and systolic dysfunction have been reported in animal models of diabetes (Zhou et al. 2000; Semeniuk et al. 2002; Christoffersen et al. 2003). Several studies have established a correlation between diabetes itself and the prognosis of heart failure (Aronow and Ahn 1999; Nichols et al. 2001; Bertoni et al. 2003), which designates a “pump failure” due to structural and functional alterations. While the pathology of diabetic cardiomyopathy is not fully understood, multiple factors contribute to the distinctive loss of myocardial contractility. Left ventricular thickness and mass are augmented in diabetic patients (Devereux et al. 2000; Ilercil et al. 2001). Calcium homeostasis, which regulates contractility, is also altered in diabetic cardiomyocytes (reviewed by Cessario et al. 2006). In fact, the cardiovascular-related deaths of diabetic patients can be predicted using the coronary calcium score (Agarwal et al. 2012).

A number of factors contributing to cardiac function are controlled by the mitochondrion. The mitochondrion is a semi-autonomous cytoplasmic organelle responsible for oxidative phosphorylation in eukaryotes. Yielding ATP through the catabolism of organic nutrient molecules, the number of mitochondria present in a cell is generally proportional to its energetic demand. Cellular transport processes and conformational changes in contractile systems require significant energetic input. In order to prevent failure of the heart, cardiomyocytes contain

numerous large mitochondria that depend on carbohydrates for approximately thirty per cent of their energetic needs, with the remaining seventy per cent of energy derived from fatty acids (reviewed by Neely and Morgan 1974). Furthermore, mitochondria are integrally involved in key cellular functions, such as maintaining calcium homeostasis, inducing cell signaling through the generation of reactive oxygen species (ROS), and initiating apoptosis.

Various significant changes in the diabetic heart occur at the level of the mitochondrion. An increased cellular and mitochondrial fatty acid uptake as well as an elevated FAO – representing approximately ninety per cent of utilized fuels – have been reported in hearts of several diabetic animal models (reviewed by Carley and Severson 2005). Nevertheless, due to the lipid accumulation observed in diabetic rat (Zhou et al. 2000) and human (Sharma et al. 2004) hearts, it has been suggested that the enhanced FAO is not sufficient to compensate for the high fat uptake. In a previous study of hearts of fructose-fed rats by our laboratory, elevated tissue concentrations of acylcarnitines suggested an inadequate FAO pathway (Lou et al. 2015). Moreover, in atrial appendages of type-2 diabetic patients, deficiencies have been reported in complex I of the mitochondrial electron transport system (ETS) by Anderson et al. (2009a) and in ETS complexes II and III by Montaigne et al. (2014). Furthermore, diabetes is associated with a markedly augmented generation of ROS (Zhou et al. 2000; Barouch et al. 2003). This may take place at complex I and/or complex III of the ETS, the primary sites of mitochondrial ROS production (reviewed by Fisher-Wellman and Neuffer 2012). Throughout the oxidation of fatty acids, ROS production may also occur during the transfer of electrons from acyl-CoA dehydrogenases to ubiquinol (Rosca et al. 2012). Antioxidant responses seem to vary between diabetes models (Aliciguzel et al. 2003; Turko and Murad 2003). In accordance with the damaging conditions, there is also evidence of a more notable myocardial autophagy in fructose-fed mice (Mellor et al.

2011). Finally, smaller mitochondria have been observed in the type-2 diabetic atrium (Montaigne et al. 2014). Fewer and smaller mitochondria suggest a lower cardiac capacity for oxidative phosphorylation. All of these characteristics are indicative of energetic inefficiency in the diabetic heart.

The study of diabetes at an early time point is crucial to elucidate the metabolic derangements leading to the progression of this disease. Treating initial changes could constitute a means of preventing the development of diabetic cardiomyopathy. The fructose-fed rat model is known to be consistent with type-2 diabetes. In addition to the traits shared by the fructose-fed rat and type-2 diabetic patients, the severity of the exhibited metabolic syndrome in this animal model can be manipulated through the intensity and the length of the fructose feeding (Dai and McNeill 1995). The subject of this study was the male Sprague-Dawley rat after receiving a standard diet and water *ad libitum* supplemented with fructose (100 g/L) for six weeks, a time point corresponding to an early stage of type-2 diabetes as the discontinuation of the fructose feeding reverses insulin resistance (Dai and McNeill 1995).

Our laboratory has previously investigated physiological and metabolic changes that occur in response to this feeding (Lou et al. 2014). The observed high fasting glucose levels, hyperinsulinemia, hypertension, and high circulating triglyceride levels (Lou et al. 2014) are characteristic of a type-2 diabetic model. Importantly, the fructose-fed rat does not present overt signs of impaired cardiac function but exhibits a decreased glucose uptake in response to insulin, consistent with insulin resistance (Lou et al. 2015). This was accompanied by increased cardiac tissue levels of triglycerides (Lou et al. 2014) and the accumulation of acylcarnitines and the diabetogenic phospholipids lysophosphatidylcholine and lysophosphatidylethanolamine (Lou et

al. 2015). Together, these findings confirm that, in addition to total body insulin resistance, the fructose-fed rat model possesses all classical features of the type-2 diabetic heart.

The main objectives of this study were the evaluation of cardiac mitochondrial function and signaling events during early diabetes, using the fructose-fed rat model. For this purpose, we posed several questions:

- (i) What are the effects of fructose feeding on indices of cellular and mitochondrial fatty acid uptake?
- (ii) Does mitochondrial FAO commensurate with indices of fatty acid uptake?
- (iii) What are the effects of fatty acid uptake and/or oxidation on the mitochondrial ETS and ROS production?
- (iv) What are the causes of the state of oxidative stress?

Based on our model's early state of diabetes and on our previous findings in skeletal muscle (Warren et al. 2014), we hypothesized that cardiac mitochondria of fructose-fed rats would manifest unaffected ETS, but significant metabolic derangements, such as increased fatty acid uptake and oxidation, increased formation of ROS, decreased antioxidant counter-regulation, and marked changes in cardiac metabolic signaling.

## Chapter 2

# Methodology

## 2.1 Animals

Acclimatized male Sprague-Dawley rats, eight weeks of age, were divided into healthy control and fructose-fed experimental groups. For six weeks, control rats received standard rat chow (PicoLab Laboratory Rodent Diet 5LOD) and water *ad libitum*. The diet of age-matched fructose-fed rats consisted of standard rat chow but was supplemented with fructose (100 g/L) drinking water (Lou et al. 2014). At the end of this period, rats were anesthetized by intraperitoneal injection of pentobarbital (150 mg/kg). Their hearts were removed and perfused in a non-working Langendorff mode with Krebs-Henseleit solution for 10 min. For high-resolution respirometry (section 2.2), the left ventricular wall was immediately processed for mitochondrial isolation. Additional whole hearts were frozen in liquid nitrogen with Wollenberger clamps, pulverized, and stored at -80°C for later use in immunoblots (section 2.4), enzyme activity assays (section 2.5), and molecular tissue level assays (section 2.6).

## 2.2 Integrated Mitochondrial Function Measurement

### 2.2.1 Mitochondrial Isolation

Isolated mitochondria were used for high-resolution respirometry. In the absence of cytosolic metabolism, mitochondrial factors could be regarded as the sole contributors to experimental

results (Brand and Nicholls 2011). Furthermore, the elimination of cellular barriers and transporters facilitated the manipulation of the mitochondrial milieu. This shortened the duration of the assays and allowed for the completion of a large number of substrate and/or inhibitor protocols per rat heart.

A crude mitochondrial isolation was carried out using a modified version of the methods of King et al. (2007). All steps were performed on ice or at 4°C. The left ventricle of the hearts of control and fructose-fed rats was collected in 15 mL of mitochondrial isolation buffer (Appendix A.1), rinsed in another 20 mL, blotted dry, and weighed. The tissue was roughly chopped with scissors and rinsed in 20 mL of the same buffer. The tissue was further minced with a single edge blade and added to 10 mL of mitochondrial isolation buffer with defatted bovine serum albumin (BSA; 2 g/L; Sigma-Aldrich A6003) per gram of tissue. The mixture was homogenized twice with a tissue processor (Polytron PT 1600 E) for 2.5 sec on a setting of 15, stirred with 1 mL of trypsin (30 g/L; Sigma-Aldrich T0303) per gram of heart for 10 min, and subjected to three strokes with the loose pestle of a glass Dounce homogenizer. The homogenate was centrifuged at 600 g for 10 min to pellet cellular debris. The resulting supernatant was filtered through three layers of gauze to remove fat and centrifuged at 3,100 g for 10 min. The mitochondrial pellet was gently resuspended in a small volume of mitochondrial isolation buffer and centrifuged at 3,100 g for 10 min once more. The washed mitochondrial pellet was resuspended in 172  $\mu$ L of suspension buffer (Appendix A.2) per gram of mitochondrial pellet. A portion of each sample was aliquoted and stored at -80°C for protein concentration determination by Bradford assay and the enzymatic activity assays of the ETS complexes (section 2.5.1) and  $\beta$ -hydroxyacyl-CoA dehydrogenase ( $\beta$ HADH; section 2.5.8).

## 2.2.2 High-Resolution Respirometry

Isolated mitochondria were added to calibrated high-resolution respirometry chambers (Oroboros Oxygraph 2-K) containing 2 mL of mitochondrial respiration medium (Mir05; Appendix A.3; Gnaiger et al. 2000). The amount of prepared mitochondria was selected to produce respiration rates high enough to minimize electrode noise while ensuring sufficient oxygen levels for protocol completion. The order of the protocols was rotated from day-to-day to account for the potential decline in the condition of isolated mitochondria over time. Oxygen consumption was measured at 37°C and atmospheric air saturation. It was recorded with Oroboros Datlab software. Nine high-resolution respirometry protocols (Table 2.1) were used to evaluate mitochondrial function and capacity in the control and fructose-fed groups.

Table 2.1 Assays for mitochondrial respiration in isolated rat heart mitochondria

Protocols	Mitochondrial Targets
<i>TCA Cycle and ETS</i>	
PM: pyruvate (5 mM) + malate (2 mM)	Pyruvate carrier, PDH complex, CI
G: glutamate (40 mM)	Glutamate-aspartate carrier, GDH, CI
GM: glutamate (40 mM) + malate (8 mM)	Glutamate-aspartate carrier, CI
S(Rot): succinate (10 mM) + rotenone (0.5 μM)	CII/SDH
AsTm: ascorbate (2 mM) + TMPD (0.5 mM)	CIV
<i>FAO (TCA Cycle and ETS)</i>	
PalCar: palcar (2.5 μM - 15 μM) + malate (4 mM)	CT, CPT2, long-chain FAO
PalCoA: palCoA (0.02 mM) + car (1.25 mM) + malate (2 mM)	CPT1, CT, CPT2, long-chain FAO
OctCar: octcar (0.33 mM) + malate (2 mM)	CT, CPT2, medium-chain FAO
ActCar: acetylcar (5 mM) + malate (2 mM)	CT, CAT

Abbreviations: tricarboxylic acid (TCA), electron transport system (ETS), fatty acid β-oxidation (FAO), N,N,N',N'-tetramethyl-p-phenylenediamine (TMPD), complex I (CI), complex II (CII), complex III (CIII), complex IV (CIV), pyruvate dehydrogenase (PDH), glutamate dehydrogenase (GDH), succinate dehydrogenase (SDH), palmitoylcarnitine (palcar), palmitoyl-CoA (palCoA), carnitine (car), octanoylcarnitine (octcar), acetylcarnitine (acetylcar), carnitine translocase (CT), carnitine palmitoyltransferase-I (CPT1), carnitine palmitoyltransferase-II (CPT2), and carnitine acetyltransferase (CAT).

## Metabolic Substrates

High-resolution respirometry protocols were collectively designed to target certain complexes, transporters, and enzymes (Table 2.1) with combinations of substrates and/or inhibitors. Nevertheless, the respiratory states of each protocol were dependent on the entirety of the appropriate metabolic pathways, i.e. the breakdown of substrates into reducing equivalents for entry into the ETS, resulting in an electron flux to complex IV and the final reduction of oxygen to water.

**PM**: The pyruvate carrier transports pyruvate into the matrix, where it is transformed to acetyl-CoA by the PDH complex. When sparked by malate, citrate synthase of the tricarboxylic acid (TCA) cycle catalyzes the condensation of oxaloacetate and acetyl-CoA. To re-establish the malate-fumarate equilibrium in the presence of added malate, there is an increase in fumarate. This results in an inhibited flux from succinate to fumarate. Moreover, oxaloacetate produced from the oxidation of malate inhibits complex II/succinate dehydrogenase (SDH). Thus, the PM protocol induces a flux of electrons through complex I of the ETS (Gnaiger 2012).

**G**: Glutamate as the sole substrate is transported into the matrix by the glutamate-aspartate carrier and is oxidized by glutamate dehydrogenase (GDH). The accumulation of fumarate inhibits complex II/SDH (Gnaiger 2012).

**GM**: In the presence of malate, the malate-aspartate shuttle uses glutamate to produce aspartate and  $\alpha$ -ketoglutarate (Puchowicz et al. 2004). The accumulation of fumarate in the presence of high malate inhibits complex II/SDH and GDH, and the TCA cycle provides electrons to complex I as described above (Gnaiger 2012).

**S(Rot)**: With the inhibition of complex I by rotenone, succinate provides electrons to complex II/SDH.

**AsTm**: N,N,N',N'-tetramethyl-p-phenylenediamine (TMPD) is employed as an artificial substrate for reducing cytochrome *c*, thereby providing electrons to complex IV. Ascorbate maintains TMPD in a reduced state.

**PalCar\***: Palmitoylcarnitine is translocated into the matrix by carnitine translocase. It is converted to palmitoyl-CoA by carnitine palmitoyltransferase-II (CPT2) before undergoing long-chain FAO to produce acetyl-CoA.

**PalCoA\***: Palmitoyl-CoA in the presence of carnitine utilizes carnitine palmitoyltransferase-I (CPT1) to form palmitoylcarnitine, which follows the same path as described above.

**OctCar\***: Octanoylcarnitine is translocated into the matrix by carnitine translocase. It is converted to octanoyl-CoA by CPT2 and enters medium-chain FAO to yield acetyl-CoA.

**ActCar\***: Acetylcarnitine is also translocated into the matrix by carnitine translocase but is converted to acetyl-CoA by carnitine acetyltransferase.

\*Malate was included in all FAO protocols to spark the entry of acetyl-CoA into the TCA cycle and stimulate a flux of electrons through complex I.

### Substrate Concentrations

In a preliminary mitochondrial preparation, substrate titrations were performed to determine optimal concentrations of ETS, TCA cycle, and FAO substrates (Table 2.1) so that differences in high-resolution respirometry measurements were not due to substrate limitation. As high concentrations of palmitoylcarnitine have a detergent effect on the mitochondrial membranes that

depends on the membrane composition of a given preparation (Červinková et al. 2008), a palmitoylcarnitine titration was performed each day to identify the optimal concentration for maximal respiration. A single addition of this concentration was applied to the PalCar protocol.

### Respiratory States

Mitochondrial function and capacity was assessed at multiple respiratory states. First, under saturating levels of ADP, substrate oxidation is coupled to ATP production by oxidative phosphorylation (OXPHOS). Then, oligomycin (2 µg/mL) inhibits ATP synthase to induce LEAK, the respiration compensating for proton leak, proton slip, cation cycling, and electron slip (Brand et al. 1994). In the AsTm protocol, the addition of azide (100 mM) inhibits respiration by blocking complex IV, revealing the chemical background to be subtracted from OXPHOS (Gnaiger et al. 1998). The measurements were normalized to protein concentration.

Further respiratory states were measured in separate PM and S(Rot) assays and expressed as percent variations of their preceding states. For example, to validate the quality of the isolated mitochondria, cytochrome *c* (10 µM) was added after OXPHOS to test the condition of the outer mitochondrial membrane (Kuznetsov et al. 2004) in the first PM assay of each day. The cytochrome *c* effect showed the preserved integrity of the outer mitochondrial membrane with OXPHOS increases of  $8.44 \pm 1.43\%$  in the control group and  $6.12 \pm 0.87\%$  in the fructose-fed group. Moreover, an uncoupler titration (0.5 µM steps) was included in discrete PM and S(Rot) assays to obtain the maximum uncoupled respiration. Uncoupling agents, such as the protonophore carbonyl cyanide 4-(trifluoromethoxy)phenylhydrazone (FCCP), allow protons to move back into the matrix by means other than the ATP synthase, disconnecting electron transport from ATP synthesis. Consequently, the gradual titration of an optimal uncoupler concentration can stimulate the ETS and reveal its greatest respiratory capacity. Finally, mitochondrial uncoupling proteins

were examined after LEAK in an S(Rot) assay by inhibiting uncoupling proteins and adenine nucleotide translocase (ANT) with GDP (0.5 mM) and carboxyatractyloside (5  $\mu$ M), respectively.

### Chemicals for High-Resolution Respirometry

The majority of the respiratory chemicals were sourced and handled as detailed by Eigentler et al. (2012). The following products were obtained from Sigma-Aldrich, unless otherwise stated. Pyruvate (P2256) was freshly dissolved in double distilled water. Stock solutions of acetylcarnitine (A6706), ascorbate (A4034), azide (S2002), carboxyatractyloside (C4992), carnitine (C0283), cytochrome *c* (C7752), GDP (G7127), glutamate (G1626), malate (M1000), octanoylcarnitine (Tocris Bioscience 0605), palmitoylcarnitine (P4509), palmitoyl-CoA (P9716), succinate (S2378), and TMPD (T3134) were prepared in double distilled water and stored at -20°C. ADP (A5285) stocks with free Mg<sup>2+</sup> (0.6 mole of magnesium chloride per mole of ADP) were prepared in double distilled water and stored at -80 °C. Stocks of FCCP (C2920), oligomycin (Abcam ab141829), and rotenone (R8875) were prepared in absolute ethanol and kept at -20°C.

## **2.3 Protein Samples**

### **2.3.1 Total Tissue Homogenate**

Total heart tissue homogenate was prepared by high-speed shaking (Qiagen TissueLyser II) with stainless steel beads (Qiagen 69989) at 25 Hz for 2 min in tubes containing radioimmunoprecipitation assay (RIPA) buffer (Appendix B.1) and protease inhibitors (Appendix B.2). The mixture was centrifuged at 4°C and 800 g for 10 min. The resulting supernatant was referred to as total tissue homogenate, and the pelleted cell debris was discarded.

### **2.3.2 Subcellular Fractions**

The differential centrifugation protocol used for the fractionation of various cellular components was derived from a combination of the methods of Cox and Emili (2006) and Dimauro et al. (2012). The purity of the fractions was verified through the protein expression of subcellular markers normalized to Ponceau S staining; contamination was presented relative to the amount of marker present in its designated fraction (Table 2.2) All steps were performed at 4°C or on ice. Heart tissue was homogenized (Qiagen TissueLyser II) at 25 Hz for 2 min with a detergent-free homogenization buffer (Appendix B.3), protease inhibitors (Appendix B.2), and a stainless steel bead. The mixture was centrifuged at 800 g for 15 min. This first pellet was set aside for the isolation of the nuclear fraction. The supernatant was spun at 800 g for a second 15 min to pellet remaining cellular debris. Its supernatant was considered largely nuclei-free and was used for mitochondrial and membrane isolations.

#### Nuclear Fraction

The first pellet was resuspended in detergent-free homogenization buffer (Appendix B.3), vortexed at maximum speed for 15 sec, and centrifuged at 500 g for 15 min. The supernatant was poured off, and this step was repeated to wash the nuclear pellet. The nuclear pellet was resuspended in detergent-free homogenization buffer (Appendix B.3) and vortexed at maximum speed for 15 sec before being centrifuged at 1,000 g for 15 min. The washed nuclear pellet was resuspended in nuclear extraction buffer (Appendix B.4), lysed by 20 passages through an 18-gauge needle, and centrifuged at 9,000 g for 30 min. The supernatant was the nuclear fraction.

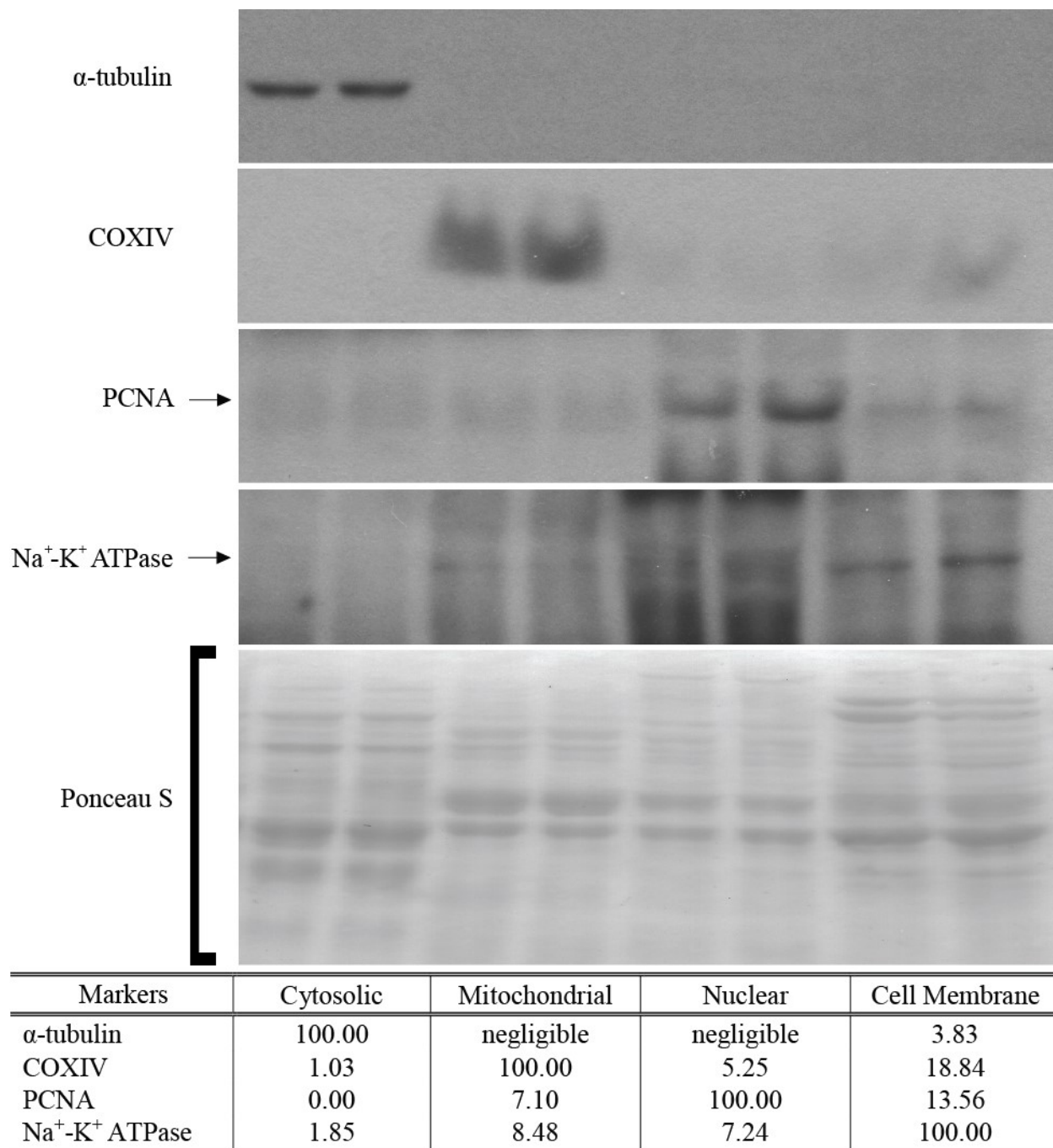


Figure 2.1 Presence of subcellular compartment markers in subcellular fractions. The expressions of  $\alpha$ -tubulin, cytochrome *c* oxidase IV (COXIV), proliferating cell nuclear antigen (PCNA), and  $\text{Na}^+$ - $\text{K}^+$  ATPase were measured by immunoblotting and used as markers of cytosol, mitochondria, nuclei, and cell membranes, respectively. Protein expression was normalized to the ponceau S staining of the appropriate lane. Contamination was calculated as a percentage (%) relative to the normalized marker expression of the respective fraction. The table above contains the mean values obtained from two independent fraction preparations of two samples per fraction. Representative images are presented to illustrate the relative levels of contamination.

### Mitochondrial Fraction

The nuclei-free supernatant was spun at 11,000 g for 10 min. The supernatant was set aside for cell membrane fractionation. The resulting mitochondrial pellet was washed through resuspension in detergent-free homogenization buffer (Appendix B.3) and centrifugation at 11,000 g for 10 min. The final mitochondrial pellet was resuspended in a small amount of detergent-free homogenization buffer (Appendix B.3).

### Cell Membrane Fraction

The designated supernatant underwent ultra-centrifugation at 100,000 g for 1 hr. The cytosolic supernatant was collected, while the pellet was resuspended in membrane extraction buffer (Appendix B.5) and left to incubate on ice for 1 hr. The suspension was centrifuged at 9,000 g for 30 min. The supernatant was designated as the cell membrane fraction.

## **2.4 Immunoblots**

For use in the Laemmli SDS-PAGE system, all protein samples (section 2.3) were reduced and denatured by 10 to 15 min of boiling in 5× Laemmli sample buffer (Appendix C.1). Equal amounts of protein determined by Bradford assay were loaded into the wells of 7.5 to 15% SDS-PAGE gels – 30 µg of protein for total tissue homogenates and cytosolic fractions and 15 µg of protein for other fractions – which were run at 85 to 95 V. Protein was transferred from the gels to 0.45 µm pore size nitrocellulose membranes (Bio-Rad 162-0115) in transfer buffer (Appendix C.2) for either 3 hr at 95 V or overnight at 30 V. The efficiency of protein transfer was assessed and confirmed by Ponceau S (Sigma-Aldrich P7170) staining. Membranes were blocked in BSA (50 g/L; Sigma-Aldrich A7906) or casein (Abcam ab126587) for a minimum of 1 hr. The primary and secondary antibody dilution factors, blocking solutions, and incubation periods were optimized for

the proteins of interest. Three 5 min washes with tris-buffered saline and Tween 20 (TBST; Appendix C.3) followed each antibody incubation. Chemiluminescent signals were obtained with Amersham ECL Western Blotting Detection Reagent (GE Life Sciences RPN2106) or Amersham ECL Prime Western Blotting Detection Reagent (GE Life Sciences RPN2232). The density of the bands was quantified using ImageJ software (National Institutes of Health) with background signal accounted for. Densitometric values were normalized to  $\alpha$ -tubulin (mouse monoclonal; Abcam ab7291), cytochrome *c* oxidase IV (COXIV; mouse monoclonal; Abcam ab14744), lamin A/C (mouse monoclonal; Cell Signaling Technology 4777), or Na<sup>+</sup>-K<sup>+</sup> ATPase (rabbit polyclonal; Cell Signaling Technology 3010) as loading controls for cellular/cytosolic, mitochondrial, nuclear, or membrane proteins, respectively.

The following proteins were detected with their respective antibodies: adenosine monophosphate-activated protein kinase- $\alpha$  (total AMPK $\alpha$ ; rabbit polyclonal; Cell Signaling Technology 2532), phosphorylated (Thr172) adenosine monophosphate-activated protein kinase- $\alpha$  (pAMPK $\alpha$ ; rabbit polyclonal; Cell Signaling Technology 2531), carnitine palmitoyltransferase-I isoform B (CPT1B; rabbit polyclonal; Abcam ab104662), cytochrome *c* oxidase IV subunit 2 isoform B (COXIV2B; rabbit polyclonal; Abcam ab70112), glutathione peroxidase 1 (GPX1; goat polyclonal; Acris Antibodies AP32028PU-N), hydroxynoneal Michael adducts (HNE; rabbit polyclonal; EMD Millipore 393207), mitochondrial transcription factor A (TFAM; rabbit polyclonal; Abcam ab131607), nuclear factor erythroid 2-related factor 2 (NRF2; rabbit polyclonal; EMD Millipore ABE413), peroxisome proliferator-activated receptor- $\alpha$  (PPAR $\alpha$ ; rabbit polyclonal; Abcam ab8934), peroxisome proliferator-activated receptor- $\gamma$  coactivator-1 $\alpha$  (PGC-1 $\alpha$ ; rabbit polyclonal; Abcam ab54481), pyruvate dehydrogenase kinase 2 (PDK2; rabbit monoclonal; Abcam ab68164), pyruvate dehydrogenase kinase 4 (PDK4; rabbit polyclonal; Abcam ab89295), sirtuin 1 (SIRT1;

rabbit polyclonal; Santa Cruz Biotechnology sc-15404), sirtuin 3 (SIRT3; rabbit polyclonal; Santa Cruz Biotechnology sc-99143), thioredoxin reductase 2 (TXNRD2; rabbit polyclonal; Thermo Scientific PA1-20940), cluster of differentiation 36 (CD36; rabbit monoclonal; Abcam ab133625), and uncoupling protein 3 (UCP3; rabbit polyclonal; Abcam ab3477). Goat anti-mouse (IgG-HRP; Santa Cruz Biotechnology sc-2055), goat anti-rabbit (IgG-HRP; Santa Cruz Biotechnology sc-2054), and donkey anti-goat (IgG-HRP; Santa Cruz Biotechnology sc-2056) secondary antibodies were used.

## **2.5 Enzyme Activity Assays**

The preparation of samples was tailored to each assay's requirements. In certain assays, the use of a tissue processor (Polytron PT 1600 E), rather than the high-speed shaker (Qiagen TissueLyser II) described in section 2.3, limited the enzymatic damage that could result from over-homogenization. The protein concentration of all samples was determined by Bradford assay. If samples were not assayed immediately, they were stored at -80°C and used within a week. The activity of the following enzymes was measured by spectrophotometric assays dependent on colorimetric reactions.

### **2.5.1 Electron Transport System Complexes**

ETS complex activity assays were performed to complement the findings of high-resolution respirometry protocols (section 2.2.2). These microplate assays were conducted using aliquoted samples of crude mitochondrial isolate (section 2.2.1). The preparation of the mitochondria for the assays and the assays themselves were derived from the methods of Kirby et al. (2007) and Spinazzi et al. (2012). Prior to each assay, the mitochondria were diluted in a hypotonic lysis buffer

composed of potassium phosphate (25 mM; Fisher Scientific P285) and magnesium chloride (5 mM; Sigma-Aldrich M2393) and pH adjusted to 7.2 at 4°C. They were subjected to three liquid nitrogen freeze-thaw cycles to disrupt mitochondrial membranes and were centrifuged at 4°C and 1,000 g for 1 min to pellet any ensuing debris.

### Complex I

Complex I activity was measured at 30°C and 340 nm as demonstrated by the rotenone-sensitive oxidation of NADH.



A baseline absorbance of the sample was established in the assay reagent consisting of potassium phosphate (50 mM; pH 7.5 at 30°C), defatted BSA (2.5 mg/mL), NADH (0.13 mM; Sigma-Aldrich N4504), potassium cyanide (2 mM; Sigma-Aldrich 207810), and antimycin A (10 µg/mL; Sigma-Aldrich A8674). The reaction was commenced by the addition of ubiquinone (65 µM; Sigma-Aldrich C7956). The decrease in absorbance was monitored for 3 min. The linearity of this reaction is limited to 1 to 2 min. In order to distinguish the contribution of complex I to the reaction, rotenone (1 mg/mL) was included in a parallel set of wells. All reaction conditions were corrected for baseline readings. Specific complex I activity is the rotenone-sensitive activity ( $r_A$ ). Complex I activity ( $v_{CI}$ ) was calculated according to Equation 1 and was normalized to protein concentration.

Equation 1.

$$v_{CI} = \frac{r_A}{l \cdot \epsilon_{NADH} \cdot n_{NADH}} \cdot \frac{V_{well}}{V_{sample}}$$

$v_{CI}$ : Complex I activity (µmol/mL/min)

$r_A$ : Rate of absorbance change (min<sup>-1</sup>)

$l$ : Optical path length (cm)

$\epsilon_{NADH}$ : Extinction coefficient of NADH at 340 nm ( $6.22 \text{ mM}^{-1} \cdot \text{cm}^{-1}$ )

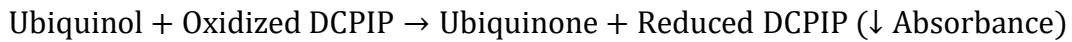
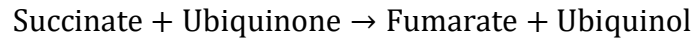
$n_{NADH}$ : Stoichiometric number of NADH in the reaction (1)

$V_{well}$ : Total volume of each well's contents ( $\mu\text{L}$ )

$V_{sample}$ : Volume of the sample in each well ( $\mu\text{L}$ )

## Complex II

Complex II activity was measured at  $30^\circ\text{C}$  and 600 nm as indicated by the malonate-sensitive reduction of dichlorophenolindophenol (DCPIP).



The assay reagents consisted of potassium phosphate (25 mM; pH 7.5 at  $30^\circ\text{C}$ ), BSA (1 mg/mL), succinate (20 mM), DCPIP (50  $\mu\text{M}$ ; Sigma-Aldrich 33125), potassium cyanide (2 mM), antimycin A (10  $\mu\text{g/mL}$ ), and rotenone (2  $\mu\text{g/mL}$ ). The addition of ubiquinone (65  $\mu\text{M}$ ) started the reaction, and the reduction in absorbance was monitored for 5 min. Like the complex I activity assay, a separate set of samples was prepared, but with malonate (10 mM; Sigma-Aldrich M1296), to inhibit complex II. Complex II activity ( $v_{CII}$ ) was calculated according to Equation 2 and normalized to protein concentration.

Equation 2.

$$v_{CII} = \frac{r_A}{l \cdot \epsilon_{DCPIP} \cdot n_{DCPIP}} \cdot \frac{V_{well}}{V_{sample}}$$

$v_{CII}$ : Complex II activity ( $\mu\text{mol/mL/min}$ )

$r_A$ : Rate of absorbance change ( $\text{min}^{-1}$ )

$l$ : Optical path length (cm)

$\epsilon_{DCPIP}$ : Extinction coefficient of DCPIP at 600 nm ( $19.1 \text{ mM}^{-1}\cdot\text{cm}^{-1}$ )

$n_{DCPIP}$ : Stoichiometric number of DCPIP in the reaction (1)

$V_{well}$ : Total volume of each well's contents ( $\mu\text{L}$ )

$V_{sample}$ : Volume of the sample in each well ( $\mu\text{L}$ )

### Complex III

Complex III activity was measured at  $30^\circ\text{C}$  and  $550 \text{ nm}$  through the reduction of cytochrome  $c$ , which is sensitive to antimycin A.



The reagents for this assay were potassium phosphate ( $25 \text{ mM}$ ;  $\text{pH } 7.5$  at  $30^\circ\text{C}$ ), n-dodecyl  $\beta$ -D-maltoside ( $1 \text{ mM}$ ; Sigma-Aldrich D4641), rotenone ( $2 \mu\text{g/mL}$ ), potassium cyanide ( $1 \text{ mM}$ ), ethylenediaminetetraacetic acid (EDTA;  $0.1 \text{ mM}$ ; Sigma-Aldrich 03690), and oxidized cytochrome  $c$  ( $75 \mu\text{M}$ ). The reaction began with the addition of decylubiquinol ( $0.2 \text{ mM}$ ) prepared from decylubiquinone (Sigma-Aldrich D7911), and antimycin A ( $10 \mu\text{g/mL}$ ) was used to inhibit complex III in a parallel reaction sample set. The increase in absorbance at  $550 \text{ nm}$  was monitored for  $3 \text{ min}$ . The linearity of this reaction is limited to  $1$  to  $2 \text{ min}$ . Complex III activity ( $v_{CIII}$ ) was calculated based on Equation 3 and was normalized to protein concentration.

Equation 3.

$$v_{CIII} = \frac{r_A}{l \cdot \epsilon_{\text{cyt.}c} \cdot n_{\text{cyt.}c}} \cdot \frac{V_{well}}{V_{sample}}$$

$v_{CIII}$ : Complex III activity ( $\mu\text{mol/mL/min}$ )

$r_A$ : Rate of absorbance change ( $\text{min}^{-1}$ )

$l$ : Optical path length ( $\text{cm}$ )

$\epsilon_{\text{cyt.}c}$ : Extinction coefficient of cytochrome  $c$  at  $550 \text{ nm}$  ( $18.5 \text{ mM}^{-1}\cdot\text{cm}^{-1}$ )

$n_{\text{cyt.c}}$ : Stoichiometric number of cytochrome  $c$  in the reaction (1)

$V_{\text{well}}$ : Total volume of each well's contents ( $\mu\text{L}$ )

$V_{\text{sample}}$ : Volume of the sample in each well ( $\mu\text{L}$ )

### Complex IV

Complex IV activity was measured at 30°C and 550 nm as designated by the potassium cyanide-sensitive oxidation of cytochrome  $c$ .



The assay reagent was composed of potassium phosphate (50 mM; pH 7.0), n-dodecyl  $\beta$ -D-maltoside (0.45 mM), and reduced cytochrome  $c$  (50  $\mu\text{M}$ ). The reaction was started by adding mitochondria, and the reduction in absorbance at 550 nm was monitored for 3 min. The decline in absorbance is exponential and is usually maximal within 1 to 2 min. The specificity of this reaction for complex IV activity is close to maximal; therefore, it does not require a separate sample reaction with potassium cyanide to inhibit complex IV. Complex IV activity ( $v_{\text{CIV}}$ ) was calculated according to Equation 4 and was normalized to protein concentration.

Equation 4.

$$v_{\text{CIV}} = \frac{r_A}{l \cdot \epsilon_{\text{cyt.c}} \cdot n_{\text{cyt.c}}} \cdot \frac{V_{\text{well}}}{V_{\text{sample}}}$$

$v_{\text{CIV}}$ : Complex IV activity ( $\mu\text{mol/mL/min}$ )

$r_A$ : Rate of absorbance change ( $\text{min}^{-1}$ )

$l$ : Optical path length (cm)

$\epsilon_{\text{cyt.c}}$ : Extinction coefficient of cytochrome  $c$  at 550 nm ( $18.5 \text{ mM}^{-1} \cdot \text{cm}^{-1}$ )

$n_{\text{cyt.c}}$ : Stoichiometric number of cytochrome  $c$  in the reaction (1)

$V_{\text{well}}$ : Total volume of each well's contents ( $\mu\text{L}$ )

$V_{\text{sample}}$ : Volume of the sample in each well ( $\mu\text{L}$ )

## 2.5.2 Citrate Synthase

Citrate synthase is the first enzyme of the TCA cycle responsible for the condensation reaction of acetyl-CoA and oxaloacetate to form citrate. Since it is an exclusive mitochondrial matrix marker (Srere 1969), a citrate synthase activity assay based on Kuznetsov et al. (2010) was used to determine the mitochondrial content (Holloszy et al. 1970; Williams et al. 1986; Hood et al. 1989) of total tissue homogenate. Pulverized heart tissue was homogenized with a tissue processor (Polytron PT 1600 E) in phosphate-buffered saline (PBS; Appendix D.1). The mixture was centrifuged at 4°C and 800 g for 10 min to pellet cellular debris. The protein concentration of the supernatant was determined by Bradford assay. It was aliquoted and stored at -80°C, if not used on the day of the preparation. A baseline absorbance was assessed at 37°C and 412 nm in microplate wells containing sample, Triton X-100 (0.25%; VWR International VW3929-2), a 5,5'-dithiobis-2-nitrobenzoic acid (DTNB; 0.1 mM; Sigma-Aldrich D8130) solution (Appendix D.2), and acetyl-CoA (0.31 mM). The reaction was started with the addition of an oxaloacetate (0.5 mM; Sigma-Aldrich O4126) solution (Appendix D.3).



For each sample, the baseline absorbance was subtracted from the reaction absorbance. The citrate synthase activity ( $v_{CS}$ ) was calculated (Equation 5) and normalized to protein concentration.

Equation 5.

$$v_{CS} = \frac{r_A}{l \cdot \epsilon_{DTNB} \cdot n_{DTNB}} \cdot \frac{V_{well}}{V_{sample}}$$

$v_{CS}$ : Citrate synthase activity ( $\mu\text{mol}/\text{mL}/\text{min}$ )

$r_A$ : Rate of absorbance change ( $\text{min}^{-1}$ )

$l$ : Optical path length (cm)

$\epsilon_{DTNB}$ : Extinction coefficient of DTNB at 412 nm ( $13.6 \text{ mM}^{-1}\cdot\text{cm}^{-1}$ )

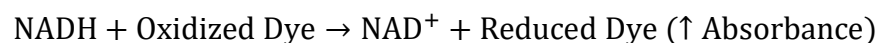
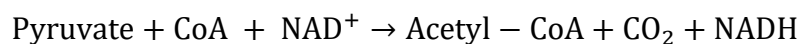
$n_{DTNB}$ : Stoichiometric number of DTNB in the reaction (1)

$V_{well}$ : Total volume of each well's contents ( $\mu\text{L}$ )

$V_{sample}$ : Volume of the sample in each well ( $\mu\text{L}$ )

### 2.5.3 Pyruvate Dehydrogenase Complex

The PDH complex is responsible for the irreversible oxidative decarboxylation of pyruvate to acetyl-CoA for entry into the TCA cycle. The total tissue homogenate for the PDH complex activity assay was prepared in the same manner as for the citrate synthase activity assay. The activity of the PDH complex was measured using a PDH enzyme activity microplate assay kit (Abcam ab109902) according to the manufacturer's instructions and recommendations. In wells coated with monoclonal antibody, the PDH complex's reduction of  $\text{NAD}^+$  to NADH was measured at room temperature and 450 nm through the coupled reduction of a reporter dye.



The PDH complex activity was the initial rate of the reaction and was normalized to citrate synthase activity.

### 2.5.4 Aconitase

The activity of aconitase, a TCA cycle enzyme, is particularly inhibited, albeit reversibly, by oxidative stress agents such as peroxynitrite, hydrogen peroxide, and superoxide (Gardner et al. 1994). Thus, aconitase activity is considered a good marker of oxidative stress. For an aconitase

activity assay, a crude mitochondrial fraction was prepared through the homogenization of rat heart tissue with antioxidant sodium chloride-Tris-EDTA (STE) buffer (Appendix D.4) using a tissue processor (Polytron PT 1600 E) and the differential centrifugation steps described in section 2.3.2. The inclusion of sodium citrate (5 mM; Sigma-Aldrich S1804) and manganese chloride (0.6 mM; Sigma-Aldrich M3634) in an STE buffer (Appendix D.4) protected aconitase from additional oxidation during the isolation process. The final mitochondrial pellet was diluted in antioxidant STE buffer (Appendix D.4) with Triton X-100 (0.05%) to further impede the inactivation of the enzyme during the assay. Aconitase activity was assayed in microplate wells containing Tris-HCl (50 mM; pH 7.4 at 4°C; Invitrogen 15504-020), NADP<sup>+</sup> (0.2 mM; Sigma-Aldrich N050), isocitrate dehydrogenase (1 unit/mL; Sigma-Aldrich I2002), and mitochondria in the presence of sodium citrate (5 mM) and manganese chloride (0.6 mM) as substrates for this assay (Gardner et al. 2002). The assay measures the absorbance of NADPH at 37°C and 340 nm, which is generated in the coupled reactions of aconitase with isocitrate dehydrogenase.



The rate at which NADPH is generated is proportional to the activity of aconitase. The baseline absorbance was accounted for in every test sample reaction. The specificity of this reaction was indicated by a full inhibition of aconitase activity by oxalomalate (2 mM; Cayman 13521). Thus, aconitase activity ( $v_{aconitase}$ ) was calculated with Equation 6 and normalized to protein concentration.

Equation 6.

$$v_{aconitase} = \frac{r_A}{l \cdot \epsilon_{NADPH} \cdot n_{NADPH}} \cdot \frac{V_{well}}{V_{sample}}$$

$v_{aconitase}$ : Aconitase activity ( $\mu\text{mol/mL/min}$ )

$r_A$ : Rate of absorbance change ( $\text{min}^{-1}$ )

$l$ : Optical path length (cm)

$\epsilon_{NADPH}$ : Extinction coefficient of NADPH at 340 nm ( $6.22 \text{ mM}^{-1}\cdot\text{cm}^{-1}$ )

$n_{NADPH}$ : Stoichiometric number of NADPH in the reaction (1)

$V_{well}$ : Total volume of each well's contents ( $\mu\text{L}$ )

$V_{sample}$ : Volume of the sample in each well ( $\mu\text{L}$ )

### 2.5.5 Carnitine Palmitoyltransferase

Carnitine palmitoyltransferases (CPTs) are key enzymes of the mitochondrial carnitine shuttle, which mediates mitochondrial fatty acid uptake. The preparation protocol for the crude mitochondrial fraction used in the CPT activity assay resembled that employed for the aconitase assay, but sodium citrate and magnesium chloride were not included in the STE buffer (Appendix D.4). The final pellet was diluted in STE buffer (Appendix D.4) for assaying purposes. The CPT activity assay was conducted in accordance with Boudina et al. (2005). Baseline absorbance measurements were read in wells containing sample, 4-(2-hydroxyethyl)-1-piperazineethanesulfonic acid (HEPES; 20 mM; pH 7.4 at 25°C; Fisher Scientific BP310), ethylene glycol tetraacetic acid (EGTA; 1 mM; Fisher Scientific O2783), sucrose (220 mM; Fisher Scientific BP220), potassium chloride (40 mM; Sigma-Aldrich P9541), defatted BSA (1.3 mg/mL), DTNB (0.1 mM), and palmitoyl-CoA (40  $\mu\text{M}$ ) at 25°C and 412 nm. The reaction was started with the addition of carnitine (1 mM).



The baseline absorbance was subtracted from the reaction absorbance and the sum of CPT1 and CPT2 activity ( $v_{CPT}$ ) was calculated using Equation 7 and normalized to protein concentration.

Equation 7.

$$v_{CPT} = \frac{r_A}{l \cdot \epsilon_{DTNB} \cdot n_{DTNB}} \cdot \frac{V_{well}}{V_{sample}}$$

$v_{CPT}$ : Total CPT activity ( $\mu\text{mol/mL/min}$ )

$r_A$ : Rate of absorbance change ( $\text{min}^{-1}$ )

$l$ : Optical path length (cm)

$\epsilon_{DTNB}$ : Extinction coefficient of DTNB at 412 nm ( $13.6 \text{ mM}^{-1} \cdot \text{cm}^{-1}$ )

$n_{DTNB}$ : Stoichiometric number of DTNB in the reaction (1)

$V_{well}$ : Total volume of each well's contents ( $\mu\text{L}$ )

$V_{sample}$ : Volume of the sample in each well ( $\mu\text{L}$ )

To determine CPT2 activity, a parallel reaction mixture was supplemented with malonyl-CoA (10  $\mu\text{M}$ ; Sigma-Aldrich M4263) to inhibit CPT1. The difference between the total CPT activity and the CPT2 activity reflects inhibitable CPT1 activity. These data were complemented by a separate microplate assay in which the several concentrations of malonyl-CoA were added (0.05, 0.1, 0.5, 1, 5, 10, 1000  $\mu\text{M}$ ) to determine the extent of CPT1 sensitivity to this inhibitor.

### 2.5.6 Superoxide Dismutase

Superoxide dismutase (SOD) is an antioxidant enzyme responsible for the dismutation of the superoxide radical into hydrogen peroxide and oxygen. The SOD activity of mitochondrial and cytosolic fractions prepared as described in section 2.3.2 was measured using an SOD activity assay kit (BioVision K335-100) according to the manufacturer's instructions and

recommendations. In microplate wells, the rate of reduced water-soluble formazan dye production was measured at 25°C and 450 nm.



This rate is linearly related to the activity of xanthine oxidase, which is inhibited by SOD. Consequently, the SOD activity per milligram of protein was calculated as function of its inhibitory effect.

### 2.5.7 Aldehyde Dehydrogenase 2

Aldehyde dehydrogenase 2 (ALDH2) is a mitochondrial enzyme involved in the oxidation of acetaldehyde to acetic acid, which results in the production of NADH. The activity of ALDH2 was examined in an assay according to the methods of Churchill et al. (2009). The baseline absorbance of cuvettes containing sodium pyrophosphate (50 mM; pH 9.5 at room temperature; Sigma-Aldrich P8010), acetaldehyde (10 mM; Sigma-Aldrich 402788), and NAD<sup>+</sup> (2.5 mM; Sigma-Aldrich N1638) was measured spectrophotometrically at room temperature and 340 nm. The reaction was initiated by the addition of a mitochondrial sample prepared in STE buffer (Appendix D.4).



The baseline absorbance was subtracted from the reaction absorbance. Equation 8 describes the calculation of ALDH2 activity ( $v_{ALDH2}$ ), which was normalized to protein concentration.

Equation 8.

$$v_{ALDH2} = \frac{r_A}{l \cdot \epsilon_{NADH} \cdot n_{NADH}} \cdot \frac{V_{cuvette}}{V_{sample}}$$

$v_{ALDH2}$ : ALDH2 activity ( $\mu\text{mol}/\text{mL}/\text{min}$ )

$r_A$ : Rate of absorbance change ( $\text{min}^{-1}$ )

$l$ : Optical path length (cm)

$\epsilon_{NADH}$ : Extinction coefficient of NADH at 340 nm ( $6.22 \text{ mM}^{-1}\cdot\text{cm}^{-1}$ )

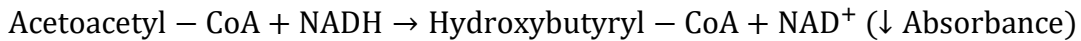
$n_{NADH}$ : Stoichiometric number of NADH in the reaction (1)

$V_{cuvette}$ : Total volume of each cuvette's contents ( $\mu\text{L}$ )

$V_{sample}$ : Volume of the sample in each cuvette ( $\mu\text{L}$ )

### 2.5.8 $\beta$ -Hydroxyacyl-CoA Dehydrogenase

$\beta$ HADH is an oxidoreductase that catalyzes the third step of FAO. The activity of this enzyme was assayed in stored aliquots of the crude mitochondrial isolate that was prepared for high-resolution respirometry (section 2.2.1). The assay was performed according to a Sigma-Aldrich protocol (EC 1.1.1.35). The reaction was initiated in wells containing potassium phosphate (100 mM; pH 7.3), acetoacetyl-CoA (90  $\mu\text{M}$ ; Sigma-Aldrich A1625), and NADH (0.1 mM) through the addition of mitochondria.



The absorbance was measured at  $37^\circ\text{C}$  and 340 nm and was corrected for the baseline absorbance of the reagents. The activity ( $v_{\beta\text{HADH}}$ ) was calculated as described by Equation 9 and was normalized to protein concentration.

Equation 9.

$$v_{\beta\text{HADH}} = \frac{r_A}{l \cdot \epsilon_{\text{NADH}} \cdot n_{\text{NADH}}} \cdot \frac{V_{\text{well}}}{V_{\text{sample}}}$$

$v_{\beta\text{HADH}}$ :  $\beta$ HADH activity ( $\mu\text{mol}/\text{mL}/\text{min}$ )

$r_A$ : Rate of absorbance change ( $\text{min}^{-1}$ )

$l$ : Optical path length (cm)

$\epsilon_{NADH}$ : Extinction coefficient of NADH at 340 nm ( $6.22 \text{ mM}^{-1}\cdot\text{cm}^{-1}$ )

$n_{NADH}$ : Stoichiometric number of NADH in the reaction (1)

$V_{well}$ : Total volume of each well's contents ( $\mu\text{L}$ )

$V_{sample}$ : Volume of the sample in each well ( $\mu\text{L}$ )

## 2.6 Assays for NAD(P)<sup>+</sup>/NAD(P)H and Malonyl-CoA

### 2.6.1 NAD(P)<sup>+</sup>/NAD(P)H

NAD<sup>+</sup> and NADH levels were determined in nuclear, mitochondrial, and cytosolic fractions. These fractions were prepared as outlined in section 2.3.2, but with slight modifications for mitochondrial and cytosolic fractions. Previously pulverized hearts (section 2.1) were homogenized with a tissue processor (Polytron PT 1600 E) in STE buffer (Appendix D.4) and subjected to ten plunges with the loose pestle of a glass Dounce homogenizer. The homogenate was centrifuged at 4°C and 850 g for 10 min to pellet cellular debris. Then, the supernatant was centrifuged at 4°C and 11,000 g for 10 min to pellet the mitochondria. The supernatant was centrifuged in spin columns (Abcam ab93349) at 4°C and 10,000 g for 1 hr to concentrate the cytosol. The mitochondrial pellet was washed through resuspension in STE buffer (Appendix D.4) followed by another spin at 11,000 g for 10 min. Protein concentration was determined by Bradford assay, and samples were snap-frozen and stored at -80°C, if not used immediately. The levels of NAD<sup>+</sup> and NADH were measured using a fluorometric microplate assay kit (Abcam ab176723) according to the manufacturer's instructions and recommendations. Samples were incubated with neutralizing and extraction reagents. The maximal rate of fluorescence increase was recorded at 540/590 nm (ex/em) for 15 min immediately after the addition of the reaction mixture. The amounts of NAD<sup>+</sup>

and NADH were determined by comparison to the standard curve and were indicative of the cell's redox state.

As the relative proportions of NADP<sup>+</sup> and NADPH drive cellular antioxidant defenses, NADP<sup>+</sup> and NADPH levels were assayed in mitochondrial and cytosolic fractions, similarly to as described above, using a fluorometric microplate assay kit (Abcam ab176724).

### **2.6.2 Malonyl-CoA**

Malonyl-CoA, which is utilized in fatty acid biosynthesis, inhibits CPT1. The malonyl-CoA concentration of total tissue homogenate subjected to two freeze-thaw cycles was measured using a competitive inhibition enzyme immunoassay kit (MyBiosource MBS701511). The colorimetric competitive inhibition with horseradish peroxidase conjugated to malonyl-CoA in microplate wells coated with a malonyl-CoA-specific antibody was determined by comparison to the standard curve.

## **2.7 Data Analysis**

Statistical analyses were conducted with GraphPad Prism software. Data are presented as mean  $\pm$  the standard error of the mean (SEM) – in the order of control group vs. fructose-fed group – with a significance of  $P < 0.05$ . Differences between the control and fructose-fed groups were determined by two-tailed unpaired Student's *t*-tests for normally distributed data. When the variance of a data set was significantly different according to an *f*-test, the Mann Whitney *t*-test was employed.

## Chapter 3

# Results

### 3.1 Reduced Mitochondrial Glucose Oxidation

#### 3.1.1 Pyruvate Dehydrogenase Complex Activity

The PDH complex regulates the entry of glycolytic products into the TCA cycle by catalyzing the irreversible oxidative decarboxylation of pyruvate to acetyl-CoA. Therefore, the activity of the PDH complex is the predominant mechanism controlling glucose oxidation. Insulin resistance is strongly associated with the dysregulation of the PDH complex (reviewed by Constantin-Teodosiu 2013). Indeed, the activity of the PDH complex was diminished in total tissue homogenates of hearts of fructose-fed rats ( $100.9 \pm 4.6$  mOD/min/CS vs.  $83.4 \pm 4.4$  mOD/min/CS,  $P = 0.017$ ; Figure 3.1A), indicating a less important contribution of glucose oxidation to the energetic state of cardiac cells and insulin resistance.

#### 3.1.2 Pyruvate Dehydrogenase Kinase 2 and 4 Expressions

The activity of the PDH complex is known to be inhibited by pyruvate dehydrogenase kinases (PDKs). Thus, the expressions of PDK2 and PDK4 were examined to elucidate the change in PDH complex activity in the fructose-fed group (Figure 3.1A). As shown in Figure 3.1B, there was no difference between the two groups in terms of cardiac PDK2 expression ( $2.01 \pm 0.23$  vs.  $2.67 \pm 0.29$ ,  $P = 0.10$ ). However, the expression of PDK4 was increased in hearts of fructose-fed rats ( $0.71 \pm 0.09$  vs.  $1.40 \pm 0.20$ ,  $P = 0.010$ ; Figure 3.1C). While PDK2 is the most abundantly

expressed PDK isoform in the heart, the regulatory activity of PDK4 is more notable (Bowker-Kinley et al. 1998). Therefore, an increased presence of PDK4 is indicative of the capacity for a higher phosphorylation and inactivation of the PDH complex.

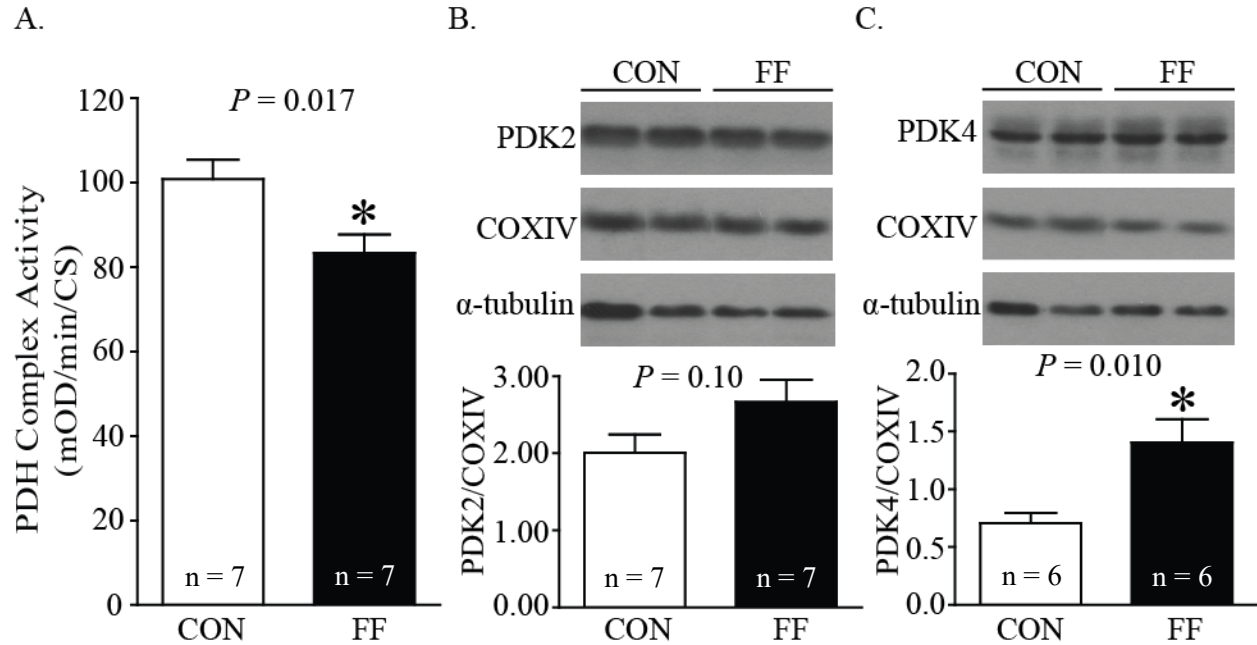


Figure 3.1 PDH complex activity (mOD/min/CS) and PDK2 and PDK4 expressions. (A) The activity of the PDH complex (n = 7) was measured spectrophotometrically in total tissue homogenates of hearts of control (CON) and fructose-fed (FF) rats. It was normalized to citrate synthase activity as an indicator of mitochondrial content. In total tissue homogenates from both groups, the cardiac protein levels of (B) PDK2 (n = 7) and (C) PDK4 (n = 6) were measured by immunoblotting and normalized to the expression of the mitochondrial marker COXIV. Data are presented as mean  $\pm$  SEM with a significance of  $*P < 0.05$ .

## 3.2 Altered Mitochondrial Function

### 3.2.1 Integrated Mitochondrial Function

The main function of the mitochondrion is the production of ATP via oxidative phosphorylation. Considering the tight coupling between electron transport and proton-motive force, the rate of mitochondrial oxygen consumption for any substrate is a measure of the mitochondrial capacity to

Table 3.1 OXPHOS (pmol O<sub>2</sub>/s/μg)

Protocols	CON	FF	P-value
<i>TCA Cycle and ETS</i>			
PM	16.98 ± 1.56 (8)	20.25 ± 1.44 (8)	0.15
G	12.13 ± 1.00 (8)	14.78 ± 1.85 (8)	0.23
GM	13.92 ± 2.17 (9)	13.50 ± 2.50 (8)	0.90
S(Rot)	14.73 ± 1.36 (8)	17.81 ± 1.47 (8)	0.15
AsTm	35.72 ± 4.09 (7)	47.64 ± 4.68 (7)	0.079
<i>FAO (TCA Cycle and ETS)</i>			
PalCar	5.85 ± 0.87 (7)	7.03 ± 0.86 (8)	0.35
<b>PalCoA</b>	<b>5.86 ± 0.68 (7)</b>	<b>9.14 ± 0.44 (8)</b>	<b>0.0011*</b>
<b>OctCar</b>	<b>7.85 ± 0.64 (8)</b>	<b>10.26 ± 0.76 (8)</b>	<b>0.030*</b>
ActCar	9.45 ± 0.97 (8)	11.57 ± 1.25 (8)	0.20

The OXPHOS respiratory state is the oxygen flux due to substrate oxidation with saturating levels of ADP. It was measured in crude mitochondrial isolates of hearts of control (CON) and fructose-fed (FF) rats (n = 7 – 9). Data were normalized to protein concentration and are presented as mean ± SEM (n) with a significance of \**P* < 0.05.

Table 3.2 LEAK (pmol O<sub>2</sub>/s/μg)

Protocols	CON	FF	P-value
<i>TCA Cycle and ETS</i>			
PM	1.39 ± 0.10 (7)	1.27 ± 0.05 (7)	0.30
G	0.75 ± 0.08 (8)	0.78 ± 0.04 (8)	0.77
GM	1.28 ± 0.18 (9)	1.18 ± 0.14 (8)	0.68
S(Rot)	3.24 ± 0.50 (7)	3.52 ± 0.35 (8)	0.65
AsTm	-	-	-
<i>FAO (TCA Cycle and ETS)</i>			
PalCar	1.10 ± 0.15 (8)	1.13 ± 0.12 (8)	0.90
PalCoA	0.92 ± 0.10 (8)	0.94 ± 0.04 (8)	0.85
OctCar	0.95 ± 0.07 (7)	1.15 ± 0.06 (8)	0.055
ActCar	0.79 ± 0.08 (7)	0.89 ± 0.12 (8)	0.53

The LEAK respiratory state is the oxygen flux due to proton leak and slip following the inhibition of ATP synthase by oligomycin. It was measured in crude mitochondrial isolates of hearts of control (CON) and fructose-fed (FF) rats (n = 7 – 9). Data were normalized to protein concentration and are presented as mean ± SEM (n) with a significance of \**P* < 0.05.

generate ATP. This rate takes the following processes into account: (i) the transport of substrates into mitochondria, (ii) the production of reducing equivalents by FAO and/or the TCA cycle, (iii) the delivery of electrons to the ETS, (iv) the reduction of oxygen, and (v) the generation of ATP.

For the TCA cycle and ETS protocols, there were no significant OXPHOS differences in cardiac mitochondria of control and fructose-fed rats (Table 3.1). Contrary to the assayed PDH complex activity (section 3.1.1), reduced PDH complex activity was not detected by high-resolution respirometry in the OXPHOS of the PM protocol (Table 3.1). Nevertheless, in comparison to the control group, OXPHOS was significantly higher in rat heart mitochondria of the fructose-fed group for the PalCoA ( $5.86 \pm 0.68$  pmol/s/ $\mu$ g vs.  $9.14 \pm 0.44$  pmol/s/ $\mu$ g,  $P = 0.0011$ ; Table 3.1) and the OctCar ( $7.85 \pm 0.64$  pmol/s/ $\mu$ g vs.  $10.26 \pm 0.76$  pmol/s/ $\mu$ g,  $P = 0.030$ ; Table 3.1) protocols. Since an OXPHOS increase was perceived with PalCoA but not PalCar, an enhanced mitochondrial fatty acid uptake due the elevation of CPT1 expression and/or activity was identified as a potential source of increased respiration. In the PM and S(Rot) protocols of both groups, OXPHOS was not increased by FCCP. This revealed that OXPHOS is not limited by the phosphorylation system in the rat heart.

The respiration in the presence of oligomycin is a direct measure of the proton leak rate across the mitochondrial membrane. Under this condition, a change in respiration can be interpreted as a change in proton leakiness or inner mitochondrial membrane potential due to uncoupling. With regard to LEAK respiration, there were no differences between hearts of control and fructose-fed rats (Table 3.2). In the S(Rot) protocol, the uncoupling protein inhibitor GDP did not further decrease oligomycin-induced LEAK. Therefore, uncoupling activity by UCP3 – the predominant uncoupling protein in the heart – was not detected. However, the expression of the mitochondrial protein UCP3 was higher in hearts of fructose-fed rats ( $0.42 \pm 0.07$  vs.  $0.91 \pm 0.05$ ,  $P = 0.0002$ ;

Figure 3.2). The addition of the ANT inhibitor carboxyatractyloside did not reveal any ANT contribution to the total LEAK.

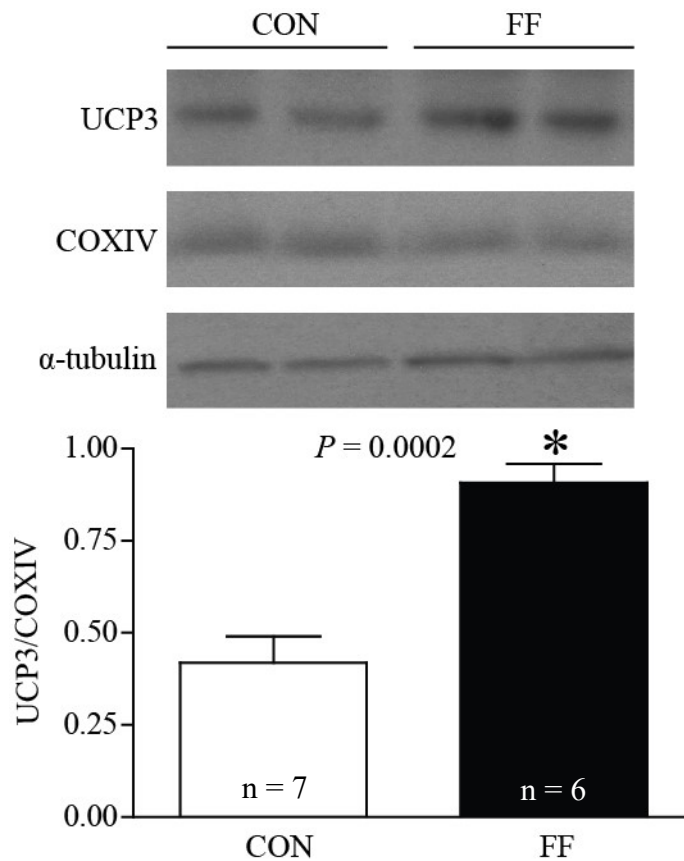


Figure 3.2 UCP3 expression in mitochondria. Protein levels were measured by immunoblotting in total tissue homogenates of hearts of control (CON) and fructose-fed (FF) rats ( $n = 6 - 7$ ) and were normalized to the expression of the mitochondrial marker COXIV, since UCP3 is an exclusively mitochondrial protein. Data are presented as mean  $\pm$  SEM with a significance of  $*P < 0.05$ .

### 3.2.2 Electron Transport System Complex Activities

Another approach to address mitochondrial bioenergetics dysfunction is the measurement of the maximum activity of individual ETS complexes I to IV. While there were no significant OXPHOS

differences between the groups for the TCA cycle and ETS protocols, these protocols revealed a trend toward a higher respiration in crude mitochondrial isolates of hearts of fructose-fed rats (Table 3.1). Consequently, it is possible that moderate changes in the complexes of the ETS were masked by the overall system behaviour. Hence, the activity of each individual ETS complex was determined.

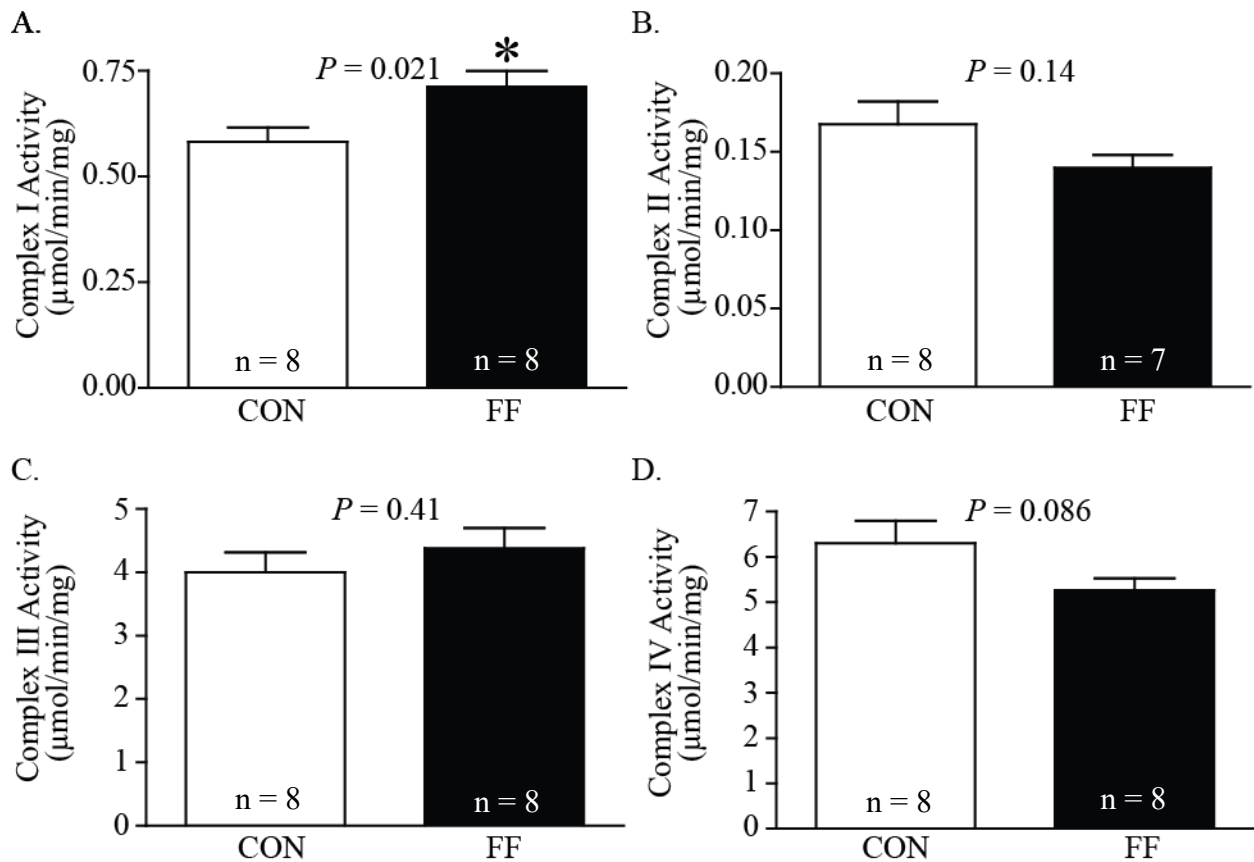


Figure 3.3 ETS complex activities ( $\mu\text{mol}/\text{min}/\text{mg}$ ). Activities were measured spectrophotometrically in crude mitochondrial isolates of hearts of control (CON) and fructose-fed (FF) rats and normalized to protein concentration ( $n = 7 - 8$ ). Data are presented as mean  $\pm$  SEM with a significance of  $*P < 0.05$ .

Complex I activity was higher in hearts of fructose-fed rats ( $0.58 \pm 0.03 \mu\text{mol}/\text{min}/\text{mg}$  vs.  $0.71 \pm 0.04 \mu\text{mol}/\text{min}/\text{mg}$ ,  $P = 0.021$ ; Figure 3.3A). There were no notable differences between the groups for the activities of complexes II ( $0.16 \pm 0.02 \mu\text{mol}/\text{min}/\text{mg}$  vs.  $0.14 \pm 0.01 \mu\text{mol}/\text{min}/\text{mg}$ ,  $P =$

0.14; Figure 3.3B), III ( $4.00 \pm 0.31 \mu\text{mol}/\text{min}/\text{mg}$  vs.  $4.38 \pm 0.32 \mu\text{mol}/\text{min}/\text{mg}$ ,  $P = 0.41$ ; Figure 3.3C), and IV ( $6.30 \pm 0.50 \mu\text{mol}/\text{min}/\text{mg}$  vs.  $5.27 \pm 0.26 \mu\text{mol}/\text{min}/\text{mg}$ ,  $P = 0.086$ ; Figure 3.3D).

### 3.3 Increased Mitochondrial Fatty Acid Oxidation

#### 3.3.1 Mitochondrial Fatty Acid Uptake

High-resolution respirometry measurements (section 3.2.1) indicate increased mitochondrial fatty acid oxidation. Since all FAO protocols included malate (Table 2.1), electrons entered the ETS via complex I. Thus, we verified that the OXPHOS increase that was observed with the PalCoA and OctCar protocols (Table 3.1) was not due to the increased complex I activity (Figure 3.3A).

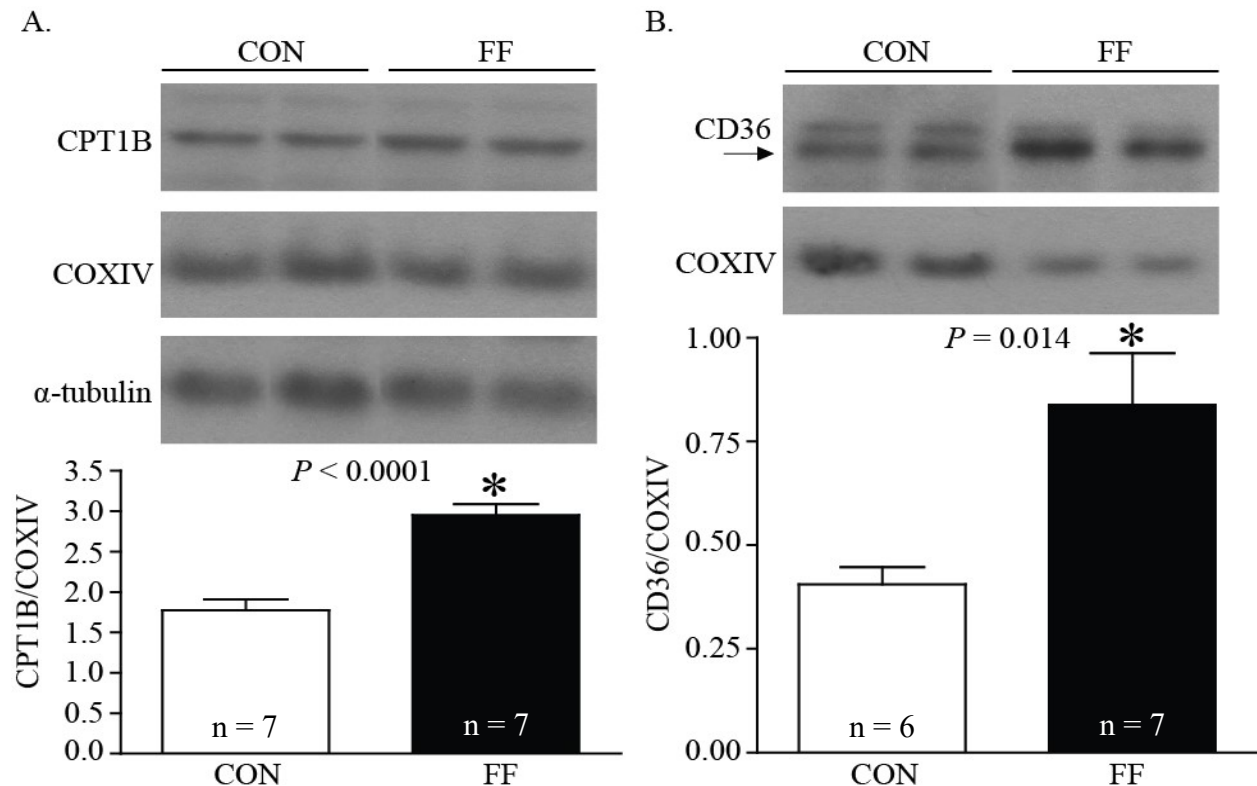


Figure 3.4 CPT1B and mitochondrial CD36 expressions. Protein levels were measured by immunoblotting in (A) total tissue homogenates ( $n = 7$ ) and (B) mitochondrial fractions ( $n = 6 - 7$ ), respectively, of hearts of control (CON) and fructose-fed (FF) rats and were normalized to the expression of the mitochondrial marker COXIV. Data are presented as mean  $\pm$  SEM with a significance of  $*P < 0.05$ .

We detected indications of increased CPT1 expression and/or activity based on the increased OXPHOS with PalCoA but not PalCar (Table 3.1). The role of CPT1 was further investigated to answer the question of whether more long-chain fatty acids could be transported into the mitochondrion, as suggested by the high-resolution respirometry data (Table 3.1).

The expression of CPT1B – the major CPT1 isoform in the heart (Weis et al. 1994) – was increased in hearts of fructose-fed rats ( $1.78 \pm 0.13$  vs.  $2.95 \pm 0.14$ ,  $P < 0.0001$ ; Figure 3.4A). Mitochondrial CD36, which has been postulated to be involved in the regulation of CPT1 and the stimulation of mitochondrial FAO (Holloway et al. 2009), was also more abundantly expressed in hearts of fructose-fed rats ( $0.41 \pm 0.04$  vs.  $0.84 \pm 0.12$ ,  $P = 0.014$ ; Figure 3.4B).

Figure 3.5A shows that the total CPT activity in hearts of fructose-fed rats was not any different from in control hearts. Using a maximum inhibitory concentration of the CPT1 inhibitor malonyl-CoA (10  $\mu$ M), CPT1 activity was lower in hearts of fructose-fed rats ( $5.21 \pm 0.18$   $\mu$ mol/min/mg vs.  $3.00 \pm 0.62$   $\mu$ mol/min/mg,  $P = 0.035$ ; Figure 3.5A). To explain the discrepancy between CPT1 activity (Figure 3.5A), CPT1B protein level (Figure 3.4A), and high-resolution respirometry data (Table 3.1), CPT activity was titrated to increasing concentrations of malonyl-CoA (0.05, 0.1, 0.5, 1, 5, 10, and 1000  $\mu$ M). Consistent with the higher CPT2 activity at 10  $\mu$ M of malonyl-CoA (Figure 3.5A), the CPT activity of the fructose-fed group was consistently higher across all malonyl-CoA concentrations (Figure 3.5C). Thus, the greater  $IC_{50}$  recorded in hearts of fructose-fed rats ( $0.54 \pm 0.15$   $\mu$ M vs.  $1.2 \pm 0.16$   $\mu$ M,  $P = 0.017$ ; Figure 3.5C) indicates a less sensitive CPT inhibition by malonyl-CoA. CPT1's affinity for malonyl-CoA was unchanged in hearts of fructose-fed rats, as indicated by unaltered  $K_i$  values ( $0.78 \pm 0.15$   $\mu$ M vs.  $0.64 \pm 0.09$   $\mu$ M,  $P = 0.47$ ; Figure 3.5D). The lower  $V_{max}$  values pointed to a depressed inhibitable CPT1 ( $61.5 \pm 2.9\%$  vs.  $47.5 \pm 2.4\%$ ,  $P = 0.0032$ ; Figure 3.5D).

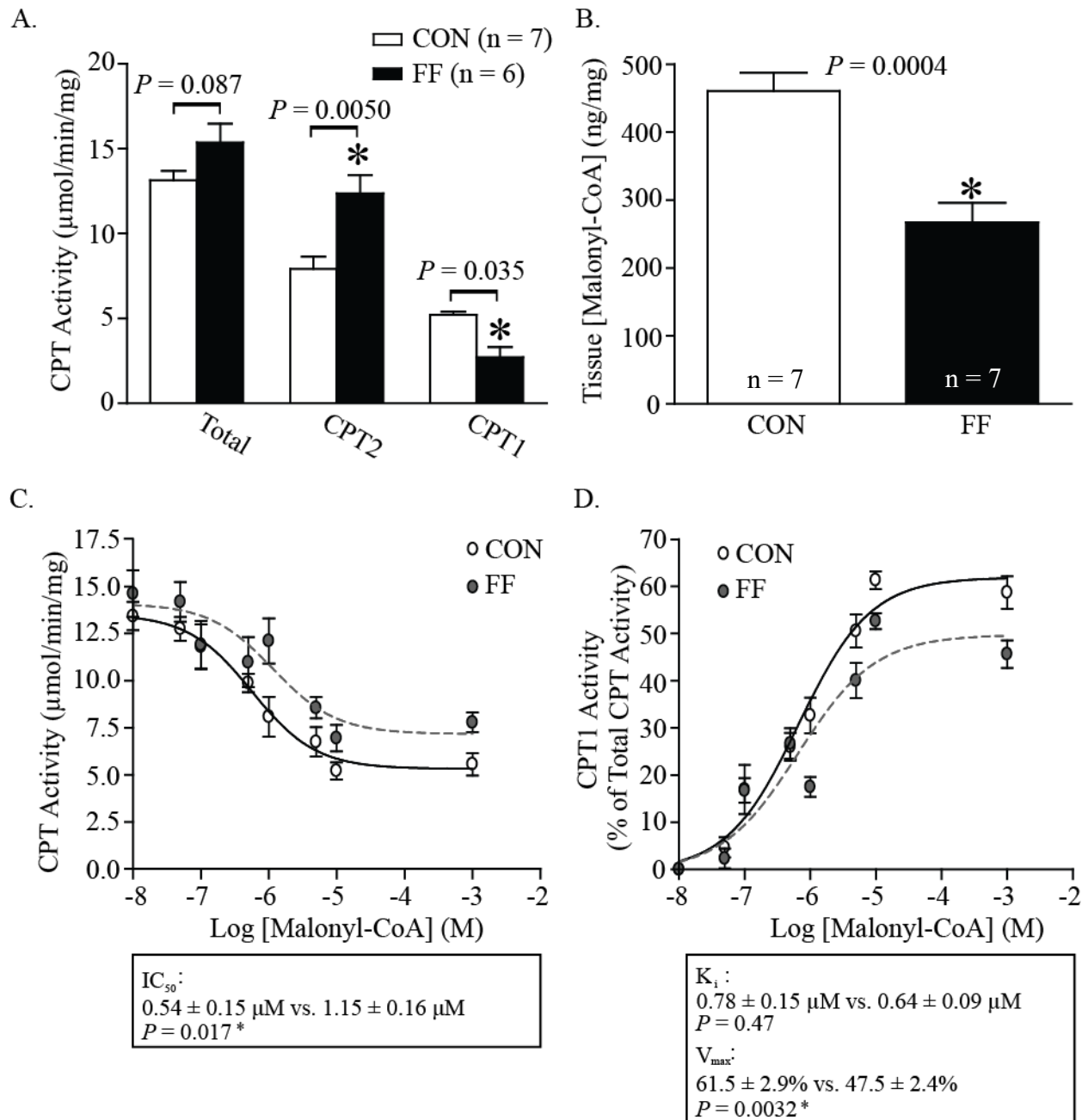


Figure 3.5 CPT activities ( $\mu\text{mol}/\text{min}/\text{mg}$ ) and malonyl-CoA tissue levels (ng/mg). The following data were obtained spectrophotometrically in hearts of control (CON) and fructose-fed (FF) rats. (A) In mitochondrial fractions, the total CPT activity was measured, and CPT1 activity was calculated following the addition of a maximum inhibitory concentration of malonyl-CoA ( $10 \mu\text{M}$ ;  $n = 6 - 7$ ). (B) The concentration of malonyl-CoA was measured in total tissue homogenates ( $n = 7$ ). (C) In mitochondrial fractions, CPT2 activity was measured with increasing malonyl-CoA concentrations ( $0.05, 0.1, 0.5, 1, 5, 10,$  and  $1000 \mu\text{M}$ ;  $n = 4 - 7$ ). (D) The inhibited CPT1 activity was calculated as the difference between the CPT activity prior to the addition of malonyl-CoA and the non-inhibited CPT2 activity at each concentration ( $n = 7$ ). Data were normalized to protein concentration and are presented as mean  $\pm$  SEM with a significance of  $*P < 0.05$ .

The concentrations of malonyl-CoA in total tissue homogenates were determined to get insight into the CPT1-malonyl-CoA dynamics in relation to overall fatty acid uptake despite apparent lower CPT1 activity. Malonyl-CoA was reduced in hearts of fructose-fed rats ( $461 \pm 27$  ng/mg vs.  $267 \pm 28$  ng/mg,  $P = 0.0004$ ; Figure 3.5B). Therefore, despite the lower inhibitable CPT1 (Figure 3.5A), the higher CPT1B expression (Figure 3.4A) coupled with lower malonyl-CoA levels (Figure 3.5B) all indicate higher mitochondrial fatty acid uptake, which is consistent with the high-resolution respirometry data (Table 3.1).

### 3.3.2 $\beta$ -Hydroxyacyl-CoA Dehydrogenase Activity

The increased OXPHOS of the OctCar protocol (Table 3.1) was CPT1-independent. To address the possibility of an augmented FAO capacity in hearts of fructose-fed rats,  $\beta$ HADH activity was examined in crude mitochondrial isolates. The activity of this key FAO enzyme was higher in fructose-fed rats ( $2.97 \pm 0.31$   $\mu\text{mol}/\text{min}/\text{mg}$  vs.  $4.09 \pm 0.33$   $\mu\text{mol}/\text{min}/\text{mg}$ ,  $P = 0.029$ ; Figure 3.6).

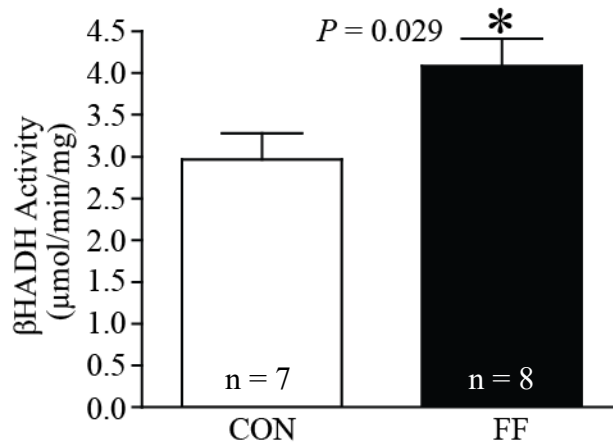


Figure 3.6  $\beta$ HADH activity ( $\mu\text{mol}/\text{min}/\text{mg}$ ). Activity was measured spectrophotometrically in crude mitochondrial isolates of heart of control (CON) and fructose-fed (FF) rats ( $n = 7 - 8$ ). Data were normalized to protein concentration and are presented as mean  $\pm$  SEM with a significance of  $*P < 0.05$ .

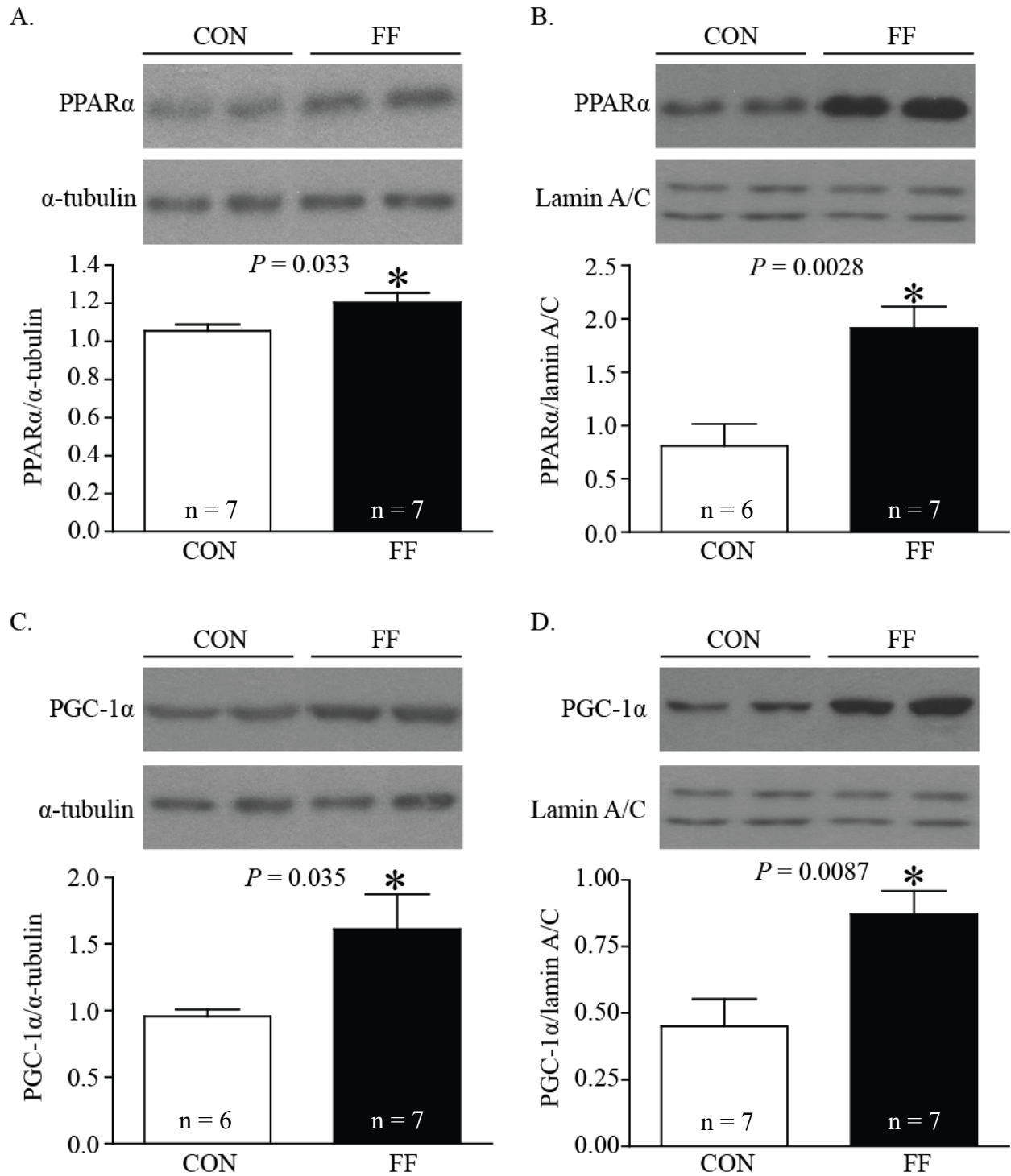


Figure 3.7 Total tissue and nuclear PPAR $\alpha$  and PGC-1 $\alpha$  expressions. The protein levels of (A and B) PPAR $\alpha$  (n = 7 and n = 6 – 7) and (C and D) PGC-1 $\alpha$  (n = 7 and n = 6 – 7) were measured by immunoblotting in (A and C) total tissue homogenates and (B and D) nuclear fractions of hearts of control (CON) and fructose-fed (FF) rats. They were normalized to the expression of  $\alpha$ -tubulin and lamin A/C as cytosolic and nuclear markers, respectively. Data are presented as mean  $\pm$  SEM with a significance of \**P* < 0.05.

### 3.3.3 Regulation of Fatty Acid Oxidation

In accordance with the previously stated findings, hearts of fructose-fed rats showed increased levels of regulatory proteins that promote fatty acid oxidation. The total ( $1.06 \pm 0.03$  vs.  $1.20 \pm 0.05$ ,  $P = 0.033$ ; Figure 3.7A) and nuclear ( $0.81 \pm 0.20$  vs.  $1.91 \pm 0.20$ ,  $P = 0.0028$ ; Figure 3.7B) expressions of the nuclear receptor protein PPAR $\alpha$  were higher in fructose-fed rats. Moreover, the expressions of the transcription co-activator PGC-1 $\alpha$  were increased in total tissue homogenates ( $0.96 \pm 0.05$  vs.  $1.61 \pm 0.26$ ,  $P = 0.035$ ; Figure 3.7C) and nuclear fractions ( $0.45 \pm 0.10$  vs.  $0.87 \pm 0.09$ ,  $P = 0.0087$ ; Figure 3.7D) of hearts of fructose-fed rats. Consistent with an increased PPAR $\alpha$ /PGC-1 $\alpha$  signaling, the heightened cell membrane expression of CD36 ( $0.24 \pm 0.03$  vs.  $0.34 \pm 0.03$ ,  $P = 0.025$ ; Figure 3.8) showed an augmented potential for cellular fatty acid uptake.

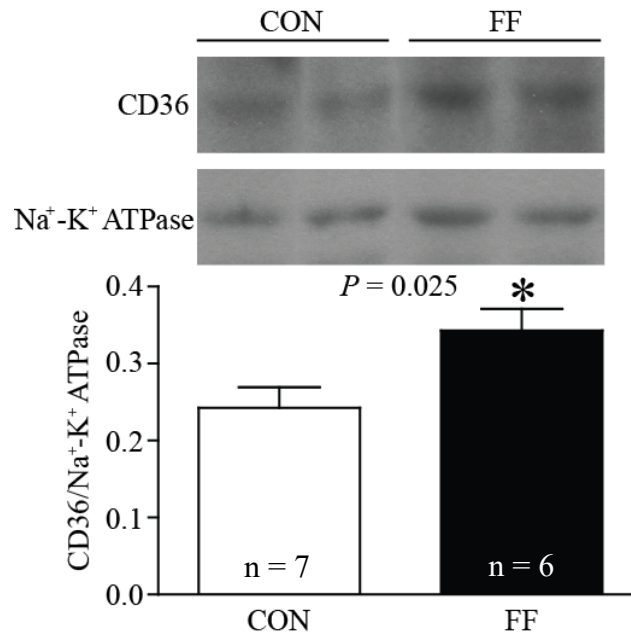


Figure 3.8 Cell membrane CD36 expression. The protein expression of CD36 in cell membrane fractions of hearts of control (CON) and fructose-fed (FF) rats was measured by immunoblotting (n = 6 – 7). Data were normalized to the expression of the cell membrane marker Na<sup>+</sup>-K<sup>+</sup> ATPase and are presented as mean ± SEM with a significance of \* $P < 0.05$ .

As reviewed by Winder and Hardie (1999), AMPK is a well-established metabolic sensor that stimulates FAO in its phosphorylated and activated form. In cytosolic fractions of hearts of fructose-fed rats, the expression of pAMPK $\alpha$  relative to total AMPK $\alpha$  was higher than in the control group ( $1.01 \pm 0.12$  vs.  $1.83 \pm 0.15$ ,  $P = 0.0026$ ; Figure 3.9). This increased proportion of pAMPK $\alpha$  is consistent with the observed reduction in malonyl-CoA tissue concentration (Figure 3.5B): pAMPK inactivates acetyl-CoA carboxylase, reducing malonyl-CoA production (Park et al. 2002).

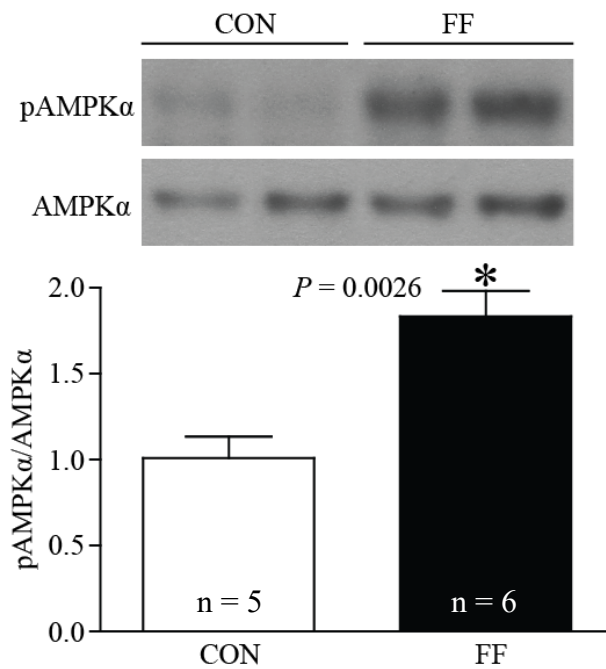


Figure 3.9 Cytosolic pAMPK $\alpha$  expression. Protein levels were measured by immunoblotting in cytosolic fractions of hearts of control (CON) and fructose-fed (FF) rats (n = 5 – 6). Data were normalized to the expression of total AMPK $\alpha$  and are presented as mean  $\pm$  SEM with a significance of  $*P < 0.05$ .

## 3.4 Elevated Oxidative Stress in Mitochondria

### 3.4.1 Markers of Oxidative Stress

As a heightened FAO produces more oxidative stress, oxidative stress was examined in hearts of fructose-fed rats. An increased oxidative stress was demonstrated by several key markers in the absence of a coordinated antioxidant defense response. The activity of aconitase, which is highly sensitive to oxidative stress (Gardner et al. 1994), was reduced in mitochondrial fractions of hearts of fructose-fed rats ( $96.4 \pm 9.4$  nmol/min/mg vs.  $46.1 \pm 4.8$  nmol/min/mg,  $P = 0.0005$ ; Figure 3.10A). Likewise, mitochondrial HNE generated by lipid peroxidation was higher in the fructose-fed group ( $1.28 \pm 0.14$  vs.  $1.83 \pm 0.20$ ,  $P = 0.042$ ; Figure 3.10B).

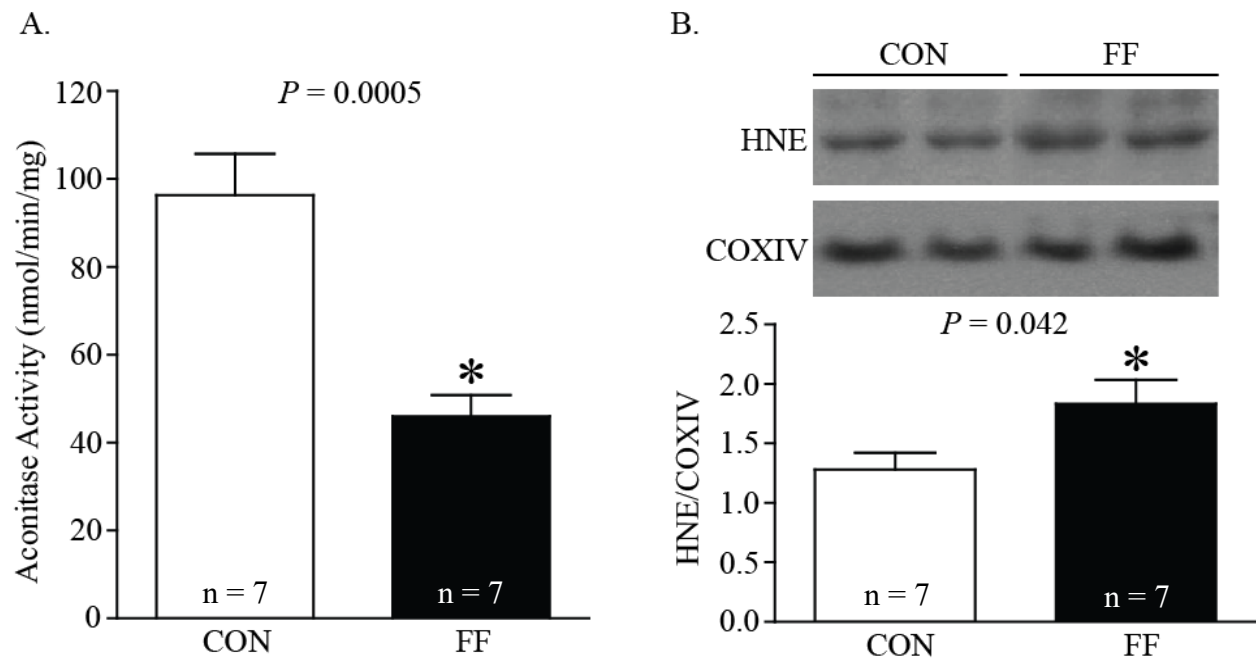


Figure 3.10 Aconitase activity (nmol/min/mg) and mitochondrial HNE expression. The following data were measured in mitochondrial fractions of hearts of control (CON) and fructose-fed (FF) rats. (A) The activity of aconitase was measured spectrophotometrically and normalized to protein concentration ( $n = 7$ ). (B) The levels of mitochondrial HNE were measured by immunoblotting and were normalized to the expression of COXIV ( $n = 7$ ). While the representative blot above depicts the most prominent band, the entire HNE profile including less apparent bands was used for analysis. Data are presented as mean  $\pm$  SEM with a significance of  $*P < 0.05$ .

### 3.4.2 Antioxidant Defenses

The expression of NRF2, an essential regulator of antioxidant responses, was heightened in hearts of fructose-fed rats ( $0.84 \pm 0.08$  vs.  $1.19 \pm 0.10$ ,  $P = 0.021$ ; Figure 3.11). The protein level of TXNRD2 was increased ( $0.21 \pm 0.04$  vs.  $0.51 \pm 0.06$ ,  $P = 0.0011$ ; Figure 3.12E) in mitochondrial fractions of hearts of fructose-fed rats. The expression of COXIV2B, which occurs under sustained metabolic stress to reduce ROS production (Srinivasan and Avadhani 2012), was also augmented in the fructose-fed group ( $0.63 \pm 0.09$  vs.  $1.01 \pm 0.08$ ,  $P = 0.012$ ; Figure 3.12F). Thus, there is activation of the antioxidant defense system in hearts of fructose-fed rats, but it is not sufficient to counteract ROS production.

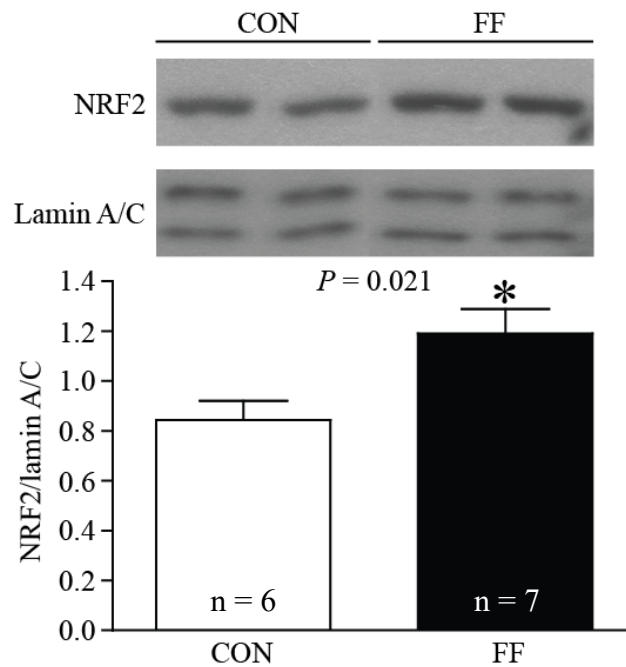


Figure 3.11 Nuclear NRF2 expression. Protein levels were measured by immunoblotting in nuclear fractions of hearts of control (CON) and fructose-fed (FF) rats ( $n = 6 - 7$ ) and were normalized to the expression of nuclear marker lamin A/C. Data are presented as mean  $\pm$  SEM with a significance of  $*P < 0.05$ .

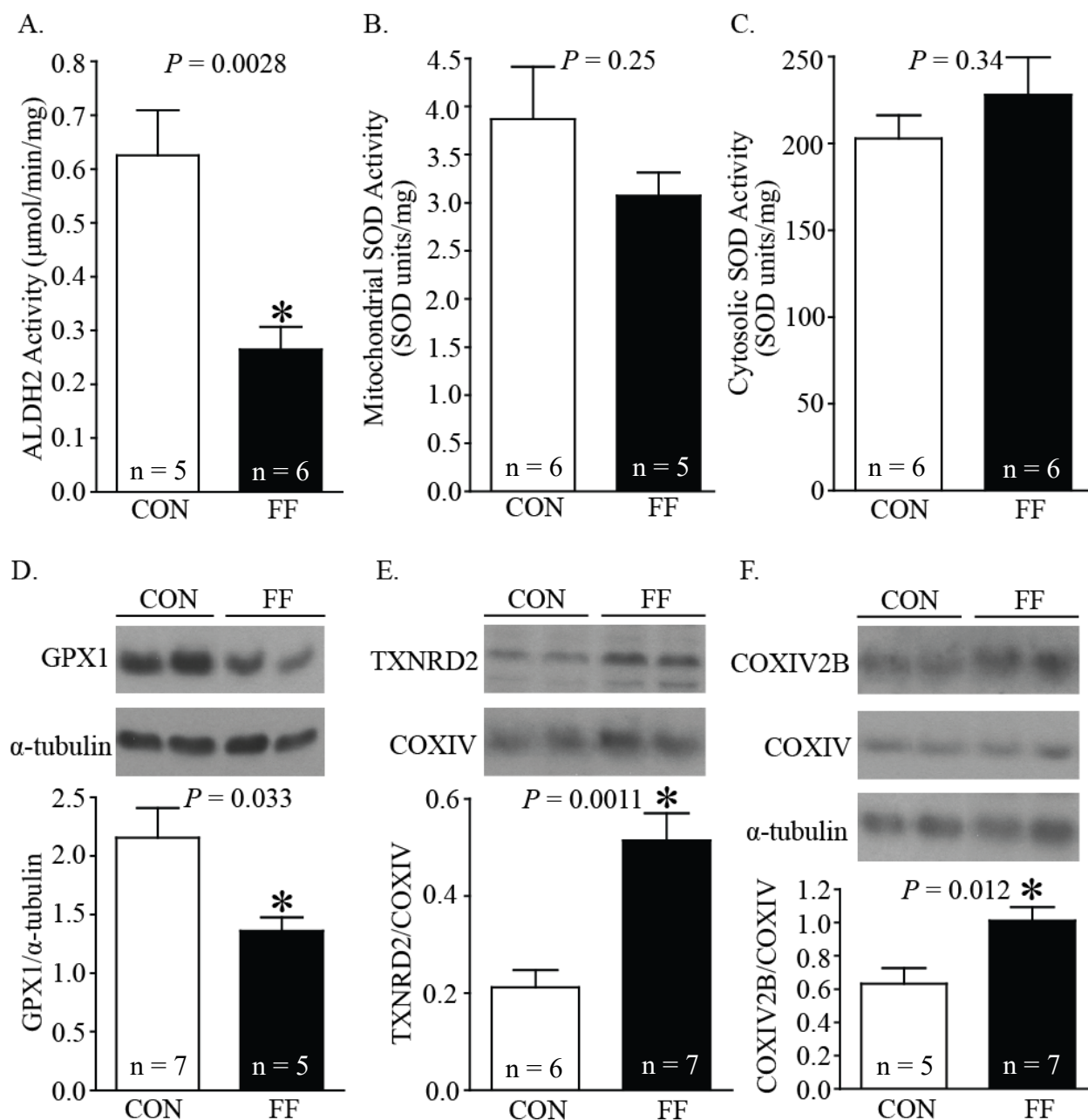


Figure 3.12 Antioxidant protein activities ( $\mu\text{mol}/\text{min}/\text{mg}$ ; SOD units/mg) and expressions. The following data were measured in hearts of control (CON) and fructose-fed (FF) rats. The activities of (A) ALDH2 (n = 5 – 6) and (B) SOD (n = 5 – 6) were measured spectrophotometrically in mitochondrial fractions and normalized to protein concentration. (C) SOD activity was also measured in cytosolic fractions (n = 6). Protein levels were measured by immunoblotting. (D) Total GPX1 (n = 5 – 7) and (F) mitochondrial COXIV2B (n = 5 – 7) were measured in total tissue homogenates and normalized to the cellular marker  $\alpha$ -tubulin and the mitochondrial marker COXIV, respectively. The protein levels of (E) TXNRD2 (n = 6 – 7) were measured in mitochondrial fractions and normalized to COXIV. Data are presented as mean  $\pm$  SEM with a significance of  $*P < 0.05$ .

ALDH2 metabolizes endogenous aldehydic products such as HNE. Yet, the activity of ALDH2 was diminished in mitochondrial fractions of the fructose-fed group ( $0.63 \pm 0.08 \mu\text{mol/mL/min}$  vs.  $0.27 \pm 0.04 \mu\text{mol/mL/min}$ ,  $P = 0.0028$ ; Figure 3.12A), affording less protection against these toxic agents. The expression of GPX1, which detoxifies hydrogen peroxide and lipid peroxides, was less abundant in total tissue homogenates of hearts of fructose-fed rats ( $2.15 \pm 0.26$  vs.  $1.36 \pm 0.11$ ,  $P = 0.033$ ; Figure 3.12D). The SOD activity responsible for the dismutation of superoxide radicals was unchanged in mitochondrial ( $3.87 \pm 0.54$  SOD units/mg vs.  $3.07 \pm 0.24$  SOD units/mg,  $P = 0.25$ ; Figure 3.12B) and cytosolic ( $203.0 \pm 13.2$  SOD units/mg vs.  $228.3 \pm 21.4$  SOD units/mg,  $P = 0.34$ ; Figure 3.12C) fractions of the two groups.

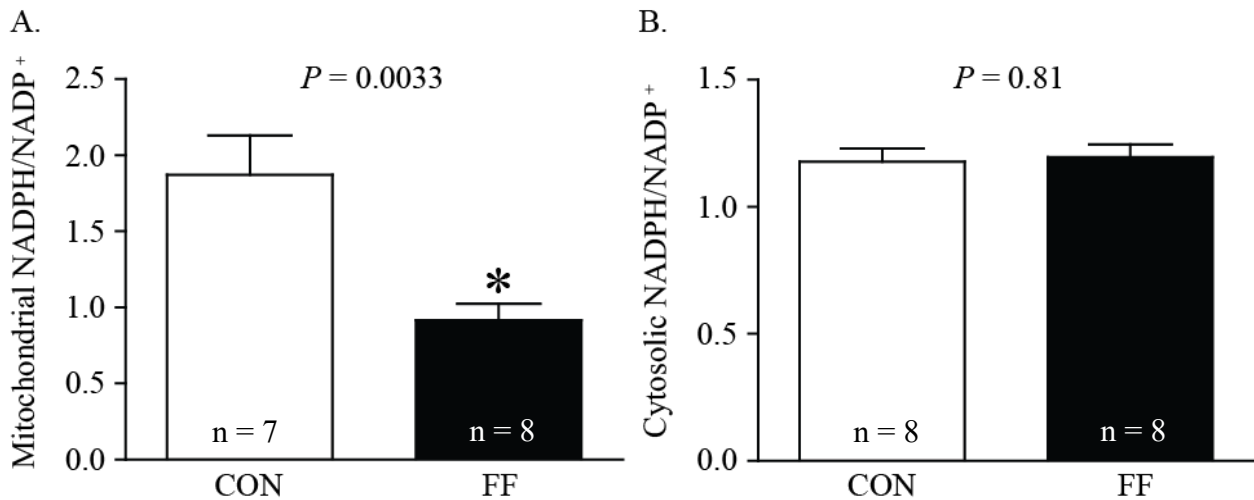


Figure 3.13 Mitochondrial and cytosolic NADPH/NADP<sup>+</sup>. The concentrations of NADPH and NADP<sup>+</sup> were measured spectrophotometrically in (A) mitochondrial (n = 7 – 8) and (B) cytosolic fractions (n = 8) of hearts of control (CON) and fructose-fed (FF) rats. Data are expressed as ratios of NADPH over NADP<sup>+</sup> and are presented as mean  $\pm$  SEM with a significance of \* $P < 0.05$ .

Additionally, the concentrations of NADPH and NADP<sup>+</sup> present in different subcellular fractions were determined, and the NADPH and NADP<sup>+</sup> ratio provides a measure of antioxidant capacity.

In hearts of fructose fed rats, the ratio of NADPH to NADP<sup>+</sup> was lower in mitochondrial ( $1.87 \pm 0.26$  vs.  $0.92 \pm 0.11$ ,  $P = 0.0033$ ; Figure 3.13A) but not cytosolic ( $1.18 \pm 0.05$  vs.  $1.20 \pm 0.05$ ,  $P =$

0.81; Figure 3.13B) fractions.

## 3.5 SIRT1 and SIRT3 Signaling

### 3.5.1 SIRT1 and SIRT3 Expressions

Sirtuins are  $\text{NAD}^+$ -dependent protein deacetylases that mediate adaptive responses to metabolic and oxidative stresses via deacetylation (Nemoto et al. 2004; Someya et al. 2010). To elucidate the interplay of enzymes and metabolic signaling involved in the changes observed in hearts of fructose-fed rats, the expressions of SIRT1 and SIRT3 were measured. There was an increased expression of SIRT1 in nuclear fractions ( $0.43 \pm 0.06$  vs.  $0.61 \pm 0.03$ ,  $P = 0.018$ ; Figure 3.14A) and SIRT3 in mitochondrial fractions ( $0.23 \pm 0.03$  vs.  $0.47 \pm 0.04$ ,  $P = 0.0004$ ; Figure 3.14B).

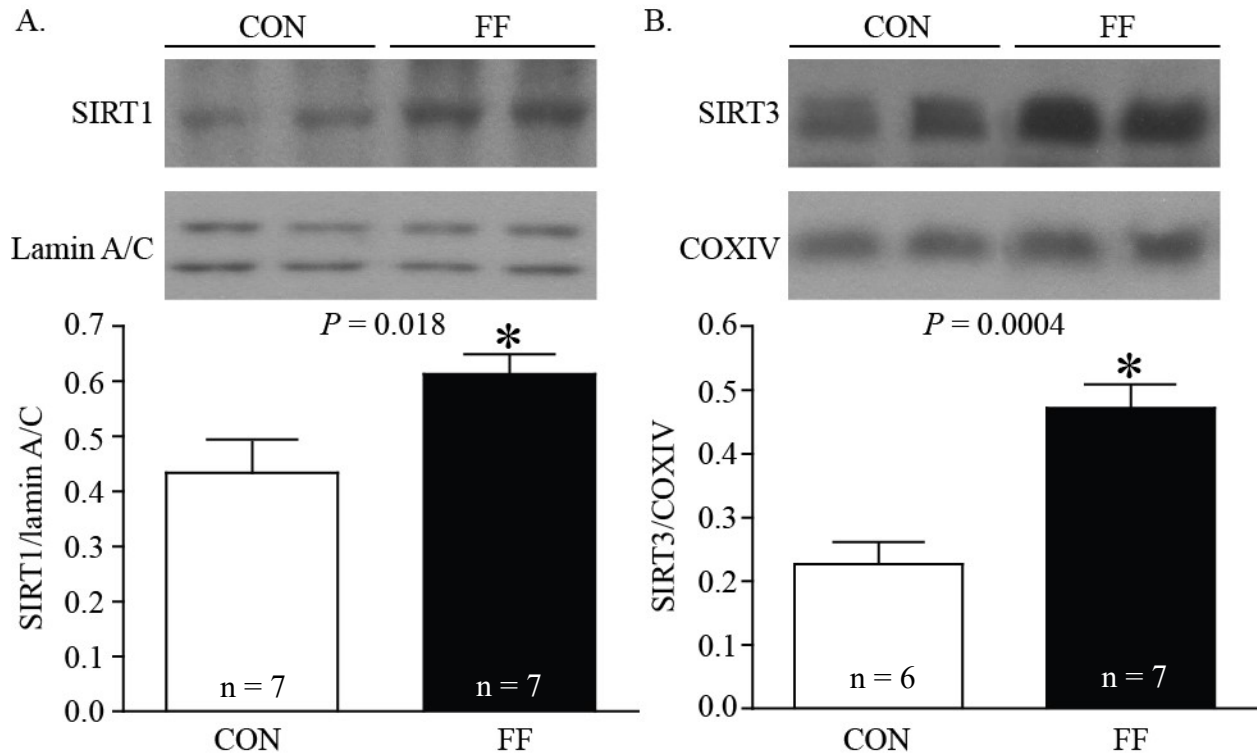


Figure 3.14 Nuclear SIRT1 and mitochondrial SIRT3 expressions. The protein levels of (A) SIRT1 ( $n = 7$ ) was measured in nuclear fractions and (B) SIRT3 ( $n = 6 - 7$ ), in mitochondrial fractions from hearts of control (CON) and fructose-fed (FF) rats by immunoblotting and were normalized to the expression of the nuclear marker lamin A/C and the mitochondrial marker COXIV, respectively. Data are presented as mean  $\pm$  SEM with a significance of  $*P < 0.05$ .

### 3.5.2 NAD<sup>+</sup>/NADH Levels

The concentrations of the sirtuin activator NAD<sup>+</sup> and the sirtuin inhibitor NADH were measured in cellular compartments to explain the level of sirtuin activation. The mitochondrial ( $0.62 \pm 0.10$  vs.  $1.22 \pm 0.19$ ,  $P = 0.016$ ; Figure 3.15A) and cytosolic ( $1.00 \pm 0.13$  vs.  $1.64 \pm 0.10$ ,  $P = 0.0034$ ; Figure 3.15B) ratios of NAD<sup>+</sup> to NADH concentrations were greater in hearts of fructose-fed rats. No difference was noted in nuclear fractions ( $0.31 \pm 0.05$  vs.  $0.43 \pm 0.06$ ,  $P = 0.13$ ; Figure 3.15C), suggesting that nuclear SIRT1 may not be active.

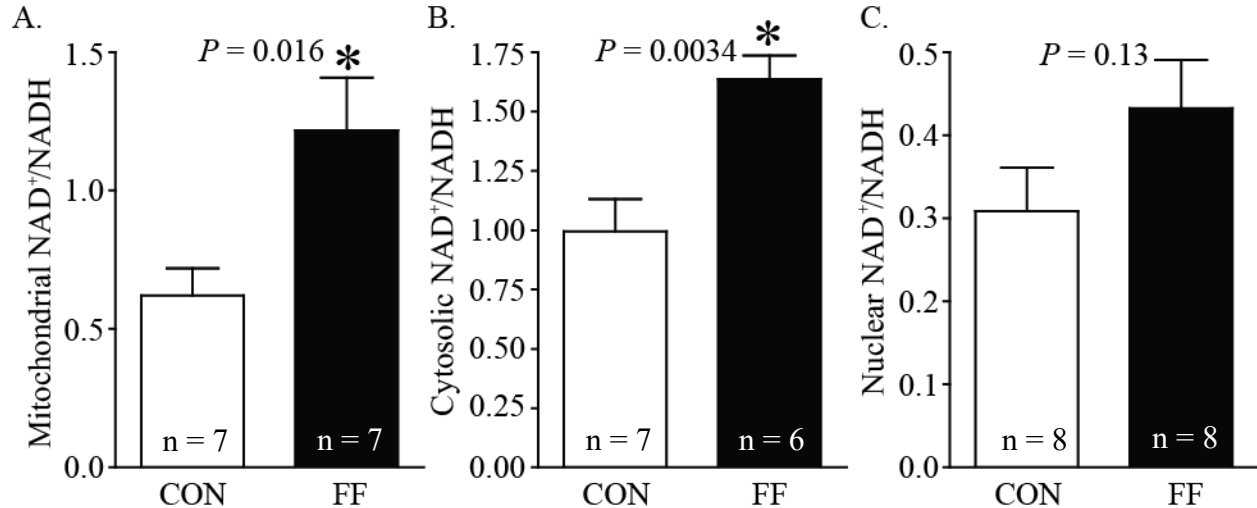


Figure 3.15 Mitochondrial, cytosolic, and nuclear NAD<sup>+</sup>/NADH. The concentrations of NAD<sup>+</sup> of NADH were measured spectrophotometrically in (A) mitochondrial (n = 7), (B) cytosolic (n = 6 – 7), and (C) nuclear (n = 8) fractions from hearts of control (CON) and fructose-fed (FF) rats. Data are expressed as ratios of NAD<sup>+</sup> over NADH and are presented as mean  $\pm$  SEM with a significance of \* $P < 0.05$ .

### 3.6 Evidence of Decreased Mitochondrial Content

Lower mitochondrial content is a possible cause for metabolic dysfunction. In this study, the mitochondrial content of hearts of control and fructose-fed rats was determined by two distinct methods. First, the activity of citrate synthase was measured ( $0.96 \pm 0.03$   $\mu\text{mol}/\text{min}/\text{mg}$  vs.  $0.81 \pm$

0.02  $\mu\text{mol}/\text{min}/\text{mg}$ ,  $P = 0.0025$ ; Figure 3.16A). The second method consisted of the comparison of the expression of the mitochondrial enzyme COXIV ( $0.27 \pm 0.03$  vs.  $0.19 \pm 0.01$ ,  $P = 0.020$ ; Figure 3.16B). The mitochondrial content as tested by these methods was decreased in hearts of fructose-fed rats.

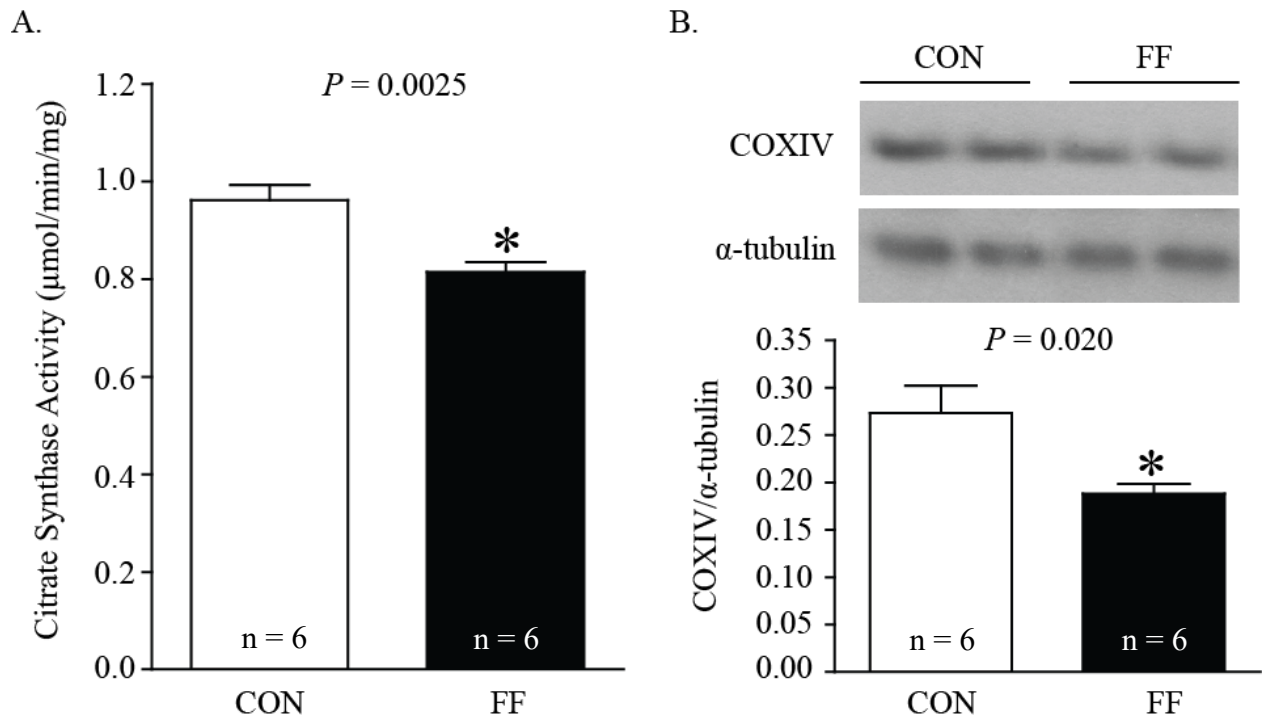


Figure 3.16 Citrate synthase activity ( $\mu\text{mol}/\text{min}/\text{mg}$ ) and total COXIV expression. (A) The activity of citrate synthase was measured spectrophotometrically in total tissue homogenates of hearts of control (CON) and fructose-fed (FF) rats ( $n = 6$ ). It was normalized to protein concentration. (B) The protein expression of COXIV in total tissue homogenates was measured by immunoblotting ( $n = 6$ ). It was normalized to the expression of  $\alpha$ -tubulin. Data are presented as mean  $\pm$  SEM with a significance of  $*P < 0.05$ .

Based on our assessment of upstream signaling molecules involved in mitochondrial biogenesis, we investigated the expression of the mitochondrial transcription factor TFAM. PGC-1 $\alpha$  coactivates NRF2, which mediates the expression of TFAM. We observed the upregulation of total and nuclear PGC-1 $\alpha$  (Figure 3.7C; Figure 3.7D) and NRF2 in nuclear fractions (Figure 3.11). However, the levels of the TFAM were not significantly changed in total tissue homogenate ( $0.67$

$\pm 0.06$  vs.  $0.72 \pm 0.05$ ,  $P = 0.52$ ; Figure 3.17A) and mitochondrial fractions ( $0.44 \pm 0.05$  vs.  $0.55 \pm 0.04$ ,  $P = 0.14$ ; Figure 3.17B).

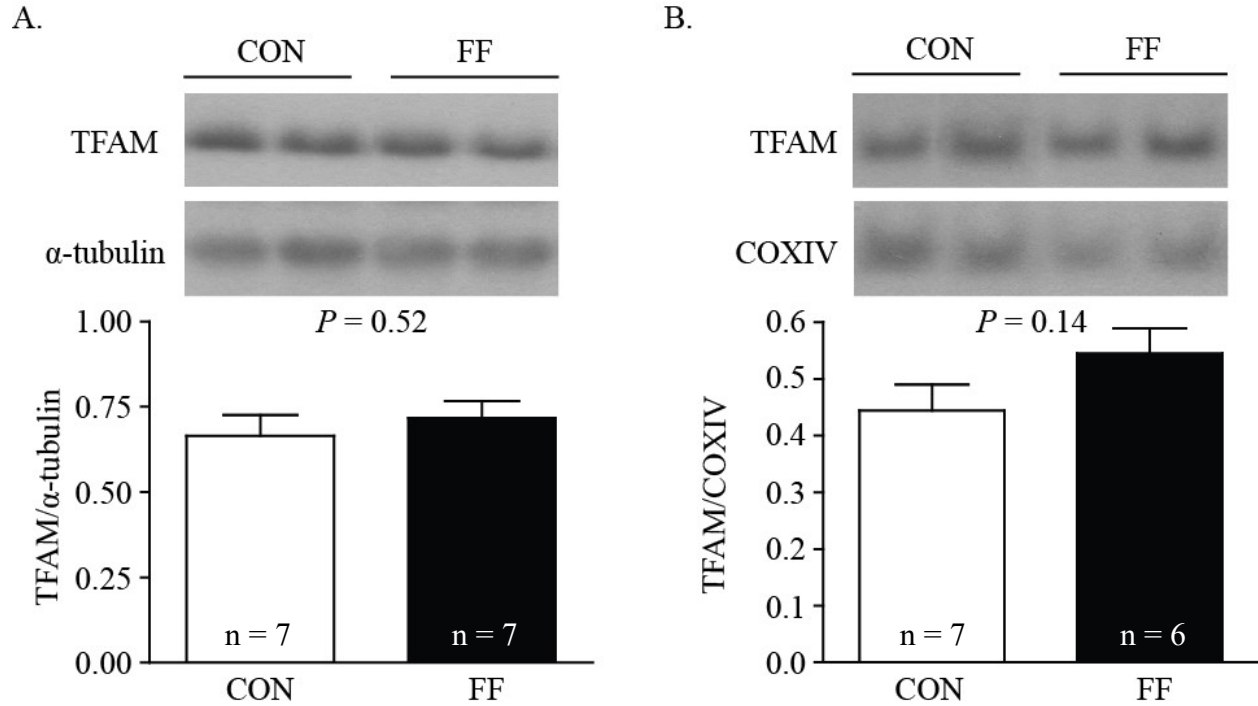


Figure 3.17 Total and mitochondrial TFAM expressions. The protein levels of TFAM in (A) total tissue homogenates (n = 7) and (B) mitochondrial fractions (n = 6 – 7) were measured by immunoblotting. They were normalized to the expressions of the cellular marker  $\alpha$ -tubulin and the mitochondrial marker COXIV, respectively. Data are presented as mean  $\pm$  SEM with a significance of  $*P < 0.05$ .

## Chapter 4

# Discussion

### 4.1 Impaired Glucose Oxidation and Insulin Resistance

The diabetic traits of the fructose-fed rat have been thoroughly described by our laboratory (Chapter 1). This model has been found to exhibit elevated fasting glucose, triglyceride, and insulin blood levels consistent with type-2 diabetes (Lou et al. 2015). Moreover, the use of the glucose tolerance and insulin sensitivity tests has confirmed total body insulin resistance (Lou et al. 2015). Insulin resistance was further detected in hearts of fructose-fed rats through a decreased insulin-stimulated rate of glucose uptake (Lou et al. 2015). Although these measurements were not repeated in the rats employed for the current study, insulin resistance was indirectly verified in hearts of fructose-fed rats through the dysregulation of the PDH complex (reviewed by Constantin-Teodosiu 2013).

The PDH complex bridges the cytosolic processes of glycolysis with the mitochondrial metabolic steps of glucose oxidation. Thus, the PDH complex acts as a central regulator of the competition between the oxidation of glucose and fatty acids. The PDH complex is activated by the glycolytic intermediate fructose-1,6-bisphosphate and by pyruvate dehydrogenase phosphatase-mediated dephosphorylation. It is predominantly inhibited by acetyl-CoA and NADH from FAO and by PDK-mediated phosphorylation. In the context of insulin resistance, myocytes rely even more on fatty acids as energetic fuels because glucose oxidation is impaired. Increased levels of fatty acids

and FAO intermediates exert negative feedback on the PDH complex (Randle et al. 1963). Therefore, the reduced PDH complex activity that we measured in hearts of fructose-fed rats is a clear indication of cardiac insulin resistance and a hallmark of diabetic metabolism. High-resolution respirometry did not detect differences in the PM protocol, but this may be due to the fact that control of mitochondrial OXPHOS under the measurement conditions is not determined by the PDH complex activity alone.

A system's ability to adapt to the fluctuating availability of energetic fuels is termed metabolic flexibility. As reviewed by Zhang et al. (2014), metabolic flexibility is largely dependent on the suppression of PDH complex activity by the four PDK isoforms. PDK2 and PDK4 are both abundantly expressed in the heart (Bowker-Kinley et al. 1998). However, PDK4 has a greater regulatory activity (Bowker-Kinley et al. 1998). Wu et al. (1998) found that conditions causing a further metabolic shift from glucose to fatty acids, such as diabetes or starvation, enhance the expression of PDK4 in rat hearts. In addition, dysregulation of PDK4 expression was identified in association with insulin resistance in rat skeletal muscle (Kim et al. 2006). Hence, it appears that the increased expression of PDK4 in hearts of fructose-fed rats is an important cause of the compromised capacity for fuel selection resulting in insulin resistance (Kelley and Mandarino 2000).

Various signaling pathways are known to contribute to the increased expression of PDK4 in insulin resistant tissues. In the presence of high free fatty acids, forkhead box class O transcription factor 1 (FOXO1) and the nuclear receptor protein PPAR $\alpha$  signal the upregulation of PDK4 (Constantin-Teodosiu et al. 2012). Furthermore, the transcription factor estrogen related receptor  $\alpha$  (ERR $\alpha$ ) has been shown to activate the expression of PPAR $\alpha$  and PGC-1 $\alpha$  (Huss et al. 2004). Araki and Motojima (2006) revealed that the transcription co-activator PGC-1 $\alpha$  is recruited to the PDK4

promoter by  $ERR\alpha$ , which further stimulates the expression of PDK4. While we did not investigate FOXO1 and  $ERR\alpha$ , we observed the increased expression of  $PPAR\alpha$  and  $PGC-1\alpha$  in total tissue homogenates as well as nuclear fractions of hearts of fructose-fed rats, indicating the significance of these signaling pathways in the development of loss of metabolic flexibility and insulin resistance.

## 4.2 Mitochondrial Electron Transport System Function

In spite of the increased complex I activity, OXPHOS is not significantly affected in hearts of fructose-fed rats. This is not surprising as respiration is ultimately dependent on various potentially rate-limiting transporters, complexes, and enzymes. Moreover, the unchanged LEAK implies efficient coupling of substrate oxidation to oxidative phosphorylation. Hence, the examination of the ETS suggests that mitochondrial function is uncompromised. This conclusion is in contrast with other studies of diabetic tissues that report: (i) decreased activity of one or more complexes of the ETS (Kelley et al. 2002; Ritov et al. 2005; Rosca et al. 2005; Anderson et al. 2009a; Croston et al. 2014; Montaigne et al. 2014), (ii) increased leak/uncoupling activity (Boudina et al. 2007; Friederich et al. 2008), and/or (iii) reduced efficiency of ATP production capacity based on respiratory control or phosphate to oxygen ratios with particular substrates (Mogensen et al. 2007; Montaigne et al. 2014).

The early stage of diabetes is likely responsible for the observed differences between our findings and other studies. Several lines of evidence support the role of mitochondrial dysfunction in the pathogenesis of insulin resistance and/or type-2 diabetes (reviewed by Sivitz and Yorek 2010). Nevertheless, it remains to be established whether mitochondrial dysfunction represents a cause or a consequence of diabetes. As the characteristics of the rat after six weeks of fructose-feeding

are consistent with an early stage of type-2 diabetes (Dai and McNeill 1995), the respiratory states measured in this model represent mitochondrial capacity and function at an early time point that precedes the advanced disease state of type-2 diabetic patients. On the other hand, the studies cited above were conducted in the context of advanced diabetes where impairments in oxidative metabolism may be consequences of the decompensated metabolism due to impaired insulin signaling.

### **4.3 Mitochondrial Fatty Acid Oxidation**

FAO consists of the mitochondrial breakdown of fatty acids to  $C_2$ -bodies, i.e. acetyl-CoA, which subsequently enters the TCA cycle. Normally, approximately seventy per cent of the energy utilized by the heart is derived from this metabolic pathway (reviewed by Neely and Morgan 1974). As described in section 4.1, diabetes induces a loss of metabolic flexibility characterized by a dependence of approximately ninety per cent on FAO (reviewed by Carley and Severson 2005). Indeed, this is the case in hearts of fructose-fed rats based on the following indications:

(i) Increased cellular fatty acid uptake:

The expression of sarcolemmal CD36 is more abundant in hearts of fructose-fed rats. Ibrahimi et al. (1999) have reported the rate-limiting nature of cellular fatty acid uptake by sarcolemmal CD36 and its importance for FAO in contracting mouse skeletal muscle. As demonstrated by Holloway et al. (2010) in the skeletal muscle of diabetic rats, the expression of CD36 is increased in correlation with nuclear PGC-1 $\alpha$  and PPAR $\alpha$ . Increased sarcolemmal CD36 has been previously reported in the heart of obese Zucker rats (Coort et al. 2004).

(ii) Increased mitochondrial fatty acid uptake:

High-resolution respirometry identified the mitochondrial long-chain fatty acyl-CoA uptake by CPT1 as the cause of the augmented OXPHOS recorded in the PalCoA protocol of the fructose-fed group. As reviewed by Kerner and Hoppel (2000), CPT1 is the rate-limiting enzyme of mitochondrial FAO. The increased expression of the primary cardiac isoform CPT1B (Weis et al. 1994), as observed in hearts of fructose-fed rats, was anticipated based on the augmented total and nuclear levels of PPAR $\alpha$  and PGC-1 $\alpha$  in the fructose-fed group (Brandt et al. 1998; Mascaró et al. 1998; Yu et al. 1998). The expressions of other isoforms A and C were not measured. However, an epigenomic study by Hidalgo et al. (2014) has suggested that an abundance of CPT1A is associated with type-2 diabetes. There was also a more abundant mitochondrial expression of CD36, which has been suggested to contribute to the regulation of CPT1 and the stimulation of mitochondrial FAO (Holloway et al. 2009). Although the mechanisms of its actions are not yet clear, mitochondrial CD36 interacts with CPT1 to augment FAO (Campbell et al. 2004; Holloway et al. 2006; Schenk and Horowitz 2006). Moreover, the tissue concentrations of the CPT1 inhibitor malonyl-CoA were reduced in our study of hearts of fructose-fed rats. This adheres to the concept of AMPK regulation of FAO, whereby an increase in pAMPK $\alpha$  reduces the production of malonyl-CoA via inhibition of acetyl-CoA carboxylase (Park et al. 2002). Similar reductions in malonyl-CoA were observed in the liver of diabetic rats (McGarry et al. 1978). In contrast, CPT activity in hearts of fructose-fed rats was less sensitive to inhibition by malonyl-CoA, as revealed by the higher IC<sub>50</sub> values. The disconnect between CPT1 levels and activity is not unusual as CPT1 activity is dependent on its inhibition and sensitivity to malonyl-CoA. Cook and Gamble (1987) have previously reported a lack of inhibition of CPT1 by malonyl-CoA in diabetic rat liver mitochondria in spite of a relatively higher total CPT activity. Together, the increased protein

expression of CPT1B, the reduced sensitivity of CPT to its inhibitor malonyl-CoA, and the decreased tissue presence of this inhibitor are consistent with the augmented uptake of long-chain fatty acyl-CoAs in cardiac mitochondria of fructose-fed rats.

(iii) Increased capacity for FAO:

Furthermore, a higher OXPHOS was measured for the OctCar protocol of the fructose-fed group. As octanoylcarnitine is a medium-chain acylcarnitine, this increased respiration was unrelated to changes in CPT1 expression, activity, or regulation. The oxidation of octanoylcarnitine depends on  $\beta$ HADH, a rate-limiting family of key FAO enzymes (Fong and Schulz 1978). Our experiments clearly demonstrate an elevated total  $\beta$ HADH activity in hearts of fructose-fed rats.

Previous studies of the late stage diabetic human heart have identified FAO as defective. Anderson et al. (2009a) and Montaigne et al. (2014) observed a decreased maximal fatty acid respiration in atrial appendages of patients suffering from long-term type-2 diabetes. By examining mitochondrial populations isolated from atrial appendages of type-2 diabetics, Croston et al. (2014) attributed this deficiency to subsarcolemmal mitochondria. However, models reflecting earlier stages of type-2 diabetes, namely those induced by high fat and sucrose/fructose feeding, show increased FAO in diabetic hearts (Gupte et al. 2013; Harmancey et al. 2012; Mansor et al. 2013; Pellieux et al. 2012). Collectively, these studies recognize FAO in the heart as increased in early stages and decreased in late stages of diabetes, depending on the progression and severity of the disease state.

## **4.4 Oxidative Stress and Antioxidant Response**

Free radicals are highly reactive species containing oxygen or nitrogen. The controlled regulation of endogenous free radicals is essential in maintaining normal cellular functions, such as signaling,

apoptosis, and ATP production. Nevertheless, damaging conditions of oxidative stress are produced when antioxidant defenses are unable to regulate levels of free radicals. The exogenous supply or the endogenous overproduction of free radicals causes several disease states and cellular ageing (reviewed by Finkel and Holbrook 2000).

Mitochondria are the main source of ROS production (reviewed by Turrens 2003). Diabetes has been found to favour oxidative stress in various tissues through the generation of free radicals, mainly in mitochondria (Chang et al. 1993; Dandona et al. 1996; Young et al. 1995), and the weakening of antioxidant defenses (McLennan et al. 1991; Saxena et al. 1993). Oxidative stress has been reported in the brain (Cheng et al. 2013), the kidneys (Bagul et al. 2015), and the heart (Padiya et al. 2014) of fructose-fed rats. Complex I and complex III are regarded as the primary sites of mitochondrial ROS production (Kwong and Sohal 1998).

However, Rosca et al. (2012) have reported that increased FAO and not the ETS itself promotes ROS production via electron leakage during the electron transfer from acyl-CoA to ubiquinol in kidney cells of early diabetic rats. Excess reducing equivalents, i.e. NADH and FADH<sub>2</sub>, provided by enhanced FAO will increase the reduction potential within the ETS complexes, thereby increasing the probability of electrons leaking to form superoxides (reviewed by Fisher-Wellman and Neuffer 2012). This situation could be worsened by an enhanced complex I activity in the absence of any corresponding increase in downstream complex activities. According to the hypothesis of Speijer (2011), FAO causes an increase in the FADH<sub>2</sub> to NADH ratio of electron flux, subsequently favouring reduced ubiquinol to oxidized ubiquinone; the scarcity of the electron acceptor ubiquinone is conducive to ROS generation. Superoxide production can also occur at complex III due to a high electron pressure (Boveris and Chance 1973).

Consistent with increased FAO, markers of oxidative stress were detected in hearts of fructose-fed rats. The activity of the ROS-sensitive TCA cycle enzyme aconitase (Gardner et al. 1994) was markedly compromised in hearts of fructose-fed rats. Furthermore, the elevated production of mitochondrial HNE indicates increased lipid peroxidation in mitochondria (Riahi et al. 2010). These findings demonstrate that the mitochondrion is an important site of ROS production in hearts of fructose-fed rats.

Key antioxidant defenses were investigated to assess cellular responses to these circumstances. Under conditions of oxidative stress, NRF2 is translocated to the nuclei to induce the expression of genes involved in antioxidant response (reviewed by Motohashi and Yamamoto 2004). Accordingly, increased levels of NRF2 were measured in nuclear fractions of hearts of fructose-fed rats. Moreover, the transcription factor NRF2, which was increased in hearts of fructose-fed rats in our experiments, has been shown to be involved in the upregulation of sarcolemmal CD36 expression in murine macrophages under conditions of oxidative stress (Ishii et al. 2004). Intriguingly, the activity of ALDH2, a mitochondrial enzyme responsible for the detoxification of HNE that is upregulated by NRF2 (reviewed by Siow et al. 2007), was decreased in hearts of fructose-fed rats.

The activity of SOD, which dismutates superoxide radicals into hydrogen peroxide and oxygen, was unchanged in mitochondrial and cytosolic fractions. This is noteworthy as the expression of SIRT3, which deacetylates and activates SOD2 (Qui et al. 2010), was increased in mitochondria of fructose-fed rat hearts. GPX1 also contributes to the detoxification of mitochondrial and cytosolic hydrogen peroxide. However, the total expression of this protein was diminished in hearts of fructose-fed rats. On the other hand, the expression of the mitochondrial ROS scavenger TXNRD2 was increased.

Furthermore, NADPH was examined as a measure of antioxidant capacity. NADPH is primarily produced by the pentose phosphate cycle. It is a key source of reducing equivalents for the replenishment of antioxidant proteins, such as TXNRD2 and glutathione disulfide (GSH). In fact, NADPH is the coenzyme of glutathione reductase, which reduces glutathione disulfide to the antioxidant glutathione. Kirsch and de Groot (2001) have proposed that NADPH directly scavenges radicals in mitochondria. In our study, NADPH concentrations were measured in mitochondrial and cytosolic fractions. The decreased ratio of NADPH to  $\text{NADP}^+$  in mitochondrial fractions of fructose-fed rat hearts testifies to the reduced potential of multiple antioxidant systems. It could also be related to an increased activity of nicotinamide nucleotide transdehydrogenase (NNT) in the inner mitochondrial membrane. In fact, NNT mutations have been associated with oxidative stress and impaired insulin secretion (reviewed by Freeman et al. 2006). Notably, the cytosolic NADPH to  $\text{NADP}^+$  ratio was unchanged in the fructose-fed group.

We also tested whether oxidative stress would lead to adaptive changes in the expression of complex IV subunit 2B because it is known to decrease ROS production under stress by increasing complex IV activity and reducing electron backlog in the ETS (reviewed by Srinivasan and Avadhani 2012). Complex IV activity was not affected in hearts of fructose-fed rats. Yet, the expression of COXIV2B was increased, representing a marker of metabolic stress. Collectively, despite a markedly enhanced oxidative stress, the antioxidant system that we examined in hearts of fructose-fed rats consisted solely of the upregulated expression of TXNRD2 and inconsequential adaptive changes in complex IV subunits.

A point of ambiguity exists within our findings at the level of mitochondrial uncoupling. The expression of UCP3 is possibly upregulated by NRF2 (Anedda et al. 2013) and PPAR $\alpha$  (Young et al. 2001), which could result in proton leak across the inner mitochondrial membrane and minimize

ROS production through a lower membrane potential. However, we were not able to detect uncoupling in isolated mitochondria using high-resolution respirometry. It is possible that some uncoupling information in our measurements was masked by concomitant changes in the mitochondrial membrane potential, which were not controlled for in this study. The high-resolution respirometry results may also suggest that UCP3 is carrying out functions other than uncoupling in this model. In fact, a growing body of evidence has established UCP3's involvement in the extrusion of lipid peroxides (Goglia and Skulachev 2003) and fatty acids from the mitochondrial matrix (Schrauwen et al. 2001).

## **4.5 Sirtuin Signaling**

Sirtuins are sensors of the cellular energy state that control essential adaptive responses by promoting metabolic stress resistance via the deacetylation of lysine residues of transcriptional regulators as well as metabolic and antioxidant enzymes (reviewed by Nogueiras et al. 2012). In the state of fasting or insulin resistance, more fatty acids enter myocytes, where they are used as primary sources of energy. Likewise, during nutrient overflow induced by high fat or fructose/sucrose feeding regimens, cellular fatty acid uptake increases (reviewed by Chabowski et al. 2008). It has been shown that under high fat feeding, the expressions (Pillai et al. 2008) and activities (Caton et al. 2011) of sirtuins are initially increased. Under fasting conditions, sirtuins are responsible for the preservation of cellular ATP production by increasing FAO, TCA cycle, and ETS activities without damaging the cell by increasing antioxidant defenses to control ROS. In the context of nutrient overflow, sirtuins efficiently eliminate accumulating fatty acids and FAO intermediates and reduce the growing lipid stores by increasing the activities of FAO, the TCA

cycle, the ETS, and antioxidant defenses. Hence, under metabolic overflow or starvation, sirtuin signaling increases FAO without toxic ROS side-effects.

To address the manner in which elevated cellular fatty acid influx increases sirtuin expression and/or activity in hearts of fructose-fed rats, we determined NAD<sup>+</sup> levels. It has been shown that fatty acids increase sirtuin activity by activation of AMPK, which increases cellular NAD<sup>+</sup> levels (Cantó et al. 2009). Hence, we have determined NAD<sup>+</sup> levels in cytosolic, mitochondrial, and nuclear fractions. In our study, we observed an increased NAD<sup>+</sup> in both cytosolic and mitochondrial fractions. The increased NAD<sup>+</sup> may be the cause for the increased SIRT1 and SIRT3 protein levels. In hearts of fructose-fed animals, increased NAD<sup>+</sup> may be the result of increased FAO as well as the mismatch between the ROS-damaged activity of the TCA cycle, e.g. reduced citrate synthase and aconitase activities, and the increased FAO. The FAO-TCA cycle mismatch is expected to further enhance NAD<sup>+</sup> levels. Recent experiments from our laboratory unveiled reduced SIRT1 activity in nuclei despite increased protein levels (communication with Dr. Michael Zaugg). SIRT3 protein levels were also increased in mitochondria, but activities were unchanged compared to control rat hearts (communication with Dr. Michael Zaugg). These observations suggest that the sirtuin signaling in hearts of fructose-fed rats is on the brink of failing after six weeks of uninterrupted fat overload. Since sirtuins are sensitive to ROS, which were massively generated in hearts of fructose-fed rats, it is likely that oxidative damage accounts for their reduced catalytic activity (Zee et al. 2010). In the context of cardiac fat overload, a failing sirtuin signaling – resulting in an insufficient antioxidant capacity, e.g. SOD and ALDH activities, and an inefficient interplay between FAO, the TCA cycle, and the ETS – is detrimental. In our model, there are indications that some sirtuin targets, e.g. complex I (Ahn et al. 2008) and  $\beta$ HADH (Hirschey et al. 2010), are possibly still functional and deacetylated. Other sirtuin targets, such as

SOD (Qui et al. 2010), ALDH (reviewed by Song et al. 2011), complex II/succinate dehydrogenase of the TCA cycle and the ETS (Cimen et al. 2010), and PGC-1 $\alpha$  as indicated by lack of TFAM upregulation (Rodgers et al. 2005), may have been insufficiently deacetylated. It is important to note that unspecific and non-enzymatically mediated acetylation due to the accumulation of C<sub>2</sub>-bodies, i.e. acetyl-CoA, in response to TCA cycle-FAO mismatch may have occurred (communication with Dr. Michael Zaugg). This is also known to increase or decrease mitochondrial enzyme activities and is likely to promote further metabolic dysregulation (Alrob et al. 2014). Experiments in our laboratory are currently investigating the degree of acetylation of key metabolic enzymes in various cellular fractions (communication with Dr. Michael Zaugg).

Despite significant overexpression of sirtuins in cardiac muscle that is aiming to “sustainably” burn abundant fatty acids, the high generation of ROS in the metabolically active cardiac muscle ultimately causes SIRT1 and SIRT3 failure. This is consistent with previous observations that the heart is among the first organs to develop insulin resistance in models of diabetes (Park et al. 2005).

## **4.6 Mitochondrial Content**

The TCA cycle enzyme citrate synthase is a marker of mitochondrial content (Srere 1969). As such, its activity is commonly used as a quantitative measure of the mitochondrial content of a given sample (Holloszy et al. 1970; Williams et al. 1986; Hood et al. 1989). Citrate synthase activity was recently demonstrated to be among the most reliable biomarkers of mitochondrial content in healthy human skeletal muscle (Larsen et al. 2012). Furthermore, the expression of the mitochondrial protein COXIV also reflects mitochondrial content. The reduction in both citrate synthase activity and COXIV expression in hearts of fructose-fed rats points to a reduced total mitochondrial content. Despite the upregulation of PGC-1 $\alpha$  and NRF2, the total and mitochondrial

levels of the mitochondrial transcription activator TFAM in normal and diabetic hearts were the same, suggesting that mitochondrial biogenesis is not elevated in hearts of fructose-fed rats. In accordance, a study by Yan et al. (2013) detected signs of reduced mitochondrial content and biogenesis in hearts of leptin-deficient diabetic mice. While the identification of the cause(s) of the decreased mitochondrial content is beyond the scope of this study, it is possible to speculate that cardiac mitochondria are damaged by the elevated oxidative stress in hearts of fructose-fed rats (Kristal et al. 1997). Such damage would likely manifest itself as visible morphological changes, such as mitochondrial swelling or shrinking and cristae distortion, as observed by Yan et al. (2013). Furthermore, compromised mitochondria may be degraded by mitophagy, as can be suggested by the observed increased expression of NRF2 in hearts of fructose-fed rats: NRF2 expression has been reported to correlate with the levels of mitophagic proteins in lungs of septic mice (Chang et al. 2015). In order to test such hypotheses, mitochondrial quantity and morphology will soon be examined by transmission electron microscopy (communication with Dr. Michael Zaugg).

## **4.7 Comparison of Cardiac and Skeletal Muscles**

Our laboratory previously examined fibres of skeletal muscles from fructose-fed rats, specifically the glycolytic EDL and the oxidative soleus (Warren et al. 2014). The aim of this study was to determine whether differential changes could be detected in glycolytic compared to oxidative skeletal muscle in early type-2 diabetes (Table 4.1).

(i) Onset of metabolic derangement:

Decreased PDH complex activity was observed in the EDL but not the soleus (Warren et al. 2014). Hence, in the fructose-fed rat, an earlier metabolic shift takes place in the heart and the EDL

compared to the soleus. This is surprising because the heart is commonly regarded as more similar to the soleus.

(ii) ETS function:

Examination of the ETS in hearts of fructose-fed rats suggests that the complexes are uncompromised. These findings adhere to those previously acquired in the skeletal muscle fibres of the fructose-fed rat. In the EDL, the substrate-specific decrease in complex I respiration was due to a reduced PDH complex activity (Warren et al. 2014). A decreased respiration was observed in the soleus for the complex II-dependent S(Rot) protocol (Warren et al. 2014). Yet, the ETS was largely unaffected as this difference was not apparent with a physiological substrate combination of pyruvate/malate/succinate (Warren et al. 2014).

(iii) TCA cycle:

The activity of the TCA cycle enzyme aconitase was decreased in the heart and the EDL (Warren et al. 2014) of the fructose-fed rat. While this enzyme is not responsible for the rate-limiting step of the TCA cycle, the reduction in its activity reveals damage to the TCA cycle, which could result in a lower oxidative capacity. Aconitase activity was not significantly different in the soleus of the fructose-fed rat (Warren et al. 2014).

(iv) Fatty acid oxidation:

High-resolution respirometry data collected from mitochondria of hearts of fructose-fed rats identified an increased OXPHOS for the PalCoA and OctCar protocols. This is similar to our previous findings in fibres of the soleus of fructose-fed rats, in which reduced levels of free carnitines and acylcarnitines were consistent with increased FAO (Warren et al. 2014).

(v) Mitochondrial ROS production:

In hearts of fructose-fed rats, the decreased aconitase activity and the increased mitochondrial HNE demonstrated mitochondrial ROS production. Aconitase activity was also negatively affected in the EDL of fructose-fed rats (Warren et al. 2014).

(vi) Antioxidant defenses:

As described in section 4.4, limited signs of heightened antioxidant defenses were detected in hearts of the fructose-fed rats. The soleus, but not the EDL, exhibited high TXNRD2 and GPX1 levels in control rats (Warren et al. 2014). Neither muscle experienced a change in the expression of these proteins after fructose feeding (Warren et al. 2014).

(vii) SIRT3 expression:

The abundant expression of the mitochondrial protein SIRT3 in the heart and the soleus (Warren et al. 2014) was further increased following fructose feeding. However, it was only present in very low levels in the EDL (Warren et al. 2014). Fibres from the EDL of fructose-fed rats (Warren et al. 2014) share similarities with SIRT3 knockout models, in which fat overload is particularly detrimental (Hirschey et al. 2011). In contrast, the soleus highly expresses SIRT3, which was further upregulated by fructose feeding (Warren et al. 2014). This enhances FAO and antioxidant capacity; thus, the soleus is able to manage fat overload without suffering ROS damage (Warren et al. 2014). In spite of the increased expression of SIRT1 and SIRT3 in hearts of fructose-fed rats, the diminished activity of SIRT1 and the unchanged activity of SIRT3 (communication with Dr. Michael Zaugg) reveal a failing sirtuin signaling. This is accompanied by insufficient antioxidant responses and increased oxidative stress. The resulting ROS damage to the TCA cycle favours TCA cycle-FAO mismatch. Ultimately, the onset of sirtuin signaling failure constitutes the tipping

point between metabolic compensation and decompensation during the progression of type-2 diabetes.

Table 4.1 Characteristics of muscle metabolism in early type-2 diabetes

Characteristics	Glycolytic EDL	Oxidative Soleus	Cardiac
Onset of metabolic derangement	Early	Late	Early
ETS function	Conserved	Conserved	Conserved
Potential TCA cycle-FAO mismatch	Yes	No	Yes
Mitochondrial ROS production	Yes	No	Yes
Antioxidant defenses	Low	High	High
SIRT3 expression	Very low	High	High
Onset of sirtuin signaling failure	From beginning	Late	Early

Findings regarding the glycolytic extensor digitorum longus (EDL) and oxidative soleus skeletal muscles were previously reported by Warren et al. (2014). Cardiac muscle findings were obtained during the current study.

## 4.8 Overall Significance

Given the extent and degree of the observed metabolic changes, the fructose-fed rat has proven to be an ideal model for cardiac studies related to metabolic derangements in early type-2 diabetes. Hence, our findings have provided a deeper understanding of the molecular changes that initially occur in the type-2 diabetic heart. The metabolic changes observed after only six weeks of fructose feeding are quite remarkable and illustrate the imminent threat of the over-consumption of soft-drinks and other fructose-containing food products. As insulin resistance is still reversible, our study emphasizes the importance of promoting behavioural changes in patients and/or exploring medical treatment options, e.g. sirtuin agonists or metformin, at an early point in the development of type-2 diabetes.

## 4.9 Limitations

The interpretation of the findings from this study are subject to the following main limitations:

- (i) While the fructose-fed rat model emulates the acquisition of type-2 diabetes resulting from Western diets, it illustrates an early time point rather than the advanced disease state that is experienced by patients with late stage type-2 diabetes.
- (ii) As time and resources did not allow for the examination of the expression and the activity of all enzymes possibly implicated in metabolic changes, certain gaps in our understanding remain.
- (iii) Although we measured nuclear protein levels for the various transcription factors including PPAR $\alpha$ , PGC-1 $\alpha$ , NRF2, and TFAM we did not directly show their binding to their respective consensus regions.
- (iv) It is possible that the final results for protein expression and activity assays may have been affected by the choice of the normalization procedure. For example, the expression of COXIV rather than that of ANT was selected for the normalization of proteins in mitochondrial fractions.
- (v) While our findings form a characterization of cardiac mitochondria after six weeks of fructose feeding, they do not identify whether the various changes constitute causes that contribute to the progression of diabetes or consequences that reflect the worsening condition.

## 4.10 Future Directions

In response to the limitations presented by this study, our laboratory is currently investigating sirtuin activity and acquiring images of mitochondria by transmission electron microscopy (communication with Dr. Michael Zaugg). Additional work could be done to strengthen the interpretation of our findings:

- (i) By examining enzymes specific to medium-chain FAO, it would be possible to identify the source of the elevated OXPHOS with the OctCar protocol in the fructose-fed group.
- (ii) A series of high-resolution respirometry protocols accounting for the potential of the inner mitochondrial membrane could reveal whether the more abundant expression of UCP3 in the fructose-fed group is associated with some features of mitochondrial uncoupling.
- (iii) It would also be beneficial to repeat measurements of mitochondrial respiratory states and mitochondrial protein expression and activity in isolated populations of interfibrillar and subsarcolemmal mitochondria.
- (iv) Furthermore, an evaluation of cardiac mitochondrial function in fructose-fed rats after shorter and longer feeding periods would reveal changes as they unfold chronologically during disease progression.
- (v) Our findings could also be furthered by adding a mitochondria-targeted antioxidant, e.g. MitoQ, to the diet of fructose-fed rats to see whether this helps preserve mitochondrial function.

- (vi) Once ambiguities have been clarified, the complete profile of mitochondrial changes in hearts of fructose-fed rats could, ultimately, be compared and contrasted with a parallel evaluation in type-2 diabetic human cardiac tissue at various stages of the disease.

# References

- Agarwal S, Cox AJ, Herrington DM, Jorgensen NW, Xu J, Freedman BI, Carr JJ, Bowden DW (2012). Coronary calcium score predicts cardiovascular mortality in diabetes: diabetes heart study. *Diabetes Care* 36: 972-7.
- Ahn BH, Kim HS, Song S, Lee IH, Liu J, Vassilopoulos A, Deng CX, Finkel T (2008). A role for the mitochondrial deacetylase Sirt3 in regulation energy homeostasis. *Proc Natl Acad Sci USA* 105: 14447-52.
- Aliciguzel Y, Ozen I, Aslan M, Karayalcin U (2003). Activities of xanthine oxidoreductase and antioxidant enzymes in different tissues of diabetic rats. *J Lab Clin Med* 142: 172-7.
- Allen RJ, Leahy JS (1966). Some effects of dietary dextrose, fructose, liquid glucose and sucrose in the adult male rat. *Br J Nutr* 20: 339-47.
- Alrob OA, Sankaralingam S, Ma C, Wagg CS, Fillmore N, Jaswal JS, Sack MN, Lehner R, Gupta MP, Michelakis ED, Padwal RS, Johnstone DE, Sharma AM, Lopaschuk GD (2014). Obesity-induced lysine acetylation increases cardiac fatty acid oxidation and impairs insulin signalling. *Cardiovasc Res* 103: 485-97.
- Anderson EJ, Kypson AP, Rodriguez E, Anderson CA, Lehr EJ, Neuffer PD (2009a). Substrate-specific derangements in mitochondrial metabolism and redox balance in the atrium of the type 2 diabetic human heart. *JACC* 54: 1891-8.
- Anderson EJ, Lustig ME, Boyle KE, Woodlief TL, Kane DA, Lin CT, Price JW, Kang L, Rabinovitch PS, Szeto HH, Houmard JA, Cortright RN, Wasserman DH, Neuffer PD

- (2009b). Mitochondrial H<sub>2</sub>O<sub>2</sub> emission and cellular redox state link excess fat intake to insulin resistance in both rodents and humans. *J Clin Invest* 119: 573-81.
- Anedda A, López-Bernardo E, Acosta-Iborra B, Saadeh Suleiman M, Landázuri MO, Cadenas S (2013). The transcription factor Nrf2 promotes survival by enhancing the expression of uncoupling protein 3 under conditions of oxidative stress. *Free Radic Biol Med* 61: 395-407.
- Araki M, Motojima M (2006). Identification of ERRalpha as a specific partner of PGC1-alpha for the activation of PDK4 gene expression in muscle. *FEBS J* 237: 1669-80.
- Aronow WS, Ahn C (1999). Incidence of heart failure in 2,737 older persons with and without diabetes mellitus. *Chest* 115: 867-8.
- Bagul PK, Deepthi N, Sultana R, Banerjee SK (2015). Resveratrol ameliorates cardiac oxidative stress in diabetes through deacetylation of NFkB-p65 and histone 3. *J Nutr Biochem* 26: 1298-1307.
- Barouch LA, Berkowitz DE, Harrison RW, O'Donnell CP, Hare JM (2003). Disruption of leptin signaling contributes to cardiac hypertrophy independently of body weight in mice. *Circulation* 108: 754-9.
- Bertoni AG, Tsai A, Kasper EK, Brancati FL (2003). Diabetes and idiopathic cardiomyopathy: a nationwide case-control study. *Diabetes Care* 26: 2791-5.
- Boudina S, Sena S, O'Neill BT, Tathireddy P, Young ME, Abel ED (2005). Reduced mitochondrial oxidative capacity and increased mitochondrial uncoupling impair myocardial energetics in obesity. *Circulation* 112: 2686-95.

- Boudina S, Sena S, Theobald H, Sheng X, Wright JJ, Hu XX, Aziz S, Johnson JI, Bugger H, Zaha VG, Abel ED (2007). Mitochondrial energetics in the heart in obesity-related diabetes: direct evidence for increased uncoupled respiration and activation of uncoupling proteins. *Diabetes* 56: 2457-66.
- Boveris A, Chance B (1973). The mitochondrial generation of hydrogen peroxide. General properties and effects of hyperbaric oxygen. *Biochem J* 134: 707-16.
- Bowker-Kinley MM, Davis WI, Wu P, Harris RA, Popov KM (1998). Evidence for existence of tissue-specific regulation of the mammalian pyruvate dehydrogenase complex. *Biochem J* 329: 191-6.
- Brand MD, Chien LF, Ainscow EK, Rolfe DF, Porter RK (1994). The causes and functions of mitochondrial proton leak. *Biochim Biophys Acta* 1187: 132-9.
- Brand MD, Nicholls DG (2011). Assessing mitochondrial dysfunction in cells. *Biochem J* 435: 297-312.
- Brandt J, Djouadi F, Kelly DP (1998). Fatty acids activate transcription of the muscle carnitine palmitoyltransferase I gene in cardiac myocytes via the peroxisome proliferator-activated receptor  $\alpha$ . *J Biol Chem* 273: 23786-93.
- Campbell SE, Tandon NN, Woldegiorgis G, Luiken JJ, Glatz JF, Bonen A (2004). A novel function for fatty acid translocase (FAT)/CD36: involvement in long chain fatty acid transfer into the mitochondria. *J Biol Chem* 279: 36235-41.

- Cantó C, Gerhart-Hines Z, Feige JN, Lagouge M, Noriega L, Milne JC, Elliott PJ, Puigserver P, Auwerx J (2009). AMPK regulates energy expenditure by modulating NAD<sup>+</sup> metabolism and SIRT1 activity. *Nature* 458: 1056-60.
- Canadian Diabetes Association (2005). Diabetes: Canada at the Tipping Point.
- Canadian Diabetes Association (2015). Diabetes Charter for Canada.
- Carley AN, Severson DL (2005). Fatty acid metabolism is enhanced in type 2 diabetic hearts. *Biochim Biophys Acta* 1734: 112-26.
- Caton PW, Nayuni NK, Khan NQ, Wood EG, Corder R (2011). Fructose induces gluconeogenesis and lipogenesis through a SIRT1-dependent mechanism. *J Endocrinol* 208: 273-83.
- Červinková Z, Rauchová H, Křiváková P, Drahotka Z (2008). Inhibition of palmitoyl carnitine oxidation in rat liver mitochondria by *tert*-butyl hydroperoxide. *Physiol Res* 57: 133-6.
- Cessario DA, Brar R, Shivkumar K (2006). Alterations in ion channel physiology in diabetic cardiomyopathy. *Endocrinol Metab Clin North Am* 35: 601-10.
- Chabowski A, Górski J, Glatz JF, Luiken JJ, Bonen A (2008). Protein-mediated fatty acid uptake in the heart. *Curr Cardiol Rev* 4: 12-21.
- Chang KC, Chung SY, Chong WS, Suh JS, Kim SH, Noh HK, Seong BW, Ko HJ, Chun KW (1993). Possible superoxide radical-induced alteration of vascular reactivity in aortas from streptozotocin-treated rats. *J Pharmacol Exp Ther* 266: 922-1000.
- Chang AL, Ulrich A, Suliman HB, Piantadosi CA (2015). Redox regulation of mitophagy in the lung during murine *Staphylococcus aureus* sepsis. *Free Radic Biol Med* 78: 179-89.

- Chen H, Charlat O, Tartaglia LA, Woolf EA, Weng X, Ellis SJ, Lakey ND, Culpepper J, Moore KJ, Breitbart RE, Duyk GM, Tepper RI, Morgenstern JP (1996). Evidence that the diabetes gene encodes the leptin receptor: identification of a mutation in the leptin receptor gene in db/db mice. *Cell* 84: 491-5.
- Cheng PW, Ho WY, Su YT, Lu PJ, Chen BZ, Cheng WH, Lu WH, Sun GC, Yeh TC, Hsiao M, Tseng CJ (2013). Resveratrol decreases fructose-induced oxidative stress, mediated by NADH oxidase via an AMPK-dependent mechanism. *Br J Pharmacol* 171: 2739-50.
- Christoffersen C, Bollano E, Lindegaard ML, Bartels ED, Goetze JP, Andersen CB, Nielsen LB (2003). Cardiac lipid accumulation associated with diastolic dysfunction in obese mice. *Endocrinology* 144: 3483-90.
- Churchill EN, Disatnik MH, Mochly-Rosen D (2009). Time-dependent and ethanol-induced cardiac protection from ischemia mediated by mitochondrial translocation of  $\epsilon$ PKC and activation of aldehyde dehydrogenase 2. *J Mol Cell Cardiol* 46: 278-84.
- Cimen H, Han MJ, Yang Y, Tong Q, Koc H, Koc EC (2010). Regulation of succinate dehydrogenase activity by SIRT3 in mammalian mitochondria. *Biochemistry* 49: 304-11.
- Constantin-Teodosiu D (2013). Regulation of muscle pyruvate dehydrogenase complex in insulin resistance: Effects of exercise and dichloroacetate. *Diabetes Metab J* 37: 301-14.
- Constantin-Teodosiu D, Constantin D, Stephens F, Laithwaite D, Greenhaff PL (2012). The role of FOXO and PPAR transcription factors in diet-mediated inhibition of PDC activation and carbohydrate oxidation during exercise in humans and the role of pharmacological activation of PDC in overriding these changes. *Diabetes* 61: 1017-24.

- Cook GA, Gamble MS (1987). Regulation of carnitine palmitoyltransferase by insulin results in decreased activity and decreased apparent  $K_i$  values for malonyl-CoA. *J Biol Chem* 262: 2050-5.
- Coort SL, Hasselbaink DM, Koonen DP, Willems J, Coumans WA, Chabowski A, van der Vusse GJ, Bonen A, Glatz JF, Luiken JJ (2004). Enhanced sarcolemmal FAT/CD36 content and triacylglycerol storage in cardiac myocytes from obese Zucker rats. *Diabetes* 53: 1655-63.
- Cox B, Emili A (2006). Tissue subcellular fractionation and protein extraction for use in mass-spectrometry-based proteomics. *Nat Protoc* 1: 1872-8.
- Crescenzo R, Bianco F, Coppola P, Mazzoli A, Valiante S, Liverini G, Iossa S (2014). Adipose tissue remodeling in rats exhibiting fructose-induced obesity. *Eur J Nutr* 53: 413-9.
- Croston TL, Thapa D, Holden AA, Tveter KJ, Lewis SE, Shepherd DL, Nichols CE, Long DM, Olfert IM, Jagannathan R, Hollander JM (2014). Functional deficiencies of subsarcolemmal mitochondria in the type 2 diabetic human heart. *Am J Physiol Heart Circ Physiol* 307: H54-65.
- Dai S, McNeill JH (1995). Fructose-induced hypertension in rats is concentration- and duration-dependent. *J Pharmacol Toxicol Methods* 33: 101-7.
- Dandona P, Thusu K, Cook S, Snyder B, Makowshi J, Armstrong D, Nicotera T (1996). Oxidative damage to DNA in diabetes mellitus. *Lancet* 347: 444-5.
- Devereux RB, Roman MJ, Paranicas M, O'Grady MJ, Lee ET, Welty TK, Fabsitz RR, Robbins D, Rhoades ER, Howard BV (2000). Impact of diabetes on cardiac structure and function: the strong heart study. *Circulation* 101: 2271-6.

- Dimauro I, Pearson T, Caporossi D, Jackson MJ (2012). A simple protocol for the subcellular fractionation of skeletal muscle cells and tissue. *BMC Res Notes* 5: 513.
- Eigentler A, Fontana-Ayoub M, Fasching M, Lassnig B, Stadlmann S, Rieger G, Haffner B, Lemieux H, Gnaiger E (2012). Selected media and chemicals for respirometry with mitochondria and permeabilized cells. *Mitochondr Physiol Network* 03.02: 1-9.
- Finkel T, Holbrook NJ (2000). Oxidants, oxidative stress and the biology of ageing. *Nature* 408: 239-47.
- Fisher-Wellman KH, Neuffer PD (2012). Linking mitochondrial bioenergetics to insulin resistance via redox biology. *Trends Endocrinol Metab* 23: 142-53.
- Fong JC, Schulz H (1978). On the rate-determining step of fatty acid oxidation in heart: inhibition of fatty acid oxidation by 4-pentenoic acid. *J Biol Chem* 253: 6917-22.
- Freeman H, Shimomura K, Cox RD, Ashcroft FM (2006). Nicotinamide nucleotide transdehydrogenase: a link between insulin secretion, glucose metabolism and oxidative stress. *Biochem Soc Trans* 34: 806-10.
- Friederich M, Fasching A, Hansell P, Nordquist L, Palm F (2008). Diabetes-induced up-regulation of uncoupling protein-2 results in increased mitochondrial uncoupling in kidney proximal tubular cells. *Biochimica et Biophysica Acta* 1777: 935-40.
- Galipeau D, Arikawa E, Sekirov I, McNeill JH (2001). Chronic thromboxane synthase inhibition prevents fructose-induced hypertension. *Hypertension* 38: 872-6.
- Gardner PR (2002). Aconitase: sensitive target and measure of superoxide. *Methods Enzymol* 349: 2-23.

- Gardner PR, Nguyen DD, White CW (1994). Aconitase is a sensitive and critical target of oxygen poisoning in cultured mammalian cells and in rat lungs. *Proc Natl Acad Sci USA* 91: 12248-52.
- Gnaiger E (2012). Mitochondrial pathways and respiratory control: an introduction to OXPHOS analysis. *Mitochondr Physiol Network* 17.18.
- Gnaiger E, Kuznetsov AV, Schneeberger S, Seiler R, Brandacher G, Steurer W, Margreiter R (2000). Mitochondria in the cold. In: *Life in the Cold*. (Heldmaier G, Klingenspor M, eds) Springer, Heidelberg, Berlin, New York: pp 431-42.
- Gnaiger E, Lassnig B, Kuznetsov A, Reiger G, Margreiter R (1998). Mitochondrial oxygen affinity, respiratory flux control and excess capacity of cytochrome *c* oxidase. *J Exp Biol* 201: 1129-39.
- Goglia F, Skulachev VP (2003). A function for novel uncoupling proteins: antioxidant defense of mitochondrial matrix by translocating fatty acid peroxides from the inner to the outer membrane leaflet. *FASEB J* 17: 1585-91.
- Gupte AA, Minze LJ, Reyes M, Ren Y, Wang X, Brunner G, Ghosn M, Cordero-Reyes AM, Ding K, Pratico D, Morrisett J, Shi ZZ, Hamilton DJ, Lyon CJ, Hsueh WA (2013). High-fat feeding-induced hyperinsulinemia increases cardiac glucose uptake and mitochondrial function despite peripheral insulin resistance. *Endocrinology* 154: 2650-62.
- Harmancey R, Lam TN, Lubrano GM, Guthrie PH, Vela D, Taegtmeier H (2012). Insulin resistance improves metabolic and contractile efficiency in stressed rat heart. *FASEB J* 26: 3118-26.

- Hidalgo B, Irvin MR, Sha J, Zhi D, Aslibekyan S, Absher D, Tiwari HK, Kabagambe EK, Ordovas JM, Arnett DK (2014). Epigenome-wide association study of fasting measured of glucose, insulin, and HOMA-IR in the genetics of lipid lowering drugs and diet network study. *Diabetes* 63: 801-7.
- Hirschey MD, Shimazu T, Goetzman E, Jing E, Schwer B, Lombard DB, Grueter CA, Harris C, Biddinger S, Ilkayeva OR, Stevens RD, Li Y, Saha AK, Ruderman NB, Bain JR, Newgard CB, Farese RV, Alt FW, Kahn CR, Verdin E (2010). SIRT3 regulates mitochondrial fatty-acid oxidation by reversible enzyme deacetylation. *Nature* 464: 121-5.
- Hirschey MD, Shimazu T, Jing E, Grueter CA, Collins AM, Aouizerat B, Stančáková A, Goetzman E, Lam MM, Schwer B, Stevens RD, Muehlbauer MJ, Kakar S, Bass NM, Kuusisto J, Laakso M, Alt FW, Newgard CB, Farese RV, Kahn CR, Verdin E (2011). SIRT3 deficiency and mitochondrial protein hyperacetylation accelerate the development of the metabolic syndrome. *Mol Cell* 44: 177-90.
- Holloszy J, Oscai LB, Don IJ, Mole PA (1970). Mitochondrial citric acid cycle and related enzymes: adaptive response to exercise. *Biochem Biophys Res Comm* 40: 1368-73.
- Holloway GP, Bezaire V, Heigenhauser GJ, Tandon NN, Glatz JF, Luiken JJ, Bonen A, Spriet LL (2006). Mitochondrial long chain fatty acid oxidation, fatty acid translocase/CD36 and carnitine palmitoyltransferase I activity in human skeletal muscle during aerobic exercise. *J Physiol* 571: 201-10.
- Holloway GP, Gurd BJ, Snook LA, Lally J, Bonen A (2010). Compensatory increases in nuclear PGC1 $\alpha$  protein are primarily associated with subsarcolemmal mitochondrial adaptations in ZDF rats. *Diabetes* 59: 819-28.

- Holloway GP, Jain SS, Bezaire V, Hann XX, Glatz JF, Luiken JJ, Harper ME, Bonen A (2009). FAT/CD36-null mice reveal that mitochondrial FAT/CD36 is required to upregulate mitochondrial fatty acid oxidation in contracting muscle. *Am J Physiol Regul Integr Comp Physiol* 297: R960-7.
- Hood D, Zak R, Pette D (1989). Chronic stimulation of rat skeletal muscle induces coordinate increases in mitochondrial and nuclear mRNAs of cytochrome c oxidase subunits. *Eur J Biochem* 179: 275-80.
- Houstis N, Rosen ED, Lander ES (2006). Reactive oxygen species have a causal role in multiple forms of insulin resistance. *Nature* 440: 944-8.
- Huss JM, Torra IP, Staels B, Giquère V, Kelley DP (2004). Estrogen-related receptor  $\alpha$  directs peroxisome proliferator-activated receptor  $\alpha$  signaling in the transcriptional control of energy metabolism in cardiac and skeletal muscle. *Mol Cell Biol* 24: 9079-91.
- Hwang IS, Ho H, Hoffman BB, Reaven GM (1987) Fructose-induced insulin resistance and hypertension in rats. *Hypertension* 10: 512-6.
- Ibrahimi A, Bonen A, Blinn WD, Hajri T, Li X, Zhong K, Cameron R, Abumrad NA (1999). Muscle-specific overexpression of FAT/CD36 enhances fatty acid oxidation by contracting muscle, reduces plasma triglycerides and fatty acids, and increases plasma glucose and insulin. *J Biol Chem* 274: 26761-6.
- Ilercil A, Devereux RB, Roman MJ, Paranica M, O'Grady MJ, Welty TK, Robbins DC, Fabsitz RR, Howard BV, Lee ET (2001). Relationship of impaired glucose tolerance to left ventricular structure and function: the strong heart study. *Am Heart J* 141: 992-8.

- Ishii T, Itoh K, Ruiz E, Leake DS, Unoki H, Yamamoto M, Mann GE (2004). Role of Nrf2 in the regulation of CD36 and stress protein expression in murine macrophages: activation by oxidatively modified LDL and 4-hydroxynonenal. *Circ Res* 94: 609-16.
- Iyer SN, Katovich MJ (1994). Effect of chronic losartan potassium treatment on fructose-induced hypertension. *Life Sci* 55: PL139-44.
- Iyer SN, Katovich MJ (1996). Vascular reactivity to phenylephrine and angiotensin II in hypertensive rats associated with insulin resistance. *Clin Exp Hypertens* 18: 227-42.
- Kelley DE, He J, Menshikova EV, Ritov VB (2002). Dysfunction of mitochondria in human skeletal muscle in type 2 diabetes. *Diabetes* 51: 2944-50.
- Kelley DE, Mandarino LJ (2000). Fuel selection in human skeletal muscle in insulin resistance: a re-examination. *Diabetes* 49: 677-83.
- Kerner J, Hoppel C (2000). Fatty acid import into mitochondria. *Biochim Biophys Acta* 1486: 1-17.
- Kim YI, Lee FN, Choi WS, Lee S, Youn JH (2006). Insulin regulation of skeletal muscle PDK4 mRNA expression is impaired in acute insulin-resistant states. *Diabetes* 55: 2311-17.
- King KL, Stanley WC, Rosca M, Kerner J, Hoppel CL, Febbraio M (2007). Fatty acid oxidation in cardiac and skeletal muscle mitochondria is unaffected by deletion of CD36. *Arch Biochem Biophys* 467, 234-8.
- Kirby DM, Thorburn DR, Turnbull DM, Taylor RW (2007). Biochemical assays of respiratory chain complex activity. *Methods Cell Biol* 80: 93-119.
- Kirsch M, de Groot H (2001). NAD(P)H, a directly acting antioxidant? *FASEB J* 15: 1569-74.

- Klöppel G, Löhr M, Habich K, Oberholzer M, Heitz PU (1985). Islet pathology and the pathogenesis of type 1 and type 2 diabetes mellitus revisited. *Surv Synth Pathol Res* 4: 110-25.
- Kraegen EW, Clark PW, Jenkins AB, Daley EA, Chisholm DJ, Storlien LH (1991). Development of muscle insulin resistance after lower insulin resistance in high-fat-fed rats. *Diabetes* 40: 1397-403.
- Kristal BS, Jackson CT, Chung HY, Matsuda M, Nguyen HD, Yu BP (1997). Defects at center P underlie diabetes-associated mitochondrial dysfunction. *Free Radic Biol Med* 22: 823-33.
- Kuznetsov AV, Lassnig B, Gnaiger E (2010). Laboratory protocol citrate synthase mitochondrial marker enzyme. *Mitochondr Physiol Network* 08.14: 1-10.
- Kuznetsov AV, Schneeberger S, Seiler R, Brandacher G, Mark W, Steurer W, Saks V, Usson Y, Margreiter R, Gnaiger E (2004). Mitochondrial defects and heterogeneous cytochrome *c* release after cardiac cold ischemia and reperfusion. *Am J Physiol Heart Circ Physiol* 286: H1633-41.
- Kwong LK, Sohal RS (1998). Substrate and site specificity of hydrogen peroxide generation in mouse mitochondria. *Arch Biochem Biophys* 350: 118-26.
- Larsen S, Nielsen J, Hansen CN, Nielsen LB, Wibrand F, Stride N, Schroder HD, Boushel R, Helge JW, Dela F, Hey-Mogensen (2012). Biomarkers of mitochondrial content in skeletal muscle of healthy young human subjects. *J Physiol* 590: 3349-60.

- Liu JE, Palmieri V, Roman MJ, Bella JN, Fabsitz R, Howard BV, Welty TK, Lee ET, Devereux RB (2001). The impact of diabetes on left ventricular filling pattern in normotensive and hypertensive adults: the strong heart study. *J Am Coll Cardiol* 37: 1943-9.
- Lou PH, Lucchinetti E, Zhang L, Affolter A, Gandhi M, Hersberger M, Warren BE, Lemieux H, Sobhi HF, Clanachan AS, Zaugg M (2014). Loss of Intralipid – but not sevoflurane-mediated cardioprotection in early type-2 diabetic hearts of fructose-fed rats: importance of ROS signaling. *PLoS One* 9: e104971.
- Lou PH, Lucchinetti E, Zhang L, Affolter A, Gandhi M, Zhakupova A, Hersberger M, Hornemann T, Clanachan AS, Zaugg M (2015). Propofol (Diprivan) and Intralipid exacerbate insulin resistance in type-2 diabetic hearts by impairing GLUT4 trafficking. *Anesth Analg* 120: 329-40.
- Maiztegui B, Borelli MI, Raschia MA, Del Zotto H, Gagliardino JJ (2009). Islet adaptive changes to fructose-induced insulin resistance:  $\beta$ -cell mass, glucokinase, glucose metabolism, and insulin secretion. *J Endocrinol* 200: 139-49.
- Mansor LS, Gonzalez ER, Cole MA, Tyler DJ, Beeson JH, Clarke K, Carr CA, Heather LC (2013). Cardiac metabolism in a new rat model of type 2 diabetes using high-fat diet with low dose streptozotocin. *Cardiovasc Diabetol* 12: 136.
- Mascaró C, Ascota E, Ortiz JA, Marrero PF, Hegardt FG, Haro D (1998). Control of human muscle-type carnitine palmitoyltransferase I gene transcription by peroxisome proliferator-activated receptor. *J Biol Chem* 273: 8560-3.
- McGarry JD, Stark MJ, Foster DW (1978). Hepatic malonyl-CoA levels of fed, fasted and diabetic rats as measured using a simple radioisotopic assay. *J Biol Chem* 253: 8291-3.

- McLennan SV, Heffernan S, Wright L, Rae C, Fisher E, Yue DK, Turtle JR (1991). Changes in hepatic glutathione metabolism in diabetes. *Diabetes* 40: 344-8.
- Mellor KM, Bell JR, Young MJ, Ritchie RH, Delbridge LM (2011). Myocardial autophagy activation and suppressed survival signaling is associated with insulin resistance in fructose-fed mice. *J Mol Cell Cardiol* 50: 1035-43.
- Mogensen M, Sahlin K, Fernstrom M, Glintborg D, Vind BF, Beck-Nielsen H, Hojlund K (2007). Mitochondrial respiration is decreased in skeletal muscle of patients with type 2 diabetes. *Diabetes* 56: 1592-9.
- Montaigne D, Marechal X, Coisne A, Debry N, Modine T, Fayad G, Potelle C, El Arid JM, Mouton S, Sebti Y, Duez H, Preau S, Remy-Jouet I, Zerimech F, Koussa M, Richard V, Neviere R, Edme JL, Lefebvre P, Staels B (2014). Myocardial contractile dysfunction is associated with impaired mitochondrial function and dynamics in type 2 diabetic but not in obese patients. *Circulation* 130: 554-64.
- Motohashi H, Yamamoto M (2004). Nrf2-Keap1 defines a physiologically important stress response mechanism. *Trends Mol Med* 10: 549-57.
- Musselman LP, Fink JL, Narzinski K, Ramachandran PV, Hathiramani SS, Cagan RL, Baranski TJ (2011). A high-sugar diet produces obesity and insulin resistance in wild-type *Drosophila*. *DMM* 4: 842-9.
- Neely JR, Morgan HE (1974). Relationship between carbohydrate and lipid metabolism and the energy balance of heart muscle. *Annu Rev Physiol* 36: 413-59.

- Nemoto S, Fergusson MM, Finkel T (2004). Nutrient availability regulates SIRT1 through a forkhead-dependent pathway. *Science* 306: 2105-8.
- Nichols GA, Hillier TA, Erbey JR, Brown JB (2001). Congestive heart failure in type 2 diabetes: prevalence, incidence, and risk factors. *Diabetes Care* 24: 1614-9.
- Nogueiras R, Habegger KM, Chaudhary N, Finan B, Banks AS, Dietrich MO, Horvath TL, Sinclair DA, Pfluger PT, Tschöp MH (2012). Sirtuin 1 and sirtuin 3: physiological modulators of metabolism. *Physiol Rev* 92: 1479-514.
- Padiya R, Chowdhury D, Borkar R, Srinivas R, Pal Bhadra M, Banerjee SK (2014). Garlic attenuates cardiac oxidative stress via activation of PI3K/AKT/Nrf2-Keap1 pathway in fructose-fed diabetic rat. *PLoS One* 9: e94228.
- Park SH, Gammon SR, Knippers JD, Paulsen SR, Rubink DS, Winder WW (2002). Phosphorylation-activity relationships of AMPK and acetyl-CoA carboxylase in muscle. *J Appl Physiol* 92: 2475-82.
- Park SY, Cho YR, Kim HJ, Higashimori T, Danton C, Lee MK, Dey A, Rothermel B, Kim YB, Kalinowski A, Russell KS, Kim JK (2005). Unraveling the temporal pattern of diet-induced insulin resistance in individual organs and cardiac dysfunction in C57BL/6 mice. *Diabetes* 54: 3530-40.
- Pellieux C, Montessuit C, Papageorgiou I, Pedrazzini T, Lerch R (2012). Differential effects of high-fat diet on myocardial lipid metabolism in failing and nonfailing hearts with angiotensin II-mediated cardiac remodeling in mice. *Am J Physiol Heart Circ Physiol* 302: H1795-805.

- Phielix E, Schrauwen-Hinderling VB, Mensink M, Lenaers E, Meex R, Hoeks J, Kooi ME, Moonen-Kornips E, Sels JP, Hesselink MK, Schrauwen P (2008). Lower intrinsic ADP-stimulated mitochondrial respiration underlies in vivo mitochondrial dysfunction in muscle of male type 2 diabetic patients. *Diabetes* 57: 2943-9.
- Phillips MS, Liu Q, Hammond HA, Dugan V, Hey PJ, Caskey CJ, Hess JF (1996). Leptin receptor missense mutation in the fatty Zucker rat. *Nat Genet* 13: 18-9.
- Pillai JB, Chen M, Rajamohan SB, Samant S, Pillai VB, Gupta M, Gupta MP (2008). Activation of SIRT1, a class III histone deacetylase, contributes to fructose feeding-mediated induction of the alpha-myosin heavy chain expression. *Am J Physiol Heart Circ Physiol* 294: H1388-97.
- Puchowicz MA, Varnes ME, Cohen BH, Friedman NR, Kerr DS, Hoppel CL (2004). Oxidative phosphorylation analysis: assessing the integrated function activity of human skeletal muscle mitochondria – case studies. *Mitochondrion* 4: 377-85.
- Qui X, Brown K, Hirschey MD, Verdin E, Chen D (2010). Calorie restriction reduces oxidative stress by SIRT3-mediated SOD2 activation. *Cell Metab* 12: 662-7.
- Randle PJ, Garland PB, Hales CN, Newsholme EA (1963). The glucose fatty-acid cycle. Its role in insulin sensitivity and the metabolic disturbances of diabetes mellitus. *Lancet* 1: 785-9.
- Redfield MM, Jacobsen SJ, Burnett JC, Mahoney DW, Bailey KR, Rodeheffer RJ (2003). Burden of systolic and diastolic ventricular dysfunction in the community: appreciating the scope of the heart failure epidemic. *JAMA* 289: 194-202.

- Riahi Y, Cohen G, Shamni O, Sasson S (2010). Signaling and cytotoxic functions of 4-hydroxyalkenals. *Am J Physiol* 299: E879-86.
- Ritov VB, Menshikova EV, He J, Ferrell RE, Goodpaster BH, Kelley DE (2005). Deficiency of subsarcolemmal mitochondria in obesity and type 2 diabetes. *Diabetes* 54: 8-14.
- Rodgers JT, Lerin C, Haas W, Gygi SP, Spiegelman BM, Puigserver P (2005). Nutrient control of glucose homeostasis through a complex of PGC-1alpha and SIRT1. *Nature* 434: 113-8.
- Rosca MG, Mustata TG, Kinter MT, Ozdemir AM, Kern TS, Szweda LI, Brownlee M, Monnier VM, Weiss MF (2005). Glycation of mitochondrial proteins from diabetic rat kidney is associated with excess superoxide formation. *Am J Physiol Renal Physiol* 289: F420-30.
- Rosca MG, Vazquez EJ, Chen Q, Kerner J, Kern TS, Hoppel CL (2012). Oxidation of fatty acids is the source of increased mitochondrial reactive oxygen species production in kidney cortical tubules in early diabetes. *Diabetes* 61: 2074-83.
- Rubler S, Dlugash J, Yuceoglu YZ, Kumral T, Branwood AW, Grishman A (1972). New type of cardiomyopathy associated with diabetic glomerulosclerosis. *Am J Cardiol* 30: 595-602.
- Saxena AK, Srivastava P, Kale RK, Baquer NZ (1993). Impaired antioxidant status in diabetic rat liver. Effect of vanadate. *Biochem Pharmacol* 45: 539-42.
- Schannwell CM, Schneppenheim M, Perings S, Plehn G, Strauer BE (2002). Left ventricular diastolic dysfunction as an early manifestation of diabetic cardiomyopathy. *Cardiology* 98: 33-9.

- Schenk S, Horowitz JF (2006). Coimmunoprecipitation of FAT/CD36 and CPTI in skeletal muscle increases proportionally with fat oxidation after endurance exercise training. *Am J Physiol Endocrinol Metab* 291: E254-60.
- Schrauwen P, Saris WH, Hesselink MK (2001). An alternative function for human uncoupling protein 3: Protection of mitochondria against accumulation of nonesterified fatty acids inside the mitochondrial matrix. *FASEB J* 15: 2497-502.
- Semeniuk LM, Kryski AJ, Severson DL (2002). Echocardiographic assessment of cardiac function in diabetic db/db and transgenic db/db-hGLUT4 mice. *Am J Physiol Heart Circ Physiol* 283: H976-82.
- Sharma S, Adroque JV, Golfman L, Uray I, Lemm J, Youker K, Noon GP, Frazier OH, Taegtmeyer H. Intramyocardial lipid accumulation in the failing human heart resembles the lipotoxic rat heart. *FASEB J* 18: 1692-700.
- Siow RC, Ishii T, Mann GE (2007). Modulation of antioxidant gene expression 4-hydroxynonenal: atheroprotective role of the Nrf2/ARE transcription pathway. *Redox Rep* 12: 11-5.
- Sivitz WI, Yorek MA (2010). Mitochondrial dysfunction in diabetes: from molecular mechanisms to functional significance and therapeutic opportunities. *Antioxid Redox Signal* 12: 537-77.
- Someya S, Yu W, Hallows WC, Xu J, Vann JM, Leeuwenburg C, Tanokura M, Denu JM, Prolla TA (2010). Sirt3 mediates reduction of oxidative damage and prevention of age-related hearing loss under caloric restriction. *Cell* 143: 802-12.

- Song BJ, Abdelmegeed MA, Yoo SH, Kim BJ, Jo SA, Jo I, Moon KH (2011). Post-translational modification of mitochondrial aldehyde dehydrogenase and biomedical implications. *J Proteomics* 74: 2691-702.
- Speijer D (2011). Oxygen radicals shaping evolution: why fatty acid catabolism leads to peroxisomes while neurons do without it: FADH<sub>2</sub>/NADH flux ratios determining mitochondrial radical formation were crucial for the eukaryotic invention of peroxisomes and catabolic tissue differentiation. *Bioessays* 33: 88-94.
- Spinazzi M, Casarin A, Pertegato V, Salviati L, Angelini C (2012). Assessment of mitochondrial respiratory chain enzymatic activities on tissues and cultured cells. *Nat Protoc* 7: 1235-46.
- Srere PA (1969). Citrate Synthase. *Methods Enzymol* 13: 3-11.
- Srinivasan S, Avadhani NG (2012) Cytochrome c oxidase dysfunction in oxidative stress. *Free Radic Biol Med* 53: 1252-63.
- Teff KL, Elliott SS, Tschop M, Kieffer TJ, Rader D, Heiman M, Townsend RR, Keim NL, D'Alessio D, Havel PJ (2004). Dietary fructose reduces circulating insulin and leptin, attenuates postprandial suppression of ghrelin, and increases triglycerides in women. *J Clin Endocrinol Metab* 89: 2963-72.
- Turko IV, Murad F (2003). Quantitative protein profiling in heart mitochondria from diabetic rats. *J Biol Chem* 278: 35844-9.
- Turrens JF (2003). Mitochondrial formation of reactive oxygen species. *J Physiol* 552: 335-44.
- Verma S, Bhanot S, McNeill JH (1994). Antihypertensive effects of metformin in fructose-fed hyperinsulinemic, hypertensive rats. *J Pharmacol Exp Ther* 271:1334-7.

- Warren BE, Lou PH, Lucchinetti E, Zhang L, Clanachan AS, Affolter A, Hersberger M, Zaugg M, Lemieux H (2014). Early mitochondrial dysfunction in glycolytic muscle, but not oxidative muscle, of the fructose-fed insulin-resistant rat. *Am J Physiol Endocrinol Metab* 306: E658-67.
- Weis BC, Cowan AT, Brown N, Foster DW, McGarry JD (1994). Use of a selective inhibitor of liver carnitine palmitoyltransferase I (CPT I) allows quantification of its contribution to total CPT I activity in rat heart: evidence that the dominant cardiac CPT I isoform is identical to the skeletal muscle enzyme. *J Biol Chem* 269: 26443-8.
- Williams RS, Salmons S, Newsholme E, Kaufman RE, Mellor J (1986). Regulation of nuclear and mitochondrial gene expression by contractile activity in skeletal muscle. *J Biol Chem* 261: 376-80.
- Winder WW, Hardie DG (1999). AMP-activated protein kinase, a metabolic master switch: possible roles in type 2 diabetes. *Am J Physiol Endocrinol Metab* 277: E1-10.
- Winzell MS, Ahrén B (2004). The high-fat diet-fed mouse: a model for studying mechanisms and treatment of impaired glucose tolerance and type 2 diabetes. *Diabetes* 52: S215-9.
- World Health Organization (2014). 10 Facts About Diabetes.
- Wu P, Sato J, Zahao Y, Jaskiewicz J, Popov KM, Harris RA (1998). Starvation and diabetes increase the amount of pyruvate dehydrogenase kinase isoenzyme 4 in rat heart. *Biochem J* 329: 197-201.
- Yan W, Zhang H, Liu P, Wang H, Liu J, Gao C, Liu Y, Lian K, Yang L, Sun L, Guo Y, Zhang L, Dong L, Lau WB, Gao E, Gao F, Xiong L, Wang H, Qu Y, Tao L (2013). Impaired

- mitochondrial biogenesis due to dysfunctional adiponectin-AMPK-PGC-1 $\alpha$  signaling contributing to increased vulnerability in diabetic heart. *Basic Res Cardiol* 108: 329.
- Young ME, Patil S, Ying J, Depre C, Ahuja HS, Shipley GL, Stepkowski SM, Davies PJ, Taegtmeier H (2001). Uncoupling protein 3 transcription is regulated by peroxisome proliferator-activated receptor ( $\alpha$ ) in the adult rodent heart. *FASEB J* 15: 833-45.
- Young IS, Tate S, Lightbody JH, McMaster D, Trimble ER (1995). The effects of desferrioxamine and ascorbate on oxidative stress in the streptozotocin diabetic rat. *Free Radic Biol Med* 18: 833-40.
- Yu GS, Lu YC, Gulick T (1998). Co-regulation of tissue-specific alternative human carnitine palmitoyltransferase I $\beta$  gene promoters by fatty acid enzyme substrate. *J Biol Chem* 273: 32901-9.
- Zee RS, Yoo CB, Pimentel DR, Perlman DH, Burgoyne JR, Hou X, McComb ME, Costello CE, Cohen RA, Bachschmid MM (2010). Redox regulation of sirtuin-1 by S-glutathiolation. *Antioxid Redox Signal* 13: 1023-32.
- Zhang S, Hulver MW, McMillan RP, Cline MA, Gilbert ER (2014). The pivotal role of pyruvate dehydrogenase kinases in metabolic flexibility. *Nutr Metab Lond* 11: 10.
- Zhang Y, Proenca R, Maffei M, Barone M, Leopold L, Friedman JM (1994). Positional cloning of the mouse obese gene and its human homologue. *Nature* 372: 425-32.
- Zhou YT, Grayburn P, Karim A, Shimabukuro M, Higa M, Baetens D, Orci L, Unger RH (2000). Lipotoxic heart disease in obese rats: implications for human obesity. *Proc Natl Acad Sci USA* 97: 1784-9.

Zhuhua Z, Zhiquan W, Zhen Y, Yixin N, Weiwei Z, Xiaoyong L, Yueming L, Hongmei Z, Li Q, Qing S (2015). A novel mice model of metabolic syndrome: the high-fat-high-fructose diet-fed ICT mice. *Exp Anim* 64 435-42.

# Appendices

## **Appendix A. Buffers and Solutions for High-Resolution Respirometry**

### A.1 Mitochondrial Isolation Buffer

100 mM potassium chloride (Sigma-Aldrich P9541), 50 mM MOPS (BP308), 5 mM magnesium sulfate (Sigma-Aldrich 230391), 1 mM EGTA (Fisher Scientific O2783), 1 mM ATP (Sigma-Aldrich A2383); pH 7.4 at 4°C

### A.2 Suspension Buffer

100 mM potassium chloride (Sigma-Aldrich P9541), 50 mM MOPS (BP308), 0.5 mM EGTA (Fisher Scientific O2783)

### A.3 Mitochondrial Respiration Medium (Mir05)

110 mM sucrose (Fisher Scientific L-12919), 60 mM lactobionate (Sigma-Aldrich 153516), 0.5 mM EGTA (Fisher Scientific O2783), 1g/L defatted BSA (Sigma-Aldrich A6003), 3 mM magnesium chloride (Sigma-Aldrich M2393), 20 mM taurine (Sigma-Aldrich T0625), 10 mM potassium phosphate monobasic (Fisher Scientific P285), 20 mM HEPES (Fisher Scientific BP310); pH 7.1 at 30°C

## **Appendix B. Buffers and Protease Inhibitors for Protein Sample Preparation**

### B.1 RIPA Buffer

150 mM sodium chloride (EMD Millipore SX0420), 50 mM Tris-HCl (pH 8.0 at 4°C; Invitrogen

15504-020), 10% Triton X-100 (VWR International VW3929-2), 5 g/L sodium deoxycholate (Sigma-Aldrich D6750), 1 g/L SDS (Bio Rad 1610302)

### B.2 Protease Inhibitors

1 mM PMSF (BioShop PMS123), 10 mM sodium fluoride (Sigma-Aldrich S7920), 1 mM sodium orthovanadate (Sigma-Aldrich S6508), 1 mM benzamidine (Sigma-Aldrich B6506), 10 mL/L protease inhibitor cocktail, 10 mL/L phosphatase inhibitor cocktail 2 (Sigma-Aldrich P5726), 10 mL/L phosphatase inhibitor cocktail 3 (Sigma-Aldrich P0044), 5 mM EDTA (Sigma-Aldrich 03690)/1 mM EGTA (Fisher Scientific O2783) were added when required

### B.3 Detergent-Free Homogenization Buffer

250 mM sucrose (Fisher Scientific L-12919), 50 mM Tris-HCl (pH 7.4 at 4°C; Invitrogen 15504-020), 5 mM magnesium chloride (Sigma-Aldrich M2393)

### B.4 Nuclear Extraction Buffer

20 mM HEPES (pH 7.9 at 4°C), 1.5 mM magnesium chloride (Sigma-Aldrich M2393), 0.5 M sodium chloride (EMD Millipore SX0420), 20% glycerol (Anachemia AC-4674), 0.01% Triton X-100 (VWR International VW3929-2), 0.2 mM EDTA (Sigma-Aldrich 03690), 0.2 mM EGTA (Fisher Scientific O2783)

### B.6 Membrane Extraction Buffer

20 mM Tris-HCl (pH 7.8 at 4°C; Invitrogen 15504-020), 0.4 M sodium chloride (EMD Millipore SX0420), 15% glycerol (Anachemia AC-4674), 1.5% Triton X-100 (VWR International VW3929-2), 10 g/L NP-40 (Sigma-Aldrich I8896), 5 g/L sodium deoxycholate (Sigma-Aldrich D6750), 1

g/L SDS (Bio Rad 1610302), 1 mM EDTA (Sigma-Aldrich 03690), 1 mM EGTA (Fisher Scientific O2783)

## **Appendix C. Buffers for Immunoblots**

### C.1 5× Laemmli Sample Buffer

0.3 M Tris-HCl (pH 6.8 at room temperature; Invitrogen 15504-020), 50% glycerol (Anachemia AC-4674), 25% β-mercaptoethanol (Fisher Scientific AC12547), 10% SDS (Bio Rad 1610302), 0.1 to 0.25% bromophenol blue (Bio Rad 1610404)

### C.2 Transfer Buffer

48 mM Tris-HCl (Invitrogen 15504-020), 39 mM glycine (Bio Rad 1610718), 10% methanol (Fisher Scientific A408); pH 9.2 at room temperature

### C.3 TBST

5 mM Tris-HCl (Invitrogen 15504-020), 15 mM sodium chloride (EMD Millipore SX0420), 0.1% Tween 20 (Sigma-Aldrich P7949); pH 7.5 at room temperature

## **Appendix D. Buffers/Solutions for Enzyme Activity and Tissue Level Assays**

### D.1 PBS

10 mM sodium phosphate dibasic (Sigma-Aldrich 255793), 2 mM potassium phosphate monobasic (Fisher Scientific P285)

### D.2 DTNB Solution

1.01 mM DTNB (Sigma-Aldrich D8130), 0.1 M Tris-HCl (pH 7.0 at 4°C; Invitrogen 15504-020);

pH 8.1 4°C

#### D.3 Oxaloacetate Solution

10 mM oxaloacetate (Sigma-Aldrich O4126), 0.1 M triethanolamine (pH 8.0 at 4°C; Sigma-Aldrich 90279), 1 mM EDTA (Sigma-Aldrich 03690); pH 8.0 at 4°C

#### D.4 STE Buffer

0.25 M sucrose (Fisher Scientific BP220), 5 mM Tris (pH 7.4 at 4°C; Invitrogen 15504-020), 2 mM EGTA (Fisher Scientific O2783); pH 7.4 at 4°C